Addis Ababa University

College of Natural and Computational Science

School of Earth Sciences

Crustal Structure of the Northeast African Rift System From Receiver Function Analysis

By:- Birhanu Abera

Supervisor:- Prof. Atalay Ayele

A dissertation submitted in partial fulfilment of the requirements of
Addis Ababa University for the degree of
PhD in Applied Geophysics (Seismology)

May 16, 2023

ABSTRACT

This study examines the crustal structure in different regions, including Afar, Northwest (NW) plateau, Southeast (SE) plateau, Northern Main Ethiopian Rift (NMER), and Central Main Ethiopian Rift (CMER). High-quality teleseismic data ($Mb > 6.0$) with epicentral distances of 30° to 90° were analysed. The data were collected between 2000 and 2013 from 27 temporary broadband stations in Ethiopia and Eritrea, and between February 2015 and October 2016 from 17 stations of the RiftVolc broadband network. The study reveals consistent seismic velocity in the Afar crust, except in magmatic segments. These segments have a shallow layer with fast V_s (4.5 km/s) at depths of 6-14 km. Below this layer, V_s decreases (< 3.2 km/s), and the V_p/V_s ratio increases (2.0) at lower crustal depths (20-25 km). This suggests partial melting beneath the lower crust, particularly in the western Afar region and magmatic segments. The NW Plateau exhibits fast V_s (4-4.7 km/s) in its crust, with some regions showing slow V_s (3.2 km/s) and high V_p/V_s (1.85-2.0) at mid-crustal depths (10-25 km). Partial melt is observed in specific mid-crustal areas, possibly due to the extension of the plateau or melt migration from the rift. The uppermost crust (depth <6 km) in the NMER and CMER has slow V_s due to sedimentary and/or volcanic layers. Crustal V_s exhibits lateral and depth variations. Slow V_s ($\sim$2-3 km/s) is observed beneath volcanic centres in the upper-mid crust, while the lower crust consistently shows slow V_s ($V_s < 3.5$ km/s). The slow lower crust is associated with high V_p/V_s ratios (1.9-2.0). A low V_s and a small fraction ($< 5\%$) of high V_p/V_s material in the rift system indicate possible partial melt, which is widespread in the rift valley as segmented and localized features. These findings suggest that partial melt in the lower crust beneath active magmatic rifts is more significant than previously thought. The presence of a substantial melt reservoir in the lower crust highlights the role of magmatism in crustal extension and its influence on the evolution of the rift system. In contrast, the Eastern Plateau exhibits uniform and faster V_s, with a distinct velocity contrast between the crust and upper mantle, indicating less deformation compared to the central rift zone. The estimated Moho depth in Afar ranges from 26-30 km, showing a gradual transition compared to other areas studied. Furthermore, the NW Plateau has a Moho depth ranging from 36-44 km, while the SE Plateau has a depth ranging from 36-42 km. These findings have implications for understanding continental rifting mechanisms, magmatic system formation, and long-term lithospheric evolution.

ACKNOWLEDGMENTS

Completing this dissertation would not have been possible without the support and contributions of various individuals and organizations. I extend my heartfelt gratitude to all those who have helped me throughout my doctoral journey.

Firstly, I would like to express my sincere appreciation to Addis Ababa University for giving me the opportunity to pursue my doctoral studies. I am grateful for the excellent academic environment and resources that have been made available to me during my time at the institution.

My deepest gratitude goes to my advisor, Professor Atalay Ayele, for his unwavering support, guidance, and encouragement throughout the research process. His expert knowledge, insightful feedback, and critical evaluation of my work have been invaluable in shaping this dissertation.

I would also like to acknowledge the immense contributions of my co-author, Professor Derek Keir, who has worked tirelessly with me on all the papers related to this research project. His concrete ideas, necessary scientific comments, and thoughtful discussions via Skype and other social media platforms have significantly strengthened the ideas and thoughts in this dissertation.

Furthermore, I would like to thank all the professors, mentors, and colleagues who have provided me with invaluable feedback, insights, and inspiration throughout my academic journey. Your knowledge, expertise, and support have been crucial in shaping my research and personal growth.

Finally, I express my heartfelt gratitude to my family, friends, and loved ones who have provided me with unwavering love, encouragement, and support. Your constant motivation, patience, and belief in me have been the driving force behind my success.

DECLARATION

I, Birhanu Abera, hereby declare that this dissertation, entitled **Crustal structure of the Northern East African Rift System from Receiver Function Analysis**, is the result of my original research and has been written solely by me.

The research project was conducted at Addis Ababa University under the supervision of Professor Atalay Ayele. All the data, interpretations, and conclusions presented in this dissertation are my own original work, except where otherwise stated and duly acknowledged.

I confirm that this dissertation has not been previously submitted for any degree or diploma to any institution or university, nor has it been published in any form or medium. I also confirm that this dissertation is not currently being considered for any other degree or diploma.

In conclusion, I affirm that this dissertation represents my own original work, and that I have complied with all ethical and academic standards and guidelines set forth by Addis Ababa University.

Signature: ——————————

Date: ——————————

Birhanu Abera Kibret
May 16, 2023

APROVAL & SIGNATURE

We, the members of the examining board, hereby testify to our acceptance and recommendation of the dissertation titled "Crustal Structure of the Northern East African Rift System From Receiver Function Analysis" submitted by Birhanu Abera Kibret, in partial fulfilment of the requirements for the PhD degree at Addis Ababa University.

We confirm that the candidate has successfully fulfilled all the academic requirements of Addis Ababa University and has demonstrated a deep understanding of the subject matter related to his research project.

Having carefully reviewed the dissertation, we are pleased to say that it meets the high academic standards required for the degree sought. The research project provides an original contribution to the field of study and reflects a remarkable level of research skills, critical thinking, and analytical abilities.

We extend our sincere congratulations to Birhanu Abera Kibret for his successful completion of this academic journey, and we highly recommend the award of the PhD degree from the School of Earth Sciences, Addis Ababa University.

Examination Board Members:

Name	**Signature**	**Date**
1. Prof. Atalay Ayele (Advisor)	_____	_____
2. Prof. Tilahun Mammo (Internal Examiner)	_____	_____
3. ********(External Examiner)	_____	_____
4. Prof. Worash Getaneh (Chairperson)	_____	_____

Date of Defense: June 15, 2023

DEDICATION

I dedicate this dissertation to my loving family, who have always supported and encouraged me throughout my academic journey. To my dear mom, sister, and brothers, your unwavering love and guidance have been my constant source of strength and inspiration.

I would also like to dedicate this work to my wonderful wife, who has been my rock and my partner in every sense of the word. Your hard work, kindness, patience, and unwavering support have been invaluable to me, and I could not have done this without you.

To my mentors, colleagues, and friends who have supported and motivated me to reach this new heights, thank you for your feedback and encouragement.

Moreover, I dedicate this dissertation to all those who have paved the way for me and made it possible to pursue my dreams.

And lastly, to my children, who have sacrificed so much as I pursued this journey. I am grateful for your patience and understanding when I had to miss playtime or study sessions, and for your unconditional love and support. This work is dedicated to you as a promise that I will continue to work hard and make time for our family, to ensure that we make memories and cherish each other's company.

DEFINITIONS AND ABBREVIATIONS

Abbreviations	Definitions
CMER	Central Main Ethiopian Rift
EAR	East African Rift
GF	Gaussian Filter
GPS	Global Positioning System
GSAC	Generic Seismic Application Computing
IDMC	IRIS Data Management Center
MER	Main Ethiopian Rift
NEARS	Northeast African Rift Systems
NLLS	Nonlinear Least Square
NMER	Northern Main Ethiopian Rift
ORFs	Observed Receiver Functions
ORF	Observed Receiver Function
PCF	percentage of cumulative frequency
RF	Receiver Function
RFs	Receiver Functions
RRF	Radial Receiver Function
SMER	Southern Main Ethiopian Rift
SRFs	Synthetic Receiver Functions
SRF	Synthetic Receiver Function
SWCs	Seismic Wave Conversion
SNR	signal-to-noise ratio
TRF	Transverse Receiver Function
VM	Velocity Model
VD	Velocity Discontinuity
Vs	Shear wave velocity
Vp	Compressional wave velocity
Vp/Vs	The ratio of Vp and Vs (Poisson's ratio)
WFB	Wonji fault belt
WLD	Water Level Deconvolution

Contents

List of Figures

List of Tables

CHAPTER 1

GENERAL INTRODUCTION

This thesis is structured into seven chapters to effectively present the research findings. The initial chapter serves as the general introduction, providing an overview, background, and justification for the study. Within this chapter, the background subsection focuses on providing contextual information such as the tectonic setting of the rift and crustal structure of plateaus related to the study. Additionally, introduction part justifies the study by addressing the problem statement, research questions, objectives, significance, scope, and limitations. All of these components are integrated into the general introduction part of chapter one.

Chapter two of the thesis delves into the data and methodology employed in the study. This section provides a comprehensive explanation of the data collection processes and the particular methodology adopted to conduct the research. The aim of this chapter is to offer a thorough understanding of the experimental procedures.

The subsequent three chapters encompass sections of the study that have been completed and are prepared for submission to a journal for publication. These chapters present the key findings and results of the research, which contribute to the overall understanding of the deep interior structure of Eastern Africa. The primary focus of these chapters lies in the analysis of receiver functions (RFs) to gain insights into the composition and layers of the region. Furthermore, the investigation places particular emphasis on the impact of partial melting, magmatism, and diking on seismic velocity.

The final two chapters of the thesis consist of the general discussion and the conclusion. The results and findings from the preceding chapters are thoroughly examined and interpreted in the general discussion section. This chapter provides an opportunity to delve into the implications, significance, and broader context of the research. Finally, the conclusion presents a concise summary of the entire thesis, restating the main findings, contributions, and potential areas for further research.

The overarching objective of this study was to comprehensively explore the crustal structure of eastern Africa, utilizing receiver functions (RFs) as the primary analytical tool. By investigating the composition and layers of the region, with a specific emphasis on the effects of partial melting, magmatism, and diking on seismic velocity, this research gives to the broader understanding of the geology and tectonic activities in the studied area.

Comparative studies of the crustal structure among the various regions of Ethiopia will be of utmost importance because findings from past research indicate that the crustal compositions in the region differ. Some of the varied natural features discovered in the crustal structure of the research areas include faults, sills, partial melt, and dikes (Figure 1.4). A piecemeal approach to study the region will have greater relevance if the considerable crustal structures are highlighted, relatively detailed structural data are obtained, and findings are compared across various locations, such as beneath Afar, along the Main Ethiopian Rift (MER), and on the NW and SE plateau. Figure 1.1 depicts the study area and the spatial distribution of transient broadband seismic stations utilized in Ethiopia at three different locations for this thesis. The stations are colour-coded to differentiate between the three distinct study areas, facilitating the analysis and interpretation of the data.

1.1 Overview

The Northeast African rift system (NEARS) provides an exceptional setting to investigate a diverse range of geological natural processes, including rifting, partial melting, lithospheric uplift, and continental extension (Figure 1.3). It is also an ideal location for observing how distributed continental deformation is progressively focused at oceanic spreading centres. Prior research on the EARS has examined these processes through the use of various geological and geophysical techniques, such as seismic imaging, geodetic measurements, and geochemical analyses (e.g., Corti, 2012; Ebinger, 2005).

The extension happening along the active NEARS covers the whole process of rift development, starting with continents splitting apart and ending with the creation of a seafloor. The NEARS stretches from the top of Afar to the bottom of Turkana. In the Afar region, the Ethiopian rift is one of the three parts of the Red Sea-Gulf of Aden triple junction. This area with volcanoes and the Mid-Oceanic Ridge (MER) is a great place to study different geological processes like magma movement, faults, melting of rocks, and differences in the Earth's crust. Understanding these processes is important for knowing how continents break apart and turn into oceanic rifts.

Most preceding studies have mainly focused on understanding how rifts form and their

effects, particularly in active continental rift systems like Afar and MER (Corti, 2012). However, this study is interested in a specific area called NEARS, which is part of a larger region called EARS. NEARS is important because it was where the concept of a rift valley was first introduced. A rift valley is a special geological feature with long basins that are separated by faults (Corti, 2012).

The Ethiopian rift system consists of different regions, such as Afar, NMER, CMER and SMER. These places are special because they give us a rare chance to see the actual process of continents breaking apart happening in nature (Hayward and Ebinger, 1996).

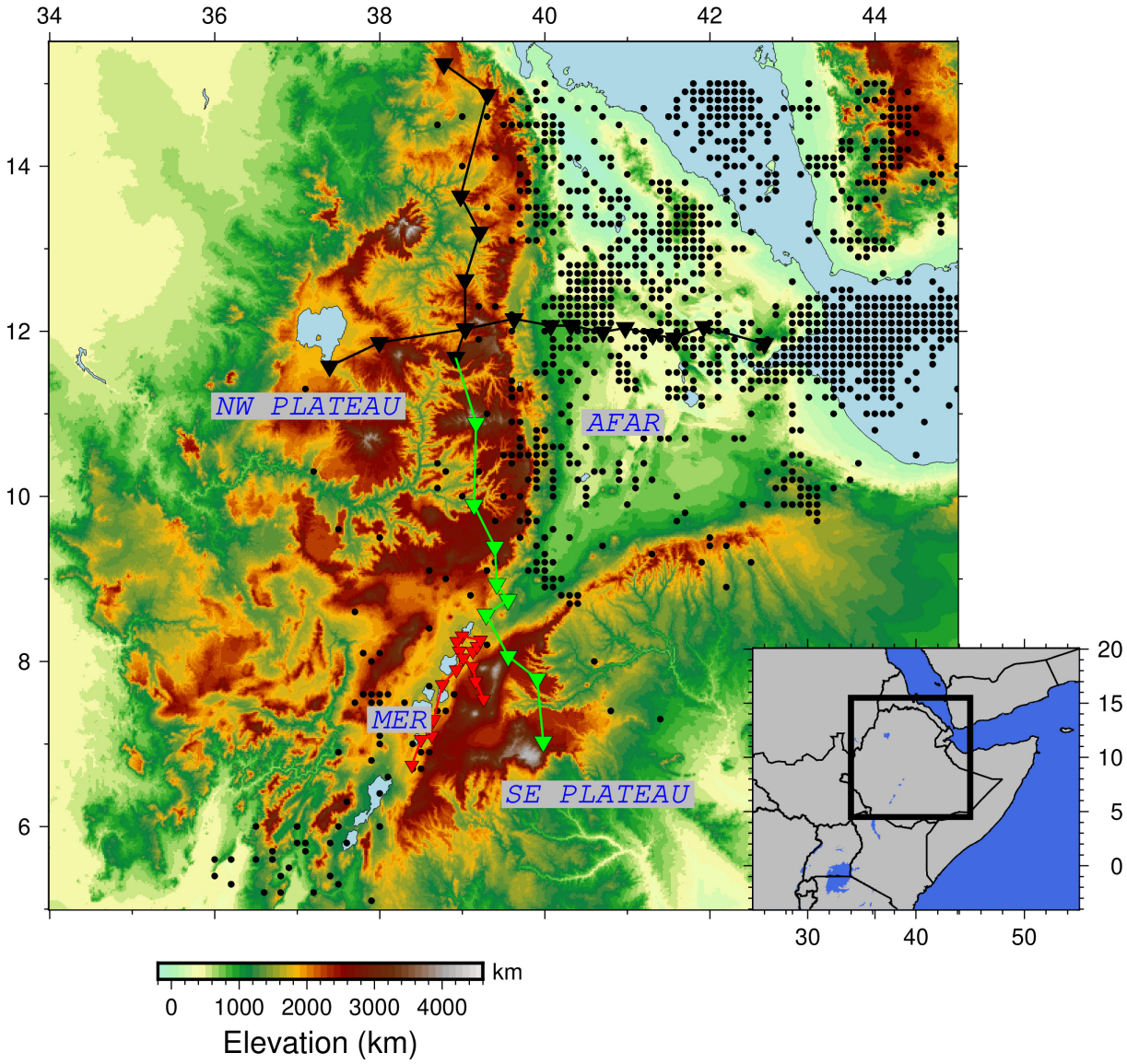

Figure 1.1: This figure depicts the temporary seismic stations used in the study, represented by three different colours of inverted triangles. The solid lines connecting the them indicate the study profile. The red inverted triangles within the MER region correspond to the study area analysed in Chapter 3, while the black inverted triangles connected by solid black lines represent the area examined in Chapter 4. The third type of inverted triangles, coloured green, represents the study discussed in Chapter 5. The black circles scattered throughout the map indicate earthquakes recorded between 1906 and 2021, obtained from the International Seismological Center (ICS) database (http://www.isc.ac.uk/). The black rectangle within the inset map outlines the study area located in the MER region.

1.2 Background

This section helps to provide a comprehensive understanding of the geological and geophysical properties of the Northeast Africa Rift System (NEARS) and the surrounding

regions, which have a complex and dynamic nature. The section covers several topics, including the NW and SE Ethiopian plateau, the Afar and MER regions, and previous crustal studies of the NEARS. It aims to summarize the key findings from previous geological and geophysical studies of the NEARS and review the various techniques used to investigate the area. The section also delves into geophysics of the area, with a focus on the parameters of Vs and the Poisson ratio (Vp/Vs) to characterize properties of crust and mantle. Additionally, the chapter discusses Mohorovicic discontinuity (Moho) of the region, which is the limit amidst crust and mantle. It summarizes the considerable findings from studies of the Moho in the NEARS region and discusses the implications of these findings for our understanding of the area's geological history. Overall, this literature review section aims to provide a solid foundation for the subsequent chapters, which will focus on our study's objectives and methods.

1.2.1 Tectonic Settings of NEARS

The NEARS is a significant part of the EAR valley and a dynamic area of interest for geological and geophysical studies. It is a representative example of a continental rift that spans a long and active part of the rift system, making it a natural laboratory for investigating the interplay between mantle dynamics, magmatic intrusion, subsurface processes, plateau uplift, and continental flood basalt (CFB) volcanism (Bastow et al., 2008; Ebinger and Casey, 2001; George et al., 1998; Sembroni et al., 2016). The NEARS is comprised of the Afar, the MER, the Northwest (NW), and the Southeast (SE) Ethiopian Plateau regions, with the Afar and MER bounded by the NW and SE plateaus (Ebinger et al., 2017).

The initiation and development of the NEARS is a result of a dynamic interplay between tectonic stretching and mantle upwelling that began during the onset of the Miocene at around 22-25 million years ago (Corti et al., 2003, 2018). Rifting advanced by a combination of thermal softening, occurrence of deformation, and reduction of crustal strength caused by the influx of hot plume material from decompression melting and intrusion of magma (Rooney et al., 2014; Rychert et al., 2012). Understanding the depth to the start of decompression melting, crustal thickness, and the nature of important boundaries such as the crust-mantle boundary and the Moho are crucial parameters in comprehending the thermal effect and the plume intensity on the rift development of the NEARS (Rychert et al., 2012). Due to the distinctive geophysical and geodynamical activity observed in each region of the NEARS, it is necessary to examine each portion of the NEARS separately to gain a complete understanding of the system.

Previous investigations have examined on various aspects of the NEARS, including its ge-

ological and geophysical properties, and different techniques which have been employed to investigate the region. For example, Rychert et al. (2012) used seismic imaging to determine composition of the crust Afar, while Bastow et al. (2008) used tomography and receiver functions to investigate the subsurface structure of the region underneath the MER. Similarly, Sembroni et al. (2016) used gravity data to study the crustal structure of the NW Ethiopian plateau, while Ebinger et al. (2017) used seismicity (Figure 1.2) and tomography to study the SE Ethiopian plateau. These studies have provided valuable insights into the NEARS, though the issue demands further research to be fully comprehended the complex and dynamic nature of this region.

Previous crustal studies in the NEARS

To increase our understanding of the fundamental processes associated with the lithosphere in the NEAR region, it is important to study the structure of the crust. Previous research has used a variety of geophysical techniques, including passive and controlled source methods such as magnetotelluric imaging and gravity data inversion (Didana et al., 2014; Kibret et al., 2019; Lewi et al., 2016). Seismological studies, such as those using receiver functions and ambient noise tomography, have also been employed in recent years to investigate the thickness and composition of the Earth's crust in the NEARS (Chambers et al., 2019; Daly et al., 2008; Dugda et al., 2005; Kibret et al., 2019, 2022; Kim et al., 2012; Stuart et al., 2006). These studies have shown that there is evidential variation in crustal thickness and composition across the NEAR region, with the crust being affected by magmatic intrusion, partial melting, and rifting (Ahmed et al., 2022; Chambers et al., 2019; Dugda and Nyblade, 2006; Dugda et al., 2007; Hammond et al., 2011).

Based on diverse geophysical methods and prior seismic imaging techniques such as RF, investigations have revealed that the crustal thickness beneath the northwestern plateau ranges from 35 to 45 km, with regions of greater thickness observed in the central part of the northwestern plateau (Ayele et al., 2004; Dugda and Nyblade, 2006; Dugda et al., 2005; Ebinger and Casey, 2001; Kibret et al., 2019; Maguire et al., 2006; Stuart et al., 2006). The eastern flank, on the other hand, is between 38-40 km thick (Cornwell et al., 2010; Dugda et al., 2005; Kibret et al., 2019, 2022). However, in the northern MER, the crustal thickness drops from 38-40 km in the south to 24 km beneath the southern Afar depression, specifically Fentale Volcano (Dugda et al., 2005; Kibret et al., 2022; Maguire et al., 2006). In our study, we focused on the structure of crust for areas where previous studies' profiles did not cross. Our results denoted that the NW plateau has a thicker crust than the SE plateau, which may be attributed to a combination of magmatic intrusion and crustal thickening.

Additionally, the 3-D representation from gravity data by Mahatsente et al. (1999) showed a dense intrusion in both the lower and upper crust in the rift centre, with crustal thinning occurring between 38-51 km beneath the plateaus and 31 km underneath the rift axis. Our findings are largely compatible with the crustal thickness traced from gravity data modelling, as well as with previous seismological studies (Kibret et al., 2019; Mammo, 2013; Tiberi et al., 2005). Overall, our study provides further insights into the rifting and uplifting processes in the NEAR region, specifically in the NW and SE plateaus.

1.2.2 The NW and SE Ethiopian plateau

The Northwest (NW) and Southeast (SE) Ethiopian Plateaus are noticeably elevated regions that present an average elevation of 2500 m above sea level. These plateaus are underlain by Precambrian and Mesozoic rocks tiled by 1-3 km thick volcanic rocks (Ismail and Abdelsalam, 2012; Pik et al., 1998; Sembroni et al., 2016; Sengor, 2001; Steiner et al., 2021). The gradual uplifting of these plateaus is an ongoing and dynamic process that has been sustained over a long period of time (Sembroni et al., 2016).

The plateaus are preceded by a huge discharge of an igneous province coherent with the very hot mantle plumes dynamic acting at the foot of the lithosphere (Corti et al., 2003). The igneous molten materials tends to intrude as a sills or dikes and exits through cracks as a lava and/or tephra rocks that form the NW and SE plateaus' uplifted flanks arise from the MER and Afar mantle plume, as magma rises through the crust and emerges at the surface (Gani and Gani, 2007).

The high topography of the NW and SE plateaus is defined by extended tectonic deformation, large-scale volcanic eruptions, anomalous subsiding of basins, and uplifting of domes resulting from substantial mantle-driven forces. The present-day elevated topography of the NW and SE plateaus is a result of the uplift that occurred along the western margin of Arabia and the Afar region around 30 million years ago (Corti et al., 2003; Rooney et al., 2014).

1.2.3 The Afar and MER

The MER and Afar region are located within the NEARS and are both key areas in the study of continental rifting and seafloor spreading. The Afar depression is a 300 km-wide region located at the intersection of the Nubian, Somali, and Arabian plates and is an example of how continental rifting leads to the establishment of incipient oceanic rifting and seafloor spreading (Sembroni et al., 2016; Weissel and Karner, 1989). The Afar crust is believed to be thin due to both tectonic and magmatic activities (Jentzsch et al., 2000).

The MER, on the other hand, is an active region segmented in three zone as NMER, CMER and SMER both in its seismicity (Figure 1.2) and volcanic active of the NEARS rift system that trends NE cross ways the Ethiopian plateau (Corti et al., 2018, 2013; Keranen and Klemperer, 2008). It is a transitional point from the continental rifting to the oceanic seafloor spreading in Afar (Dugda and Nyblade, 2006; Hayward and Ebinger, 1996; Rowland et al., 2007). Lithospheric thinning is a fundamental process associated with the modification from continent-wide to oceanic rifting, and it exposed to the magma intrusion with little crustal thinning in the MER (Biggs et al., 2011; Ebinger and Casey, 2001; Mackenzie et al., 2005; Maguire et al., 2006). Magmatic upwelling (Figure 1.3) alters the lithosphere through the process of thermal erosion, which involves the infiltration of magma and thinning of the crust due to thermo-mechanical erosion in active continental rifting zones such as the MER and Afar (Rooney, 2010; Rychert et al., 2012).

Both the Afar and MER regions are influenced by magma intrusions in the form of dikes and sills, faulting, and stretching, which make the Earth's outer layer thinner and stretched (Figure 1.3) (Bastow et al., 2011; Buck, 2004; Buck et al., 2006; Corti et al., 2003; Ebinger and Casey, 2001; Rooney et al., 2014). The crust in these areas has distinctive features, including scattered volcanic eruptions, lower basins, and raised areas called geologic domes. These features are caused by powerful forces from the molten rock beneath the Earth's surface (Ismail and Abdelsalam, 2012; Pik et al., 1998; Sembroni et al., 2016; Sengor, 2001; Steiner et al., 2021). The Ethiopian Plateau has been gradually rising over a long period and may still be changing due to ongoing processes (Sembroni et al., 2016).

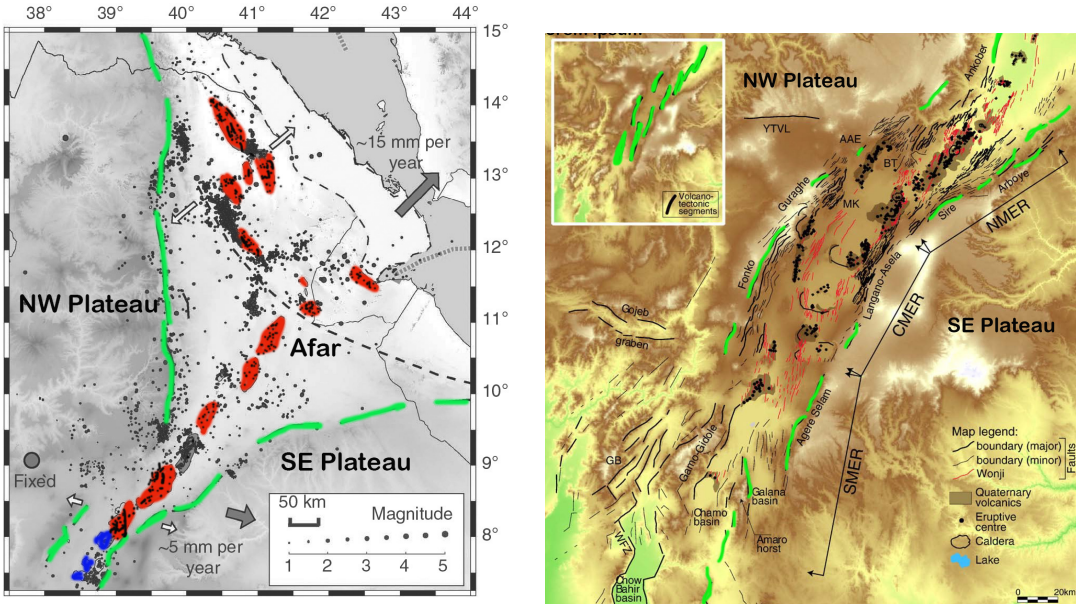

(A) (B)

Figure 1.2: (A) This figure displays the seismic activity in Afar, with the border fault pointed by the solid green line, and the volcanic cone of Afar and MER outlined by the solid red polygon. The modified image, which is based on data from Keir et al. (2011), offers insights into the tectonic features of the region. (B) This map illustrates the MER and its associated tectonic features, including the Wonji Fault Belt, which is arranged in a en-echelon and right-stepping pattern as shown in the inset. The figure provides a high-level overview of the complex tectonic environment of the MER (adapted from Boccaletti et al., 1998; Corti, 2009).

1.2.4 The shear wave velocity (Vs) of the region

Beneath Afar, there is a prevalence of slow-moving seismic waves, with velocities ranging from 3.2 to 3.3 km/s, as reported by Eshetu et al. (2021). These velocities are linked to the emergence of Pliocene flood basalts on the surface. The observed decrease in wave speed is attributed to the partial melting of the upper crust and the resulting increase in temperature, which are also evident in the area's volcanic activity and thermal manifestations (Eshetu et al., 2021). The top mantle of the Afar and MER exhibits a low wave speed anomaly, which shifts towards the west as one goes deeper (e.g., Bastow et al., 2011).

Previous studies have suggested that the high-speed lower crustal layer beneath the NW plateau may be the result of mafic rock underplating or high-density lower crustal sill intrusion during magmatism from the Oligocene to present (Cornwell et al., 2010; Hammond, 2014; Hammond et al., 2011; Kibret et al., 2019; Maguire et al., 2006; Stuart et al., 2006). This hypothesis is supported by seismic refraction data that indicate high velocities of seismic waves (Vp) in the crust beneath the plateau, with values reaching as high as 8.0 km/s

(Makris and Ginzburg, 1987). The crustal thickness of the NW plateau, on the other hand, has been estimated to be around 40-45 km based on receiver functions (Dugda et al., 2005; Hammond et al., 2011). In contrast, the crustal thickness of the SE plateau appears to be 38–40 km, as presented by receiver functions (Hammond et al., 2011; Keranen et al., 2009; Mackenzie et al., 2005; Tiberi et al., 2005). It is possible that the different crustal structures of the two plateaus are related to their distinct geologic histories.

In addition to studying the crustal structure, the NEARS region has been investigated for its seismicity and volcanic activity (Figure 1.2). The MER segment is the most seismically active region in the NEARS, with multiple moderate to large earthquakes recorded in the past century (Greenfield et al., 2019a,b; Keir et al., 2009, 006b). This high level of seismic activity is attributed to the ongoing rifting process, as well as to the complex interaction of tectonic forces and magmatic activity (Keir et al., 2009, 009b; Rowland et al., 2007). The Afar depression is also known for its volcanic activity, with several active volcanic centres, including Erta Ale, Alu-Dalafilla, and Dabbahu (Hamling et al., 2009; Hammond et al., 2011; Kendall et al., 2006). The volcanic activity in the region is considered to be associated with the extensional tectonics (Figure 1.3) and magma upwelling (Figure 1.3) associated with continental rifting (Hammond, 2014).

1.2.5 The Poisson ratio (Vp/Vs) of the region

The high V_p/V_s ratio observed in the Afar and MER regions can be attributed to the presence of mafic materials with partial melt underneath the crust (Figure 1.5). This high ratio is also observed in the NW and SE plateaus. The lithospheric weakening by hot materials assists in the continental breakup through decompression melting (Ebinger and Wijk, 2014; Samrock et al., 2018). Emplacement of hot material into the lower crust would lift the regional thermal gradient, resulting in partial melting of the crust (Cornwell et al., 2010). The produced melt increases the rate of crustal thinning (Koptev et al., 2015) and can cause ductile or brittle failure of the crystal matrix (Campione et al., 2015). Adiabatic decompressions as the plume rises and additional heat advected by the plume itself produces melt and pressurized fluid inclusions (Koptev et al., 2015). When the upper mantle is extremely hot and has partially melted, the speed of seismic waves travelling through it can decrease. Research conducted by Keranen et al. (2009) has shown that both these effects can occur at the same time. This finding is in line with the magma-driven rifting theory proposed by Buck et al. (2006).

Studies have shown a variation in Vp/Vs ratio with depth, particularly in the upper and mid-crust. For example, the Vp/Vs ratio increments with depth in the MER, indicating a

more mafic composition with depth (Hammond et al., 2011). Studies of the Afar region have shown that as depth increases, there is an increase in the ratio of seismic wave velocities (Vp/Vs), which indicates a greater degree of partial melting at greater depths (Ahmed et al., 2022; Chambers et al., 2019). On the other hand, the NW plateau shows a relatively constant Vp/Vs ratio with depth, indicating a more felsic composition throughout the upper crust (Keranen and Klemperer, 2008). The SE plateau also shows a constant Vp/Vs ratio with depth, indicating a similar felsic composition as the NW plateau (Kibret et al., 2022). Thus, the Vp/Vs ratio can be used to distinguish between the different crustal domains and their underlying structure.

Magnetotelluric surveys, as described in a study by Johnson (2012), have revealed a highly conductive mass beneath the rift axis that is estimated to be around 13 km wide and between 15 to 28 km deep, which may indicate partial melt in the crust (Figure 1.5). This finding is supported by other studies by Desissa et al. (2013); Didana et al. (2014); Hammond (2014). Another study by Mammo (2013) used modelling of dense gravity studies to identify the presence of low-density material, such as basaltic melt in a magma reservoir. Similarly, Bilham et al. (1999) from GPS measurements have shown that 80% of the extensional strain is concentrated in right stepping en echelon patterned magmatic segments where intensive dyke injections are mainly observed (Ebinger and Casey, 2001).

1.2.6 The Mohorovicic Discontinuity (Moho) of the region

The Mohorovicic discontinuity, also known as the Moho, represents a boundary between the Earth's crust and the underlying mantle, with significant alterations in seismic velocities, density, thermal pressure, chemical compositions, and rheology (e.g., Dugda et al., 2005; Kibret et al., 2019; Mackenzie et al., 2005; Maguire et al., 2006; Zhu and Kanamori, 2000). Knowing the depth at which decompression melting begins is essential for understanding the thermal structure of the mantle, computing the degree of plume effect, and deciphering the lithosphere's modification history (Rychert et al., 2012).

The Earth's crust gets thinner as we go towards the north. In the MER, it is about 36 km thick, while in most parts of Afar, it is around 25 km. In the northern region of Afar, it becomes even thinner, measuring about 15 km (Hammond et al., 2011). Recent studies involving ambient noise tomography (Chambers et al., 2019; Eshetu et al., 2021), controlled source seismic experiment Maguire et al. (2006) and gravity analysis (Lewi et al., 2016; Mammo, 2013) have helped us understand the crust better in our research areas. By using magnetotelluric surveys, scientists have found a highly conductive feature below the rift axis. It is located at depths ranging from 15 to 28 km and has a width of about 13 km.

This discovery suggests that there is a considerable amount of melted or partially melted material in the crust (Desissa et al., 2013; Didana et al., 2014; Hammond, 2014; Johnson, 2012; Lewi et al., 2016). Dense microgravity studies have also been used to study materials with low density, including melted basalt in magma reservoirs. When looking at the bigger picture, the results from gravity data modelling support the conclusions drawn from seismology about the thickness of the crust (Mammo, 2013; Tiberi et al., 2005).

1.3 Justifications of the Study

1.3.1 Statement of the problem

The Afar, NMER, CMER, and SE Plateau regions in Ethiopia and Eritrea are complex areas with diverse geologic features and tectonic processes, including magmatic intrusions, partial melting, and seismicity (Figure 1.2). However, the crustal structure of these regions and the distribution of Moho homogeneity and heterogeneity are poorly understood. Existing models of these regions have relied on limited seismic station coverage and surface geology data, without considering the architecture of the crust. Although some previous studies have provided information on crustal thickness and Moho depth, there is still a remarkable knowledge gap regarding the complex crustal structure and geodynamic processes of these regions.

To address this gap, this study aims to employ advanced seismic techniques and legacy teleseismic data from temporary broadband stations to investigate the crustal structure of the Afar, NMER, CMER, and SE Plateau regions. The study will focus on identifying major magmatic intrusions and their potential contribution to partial melting and seismicity in the lower crust. Additionally, the study will investigate the distribution of Moho heterogeneity and homogeneity in different zones. These efforts will provide valuable insights into the crustal architecture and geodynamic processes of the region, which will contribute significantly to our understanding of rift evolution and the formation of magmatic intrusions. However, accurately estimating crustal thickness and Moho depth, and identifying major melt reservoirs with limited seismic station coverage and wide station separations pose a significant challenge. Nonetheless, the findings of this study will provide new insights into the crustal structure and magmatic processes of the region and have momentous implications for future studies on geologic hazards, resource exploration, and tectonic evolution.

1.3.2 Objectives

General Objective

The aim of this study is to provide a comprehensive understanding of the structure of the Earth's crust in the NEARS region by generating one- and two-dimensional Vs and Vp/Vs models of the lithosphere. This will involve identifying the presence of magmatic additions with high or low Vs, estimating key parameters such as crustal thickness and composition, and assessing their contribution to the region's rifting processes and tectonic settings.

Specific Objectives

This thesis has three main objectives:

- To constrain architecture of the lithosphere beneath CMER and SE plateau by investigating solidified intrusions and partial melt in the upper-to-lower crust using data from 17 RiftVolc temporary broadband stations.
- To investigate major melt reservoirs, estimate Moho depths, and interpret crustal structure and geodynamic processes in the NW plateau and adjacent Afar rift using legacy data from 17 temporary broadband stations.
- To estimate crustal structure, Vs, and Vp/Vs beneath 10 transient broadband seismic stations along the NW plateau, NMER, and SE plateau, and to use these estimates to better understand the region's geology and tectonic activity.

1.3.3 Research question/Hypothesis

Here are the research questions that will be explored to pursue the overarching aims of the study, these are:

- How do the properties and composition of the mantle beneath the Afar, NMER, and CMER regions affect the progression from continental rifting to seafloor spreading, and what is the role of magma in this process?
- To what extent does the intruding magma in the upper/mid and lower crust of the study areas relate to the architecture and development of the Ethiopian plateaus, as well as the Afar, NMER, and CMER, and what are the implications for the evolution of these regions?

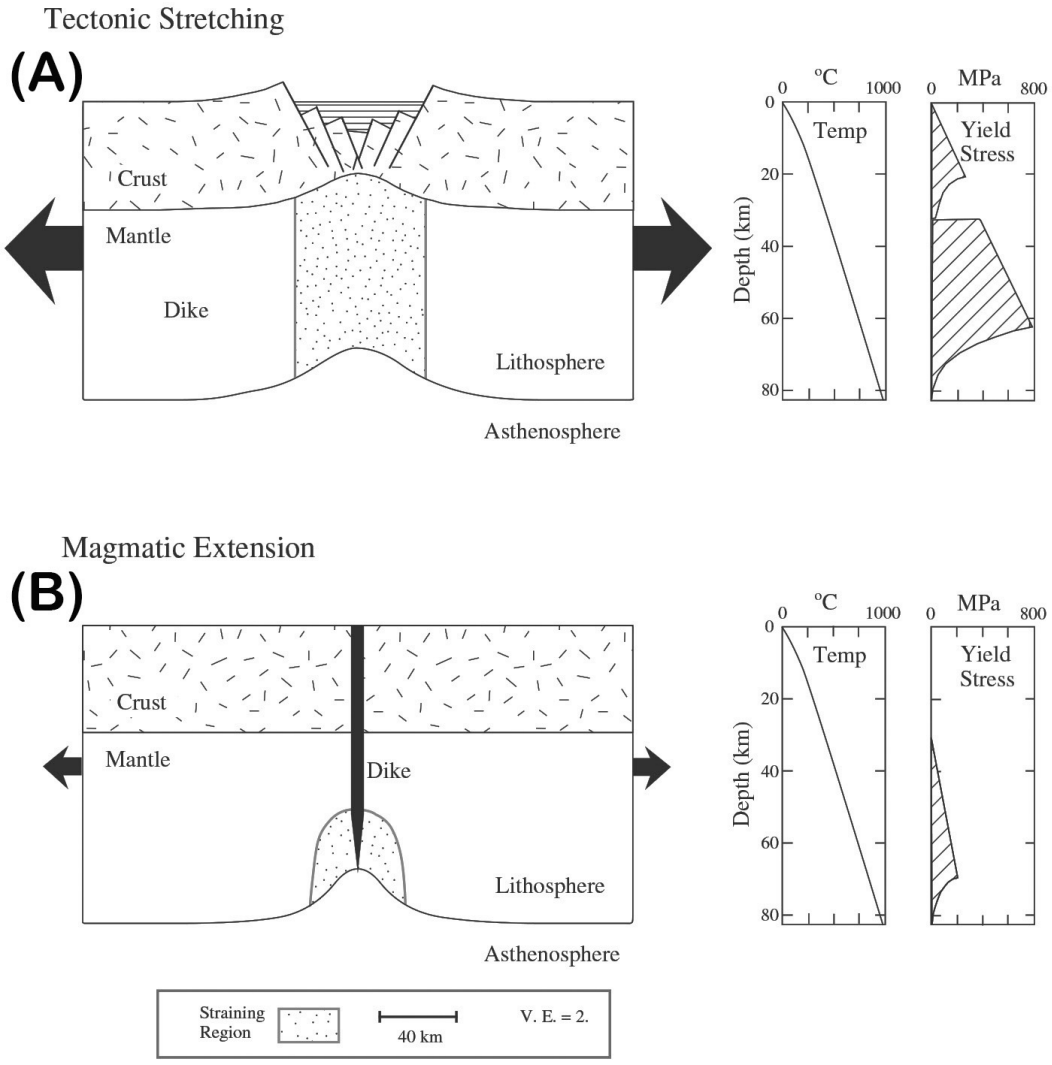

Figure 1.3: Models for rifting of the lithosphere in a rifted region. (A) shows mechanical stretching in which strain is provided by large offset faults where brittle failure is true and by ductile deformation in weaker layers. (B) shows magmatic extension caused by intrusion and subsequent heating. The strain localization and strength reduction of the lithosphere is enhanced by melt intrusion (Adapted from Buck, 2004).

- How was the intruding magma in the upper/mid and lower crust of the study areas formed and deposited, and what are the key geochemical and isotopic signatures that can provide insights into the magmatic processes involved?
- What is the relationship between the features of magma injection into the Afar, CMER, and NMER and the active rifting mechanisms involved, and how does the lithospheric framework influence the evolution of these regions?

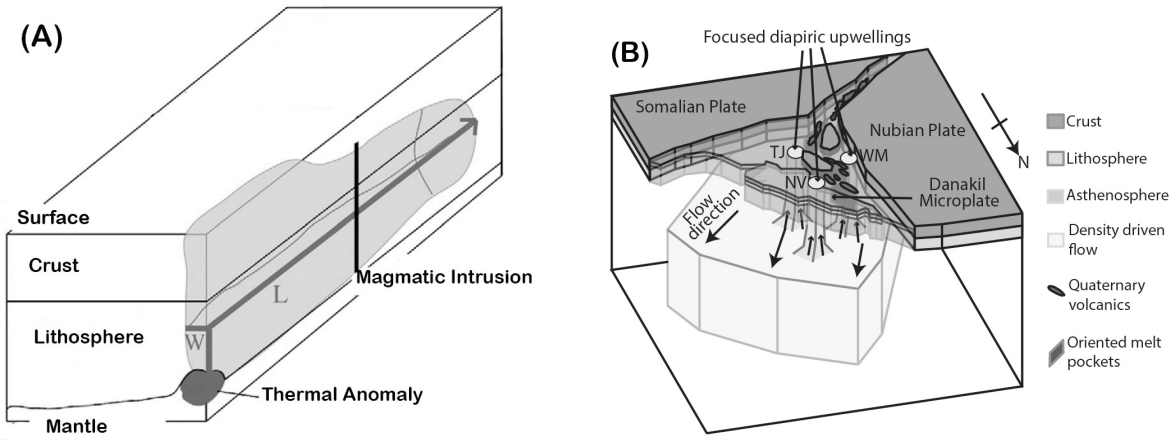

Figure 1.4: (A) A schematic view shows a large dike intrusion into continental lithosphere, adapted from (Modified from Bialas et al., 2010). The dike originates from a magma chamber situated above a thermal anomaly, and it radiates hundreds to thousands of kilometres from a central source. (B) The model suggests that passive rising of asthenosphere (Figure 1.3) in the mantle beneath Afar leads to a melt-filled mantle above 75 km. Focused diapiric thermal upwellings are superimposed on this, and melt oriented at rift axis causes considerable seismic anisotropy and large velocity anomalies (Modified from Hammond et al., 2013).

- How do Vs and Vp/Vs provide new insights into the crustal structure of the Afar, NMER, CMER, and adjacent plateaus, and what are the implications for the velocity structure, crustal thickness, Moho depth, and crustal composition?
- How do the major melt reservoirs vary across different areas in the Afar, NMER, CMER, and adjacent plateaus, and what is their potential contribution to rift-related magmatic processes, and what are the key factors that control their distribution and composition?
- What is the extent and distribution of partial melt in the lower crust underneath the NEARS, and how does it vary across different tectonic settings, and what are the key melt reservoirs in the lower crust beneath the NEARS, and how do they contribute to rift-related magmatic processes?

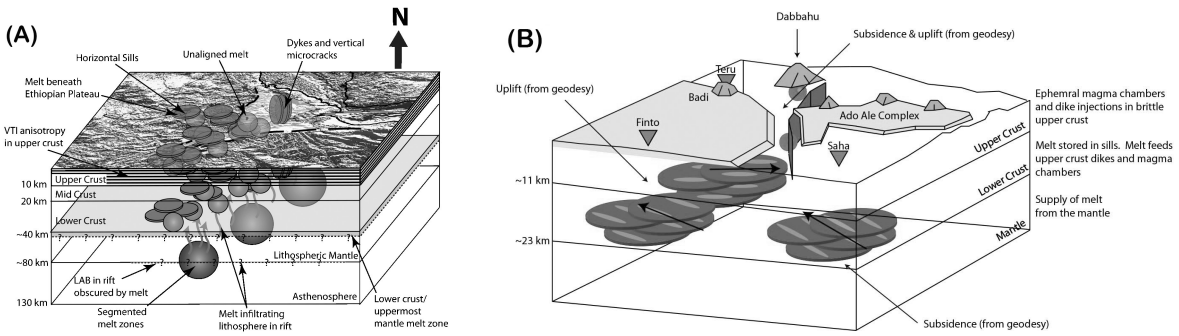

Figure 1.5: (A) This schematic illustrates the magmatic plumbing system below the Northern East African Rift (NEARS), featuring horizontal mafic intrusions in the upper crust and flat disc-shaped sills found on and off the rift in the mid and upper crustal layers. At lower depths, melt is stored in circular sills with low velocity. With the progress of rifting, melt storage transitions from horizontal to vertical sills (Adapted from Chambers et al., 2021). (B) This schematic depicts a model of the magmatic plumbing system in the Manda Hararo rift segment. In this system, melt in the lower crust is believed to be stored in stacked sills, with vertically oriented melt connecting these sills and aligned with the strain. Melt storage in the lower crust away from the rift axis can supply magma to the upper crust and the dike of the rift axis (Adapted from Hammond, 2014).

1.3.4 Significance of the study

Despite numerous studies on the magmatism and partial melting associated with continental rifts, there is a lack of research focusing on the crustal structure beneath elevated shield volcanic regions, such as Guguftu, Choke, and Guna, and its implications on subsurface materials during continental extensional (Figure 1.3) activities. Moreover, while the existing body of research has primarily focused on understanding the interactions between magmatic intrusion, partial melting, crustal thickness deviations, and tectonics in the Ethiopian rift system, there is limited knowledge about the unevenly segmented placement of magmatic upwelling beneath the Central Main Ethiopian Rift (CMER).

To address these research gaps, our study aims to provide new insights into the structure of the crust, Moho depth determination, regional and local velocity modelling, partial melting zone delimitation, low velocity material crustal inclusion, high velocity materials, and solidified magmatic intrusion, as well as crustal material homogeneity and heterogeneity beneath the CMER and adjacent regions.

By better understanding the geodynamic processes involved in magmatic activity in the CMER and the broader NEARS, our study will contribute to the advancement of the understanding of the fundamental mechanisms of continental rifting and seafloor spreading. Moreover, our findings will have important implications for the management of natural resources and geohazards in the region, as well as potential geothermal energy resources.

1.3.5 Study Scope

The scope of this study entails a comprehensive investigation of various aspects within the magmatically active regions of Ethiopia, employing advanced seismic techniques and utilizing legacy teleseismic data. The primary objectives encompass a range of focal points, including the characterization of crustal structure, determination of Moho depth, regional and local velocity modeling, identification of the partial melting zone, delineation of low-velocity material crustal inclusions, characterization of high-velocity materials, and examination of solidified magmatic intrusions. The study will primarily concentrate on the following regions:

1. Northern Main Ethiopian Rift (NMER): Previous studies have predominantly examined the upper mantle low-velocity structure of the NMER through methods such as travel-time tomography and controlled source experiments (e.g., Maguire et al., 2006). Hence, this study will primarily focus on comprehending the constituents and composition of the crust within the NMER. This includes analyzing the crust's composition, investigating the presence of diking along the major rift axis and off-axis, as well as exploring the occurrence of partial melting and its influence on the overall rifting process.

2. Central Main Ethiopian Rift (CMER): The CMER exhibits a plethora of geodynamic phenomena ranging from the uppermost crust to the upper mantle. The findings of this study will encompass the examination of magmatic intrusions, investigation of partial melting, analysis of uplift-subsidence of the crater, and exploration of crustal faulting. However, the primary focus of this study will be on understanding crustal structure, particularly the upper to lower crust. Furthermore, the study will direct attention towards segmented and solidified magmatic intrusions and the distribution of partial melt in the lower crust beneath the magmatically active CMER. Additionally, the study will explore the potential contribution of the magma plumbing system (Figure 1.5).

3. Afar region: While the entire Afar region holds significant geological interest for scientific research, this study will specifically concentrate on the central Afar region where seismic stations have been strategically deployed along a convenient trajectory. The primary focus will revolve around investigating the crustal structure beneath a designated single profile extending from the northwest plateau, traversing the CMER, and reaching Djibouti. Through this approach, the study aims to provide new insights into the role of major melt reservoirs in rift-related magmatic processes within the

northwest plateau and Afar (Figure 1.5).

4. Northwestern-to-Southeastern Ethiopian plateau: Previous studies have made attempts to estimate the Moho depth beneath the NW and SE plateau. However, this study will extend the analysis to encompass an examination of the composition of the plateau crust, in addition to investigating the presence of diking and melting, commonly observed in the rift region. The characterization of crustal structure and geodynamic processes along a profile spanning the NW plateau, NMER, and SE plateau will be carried out to gain insights into the magmatic processes, partial melting, crustal thickness variations, and incidental tectonics prevalent within these regions.

1.3.6 Limitations of the study

One potential limitation of our study is related to the accuracy and precision of the seismic data used to estimate the crustal and upper mantle structure beneath the NEAR region. While we utilized a large dataset from $\sim$44 seismic stations across the study area, the data quality and coverage can vary across the region, which could introduce some uncertainty in our velocity models. Additionally, seismic data is often subject to various noise sources, such as anthropogenic activities or weather conditions, which could affect the signal quality and potentially lead to erroneous interpretations. Despite our efforts to carefully preprocess and analyse the data, there may still be some remaining noise or biases that could affect the accuracy of our results.

The other limitations of this study are related to the complexity of the subsurface structure, and the quality and quantity of seismic data. These limitations can affect the accuracy of the estimated velocity models and interpretation of the subsurface structure. However, despite these limitations, this study provides worthful insights into the crustal and upper mantle structure beneath the different settings in the northeast African region and contributes to a better understanding of the geological and geophysical characteristics of the region. Future studies could address these limitations by increasing the density of seismic stations in areas with limited coverage, incorporating additional geological and geophysical data, and improving the quality and quantity of seismic data.

CHAPTER 2

DATA AND METHOD

This chapter presents a comprehensive exposition of the data and methodology associated with the data collection, encompassing both the pre-existing data and the data collection process in which I actively participated. The employed research methodologies are cogently elucidated throughout the entirety of this study.

2.1 Data

2.1.1 Data Set

Within the framework of our thesis, we heavily relied on archival teleseismic data derived from the Ethiopian Afar Geoscientific Lithospheric Experiment (EAGLE) (Stuart et al., 2006), as well as the Afar Consortium and RiftVolc projects conducted between 2000 and 2017 (Figure 3.2) (Greenfield et al., 2019a; Kibret et al., 2022). Our active engagement in the RiftVolc project spanned the entire data collection process, commencing with the initial deployment of seismic stations and encompassing meticulous data acquisition at regular intervals. By implementing a meticulously planned timetable, we consistently gathered data every four to six months, thereby ensuring a robust temporal coverage that proved indispensable for our comprehensive analysis.

2.1.2 Integrated Teleseismic Events

To enrich our dataset, teleseismic events recorded at specific broadband seismic stations were incorporated. Ten broadband seismic stations (ADYE, DICE, GASE, KOBE, LALE, LYDE, SEKE, SMRE, SRDE, YAYE) operated under the Afar Consortium project (AFAR; Hammond et al., 2011), led by the Universities of Bristol, Leeds, and Addis Ababa. These stations contributed 39 teleseismic events occurring between March 2007 and March 2012. Furthermore, we integrated 15 teleseismic events recorded at the BAHI station from the Seismic Investigation of Deep Structure Beneath the Ethiopian Plateau and Afar Depression

(Ethiopia) project conducted by IRIS/PASSCAL (Nyblade et al., 2000). An additional set of 54 teleseismic events originated from two stations (FINE, AWEE) during the period of 2007–2009 as part of the AFAR07 project (Guidarelli et al., 2011), led by the University of Rochester. Similarly, the AFAR0911 project, led by the University of Southampton, provided 35 teleseismic events recorded at two stations (LULE, SAHE) from 2009 to 2013 (Chambers et al., 2021). Additionally, the Eritrea Seismic Project (ESP) (Hammond, 2011) operated by Birkbeck University of London contributed 22 teleseismic events recorded at two stations (EITE & CAYE) between 2010 and 2011. Lastly, the DORA project conducted by Ecole et Observatoire des Sciences de la Terre (EOST) yielded 15 teleseismic events recorded at the RAND station from 2009 to 2012.

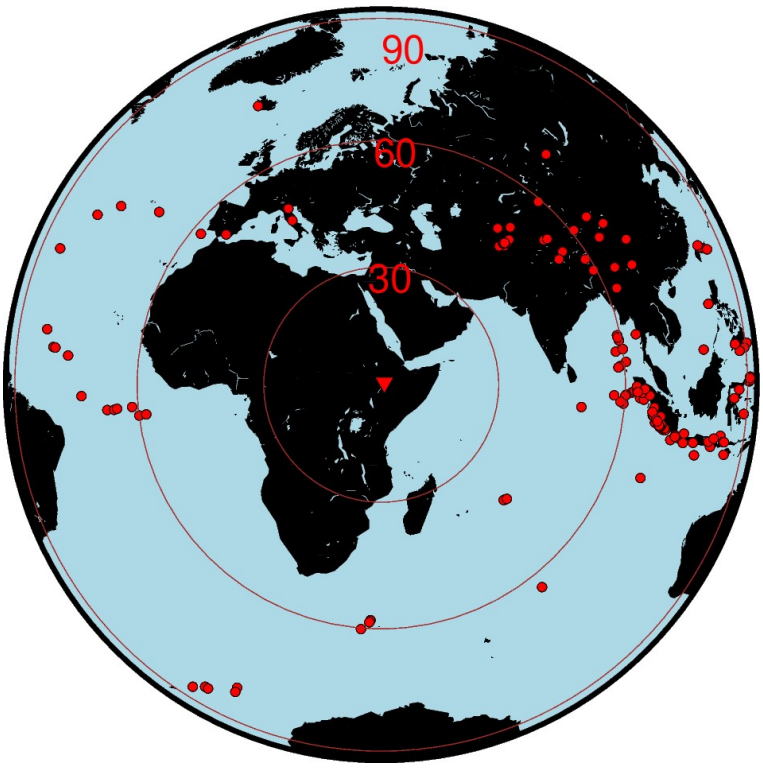

Figure 2.1: The red dots are teleseismic earthquakes used to perform the investigation carried out. Positioned at the focal point of the circles are our study areas, denoted by the red inverted triangle. The three concentric circles emanating from the red triangle describes distance from stations. These circles, delineating distances of 30°, 60°, and 90° respectively, allowed us to precisely define the range of earthquakes included in our analysis.

2.1.3 Distribution of stations

The survey areas encompass diverse regions, including the Afar depression, the Ethiopian plateaus, NMER, CMER, and SMER (Corti, 2008, 2009; Corti et al., 2020, 2013). These areas were selected to thoroughly investigate the NE African region's crustal structure, with

each representing unique geological and tectonic settings that offer valuable insights into regional dynamics. However, it is important to note that seismic station distribution within these survey areas is non-uniform. This variation arises from different projects conducted for specific purposes, resulting in variations in station density. In our study, we focused on data from the RiftVolc project, which employed a denser network of seismic stations compared to others (Chambers et al., 2019; Greenfield et al., 2019a). This increased station density allowed for a more detailed examination of seismic activity and crustal structure within the RiftVolc-covered region. By acknowledging the heterogeneous station distribution, we can effectively interpret data and results, while also accounting for potential biases and limitations associated with variations in station density. Consequently, our study ensures a comprehensive analysis while accommodating the diverse characteristics of seismic data acquired from different projects within the NEARS.

2.1.4 Instruments used

During the data acquisition phase, a diverse range of instruments was employed to capture seismic data with precision and accuracy. The instruments utilized included Guralp CMG-3T, CMG-ESP, and CMG-40T seismometers, each designed with specific natural periods of 120 s, 60 s, and 30 s, respectively (Hammond et al., 2011). These seismometers were carefully selected for their ability to capture a broad frequency range of seismic waves, enabling a comprehensive understanding of the subsurface dynamics. To supplement the seismic network, the STS-2 sensor was strategically placed at the RAND station. The STS-2 sensor offered exceptional sensitivity and stability, allowing for the collection of high-resolution seismic data at a sampling rate of 50 Hz. Its deployment at the RAND station enhanced the coverage and accuracy of the data acquisition process, particularly in capturing seismic events within a specific range of epicentral distances.

In this study, we employed the RiftVolc temporary network project, which was conducted between February 2016 and October 2017. For data acquisition, we deployed three-component broadband Guralp CMG-6TD and Guralp CMG-ESPCD seismometers, operating at a sampling rate of 50 Hz. These seismometers were specifically selected for their enhanced sensitivity and capability to record a broad frequency range, enabling us to conduct detailed monitoring of seismic activity and crustal dynamics within our study region. To facilitate comprehensive analysis, we acquired the teleseismic waveform data (Figure 3.2) and instrument responses from the RiftVolc project by downloading them from the IDMC. This approach ensured standardized data access and provided us with the opportunity to perform accurate calibration and preprocessing of the recorded seismic data.

2.1.5 Data Selection Criteria

In this study, we implemented rigorous criteria to meticulously select data of high quality and reliability. Specifically, we focused on teleseismic events surpassing a magnitude threshold (Mb) of 6.0 and occurring at epicentral distances spanning from 30° to 90° (Ammon, 1991; Dugda and Nyblade, 2006; Langston, 1979). By concentrating on teleseismic events with substantial magnitudes and appropriate epicentral distances, we aimed to capture seismic signals of significant amplitude and propagation characteristics conducive to in-depth investigation. All earthquake events utilized in this study were sourced from the esteemed IRIS Data Management Center (IDMC). Known for its comprehensive and dependable earthquake data, the IDMC served as the principal data repository, granting us access to a wide array of seismic events from diverse regions worldwide. Our reliance on the IDMC ensured the data integrity of our study and facilitated consistency in the comparison and analysis of seismic events across different projects and regions.

2.1.6 Preprocessing Raw Data

During the data preprocessing phase of this study, we implemented meticulous measures to ensure the integrity and reliability of the seismic data. We began by subjecting the initial raw data, as illustrated in Figure 2.2, to a comprehensive procedure aimed at removing environmental and instrumental influences, such as atmospheric pressure fluctuations, drift, and artifacts in the instrument response. Subsequently, we applied meticulous filtering techniques to isolate the desired frequency range, typically between 0.01 and 1 Hz.

For the processing of data for RF analysis, we utilized the widely used SAC format in conjunction with Generic Seismic Application Computing (GSAC) in the CPS software (Herrmann, 2013; Herrmann and Ammon, 2002). To ensure smoothness and minimize sudden signal variations, we applied a cosine taper function to the P-waveform signal over a 50-second duration, encompassing 10 seconds prior to and 40 seconds after the initiation of the P-wave arrival. This tapering approach effectively reduced the potential for distortions in subsequent analysis.

To address the impact of low-frequency noise on the RFs, we employed a Butterworth bandpass (BF) filter to filter all the signals. The parameters of the BF filter were set between 0.01 and 5 Hz, effectively removing undesired low-frequency noise while maintaining the stability of the RFs (e.g., Kibret et al., 2022). This filtering step played a crucial role in ensuring accurate and reliable outcomes, while also preventing aliasing when downsampling the data.

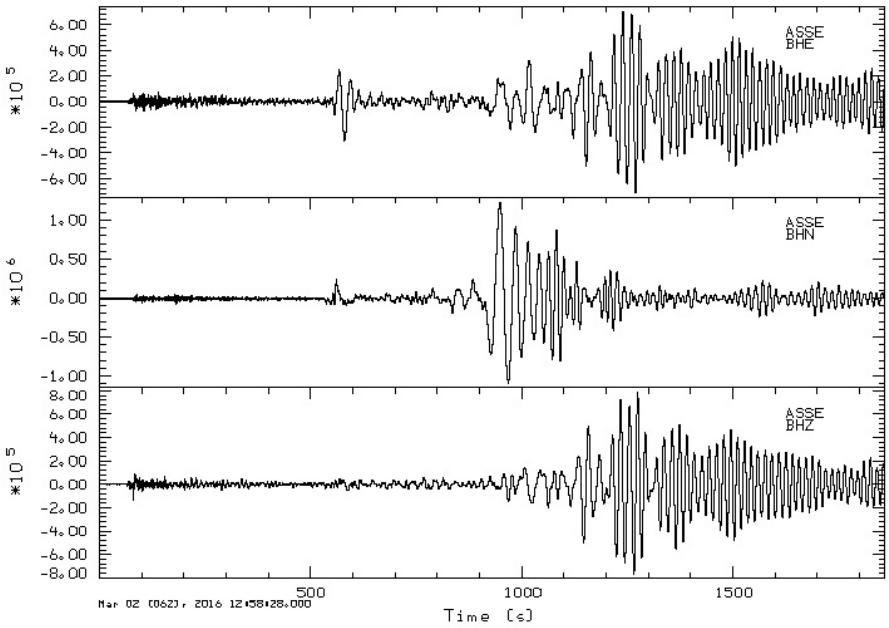

Figure 2.2: The figure presented here displays a representative example of raw teleseismic earthquakes that were recorded at the ALE station on March 5, 2002. These earthquakes had a moment magnitude (Mw) of approximately 7.5 and occurred at epicentral distances ranging from 30 to 90 degrees.

In this study, we employed stringent measures to ensure the quality and reliability of the acquired seismic data. Specifically, each three-component signal was meticulously inspected to identify and eliminate signals with low SNR. Additionally, any signals displaying improper recording in any of the three components due to instrument malfunction were excluded from the analysis. This quality control procedure aimed to ensure that only high-quality data were considered for subsequent analysis.

Regarding the software utilized for data processing, The work employed computer program in Seismology developed by Herrmann and Ammon (2002). This software facilitated a range of preprocessing steps and corrections to enhance the robustness and reliability of the data formatted in SAC. These steps included removing long-term variations through trend removal, smoothing the signal through tapering, and eliminating the average value of the signal through mean removal. Furthermore, the instrumental frequency response was corrected by implementing a pole-zero function, preserving the amplitude and phase characteristics of the recorded waveform.

In order to focus our analysis on the relevant time window, the present investigation truncated the three-component seismograms using a time extending from 10 seconds prior to the P-wave arrivals to 40 seconds after. This time window encompassed the essential seis-

mic phases necessary for receiver function analysis. To ensure further data quality, we employed a Gaussian parameter (Figure 2.6) (Owens, 1985) of 1.0 and a water level of 0.01 when computing all RFs. These parameters contributed to optimizing the computation process and ensuring reliable results, aligning with established practices in the field (Langston, 1979; Dugda et al., 2007).

Data Quality Control

In this study, we implemented data quality control procedures to ensure the selection of high-quality seismic traces for analysis. We employed several crucial steps to assess the reliability and integrity of the data, ultimately enhancing the accuracy and robustness of our study results. One essential criterion we considered during data quality control was the assessment of the signal-to-noise ratio (SNR) of the seismic traces (Dugda and Nyblade, 2006; Hammond et al., 2011). Higher SNR values indicate a stronger and more reliable signal compared to the background noise (Zhu and Kanamori, 2000). Seismic traces with low SNR are prone to distortions and uncertainties, which can compromise the accuracy of our subsequent analyses. Therefore, we excluded traces with low SNR values from further analysis to maintain the quality and reliability of our data.

Another critical factor in our selection process of quality data was ensuring the proper recording of all three components of the seismic signal. Seismic stations typically record three components: vertical (Z), north-south (N-S), and east-west (E-W). Each component provides unique information about the propagation of seismic waves. However, issues such as instrument malfunction or other factors may result in incomplete or improper recording of one or more components. To ensure the integrity of our data, we excluded traces with incomplete or improper recording of any component from our analysis.

Furthermore, we considered the magnitude and distance range of the recorded seismic events in our data quality control procedures. Higher magnitude events generally produce stronger signals that are easier to analyse accurately. Similarly, events within an optimal distance range from the recording station provide better resolution of the subsurface structures. Therefore, we excluded seismic traces associated with events falling outside the predetermined magnitude and distance ranges to ensure the overall quality and reliability of our dataset.

2.2 Method

In this study, the receiver function (RF) technique was employed to characterize the crustal structure, Moho depth, and subsurface lithology and composition. The methodology followed a step-wise approach, where each result served as input for the subsequent step, ensuring a coherent and systematic workflow. The entire analysis was conducted using the computer program in seismology (CPS) software (Herrmann, 2013). The sequential steps included:

1. Source equalization was utilized to ensure consistency (Ligorria and Ammon, 1999).
2. Rotation of N-S to R-T components was performed for data preparation.
3. Deconvolution was conducted to generate radial (Figure 2.5) and transversal RFs (Ammon, 1991; Langston, 1979).
4. Iterative inversion was employed to identify depth interfaces with P-to-S wave conversion.

The advantages of RF application were elucidated through thorough validation and quality control procedures. The quantification of result uncertainties through statistical analysis strengthened the reliability of the findings. The utilization of advanced tools, such as CPS software, facilitated efficient data processing and analysis (Herrmann, 2013). Ethical considerations were upheld throughout the study, including permissions, data protection, and the acknowledgement of contributions from other researchers and institutions.

When seismic waveforms encountered interfaces with dissimilar acoustic properties, the reflection of energy and transmission into the underlying layer occurred. This conversion of P-to-S waves enables the detection and analysis of subsurface boundaries (Ammon, 1991; Hammond et al., 2011; Keranen et al., 2009; Langston, 1979). The selection of inversion method incorporated within the Computer Program for Seismology (CPS) was based on its adaptability and simplicity. This approach facilitated the estimation of crustal structure through the inversion of observed RFs and the calculation of synthetic receiver functions (SRFs) (Figure 2.7) Herrmann (2013).

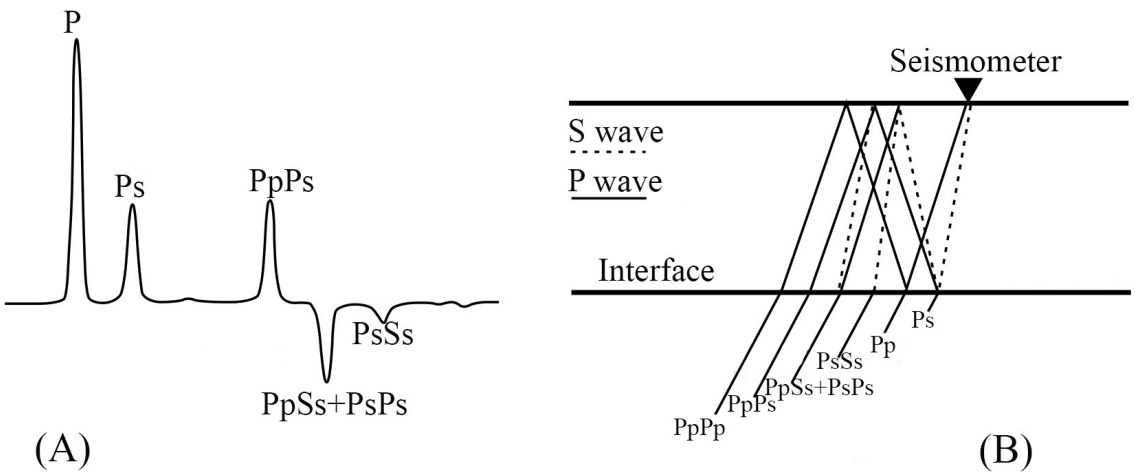

Figure 2.3: The formation of a radial receiver function through a single layer positioned above a half space. (A) P shows the direct P wave. Ps indicates the converted wave from the direct P- to -S wave. The other converted waveforms are the reverberations. (B) The Model which indicates the wave conversions when the P wave interacts with an interface, it can convert to S wave and/or to other forms of waves. The PpPp, PpPs and PpSs+PsPs are reverberations (modified from Ammon et al., 1990; Ligorria and Ammon, 1999).

The terminology employed to distinguish between the arrivals in RRF data encompasses the direct P-wave arrival (P), the P-to-S converted wave (Ps), and multiples of both waves (such as PpSs and PsPs) (Figure 2.3). The alphabetical letters in the nomenclature serve to identify the wave mode (P or S) and the path that the wave takes (direct or converted) (Ammon et al., 1990; Julia et al., 2000).

2.2.1 Source equalization approach

When a seismic event occurs, it generates waves that propagate through the Earth's subsurface. These waves can be decomposed into different components based on their particle motion: radial, transverse, and vertical (Ammon, 1991; Stuart et al., 2006). The radial (R) component is the motion along radial direction from the source to the receiver, transverse (T) component is the motion perpendicular to the radial direction, and the vertical component is the motion in the vertical direction. The source equalization approach (Ammon, 1991; Ligorria and Ammon, 1999) is a method used to calculate radial receiver function (RRF) and transverse receiver function (TRF) (Dugda and Nyblade, 2006; Stuart et al., 2006).

To calculate RRF and TRF, it is necessary to consider the contribution of both R and T components. However, the recorded seismograms are often dominated by the R component due to the seismic source radiation pattern. This dominance can lead to an imbalance in the

amplitudes of RRF and TRF (Dugda et al., 2005; Liu and Niu, 2012; Zhu and Kanamori, 2000). The source equalization approach for RF analysis involves mathematically equalizing the source term in the recorded seismic waveforms to improve the estimation of RFs. The goal is to remove or reduce the effects of source signature from the recorded data. By dividing the recorded R and T components by the source radiation pattern, the RFs are "equalized" and provide a more accurate representation of the subsurface structure.

The source equalization approach is used to calculate the radial and transverse RFs. Equation 2.6 presents the expression for the deconvolved radial earth response ($Erth_R$) in the frequency domain. It involves dividing the Fourier transform of the radial receiver function (Figure 2.3) by the Fourier transform of the vertical seismogram and multiplying it by the complex conjugate of the vertical seismogram's Fourier transform. The autocorrelation of the vertical seismogram ($AutCor_{SS}$) is used to scale the denominator, and a Gaussian function (G) (Figure 2.6) is applied as a filter to attenuate high-frequency noise (Kikuchi and Kanamori, 1982).

The source equalization approach is important in RF analysis as it helps to improve the quality and reliability of the calculated RFs. It ensures that the radial and transverse components are appropriately balanced, allowing for a better understanding of the subsurface seismic properties and wave conversion processes.

2.2.2 Rotation of N-S to R-T components

The rotation of north (N) and south (S) seismic wave components to radial (R) and transverse (T) components is an important step in RFs study. When seismic waves propagate through the Earth, they generate vibrations in all directions, which are recorded by seismometers in three different components: north-south (N), east-west (E), and vertical (Z). However, to analyse the seismic wave and the Earth's structure more effectively, it is often necessary to convert these three components into two other components that are aligned with the direction of wave propagation (Ammon, 1991; Langston, 1979).

The first step in this conversion process is to rotate the north-south (N) and east-west (E) components around the vertical (Z) axis to obtain the radial (R) and tangential (T) components (Figure 2.4). The R component is parallel to the direction of the incoming wave and contains all the P-to-SV converted energy, assuming a one-dimensional (1D) Earth model. Any energy that remains on the T component after this rotation will be due to horizontally-polarized SH waves, which arise from structures and/or anisotropy beneath the station (Ligorria and Ammon, 1999).

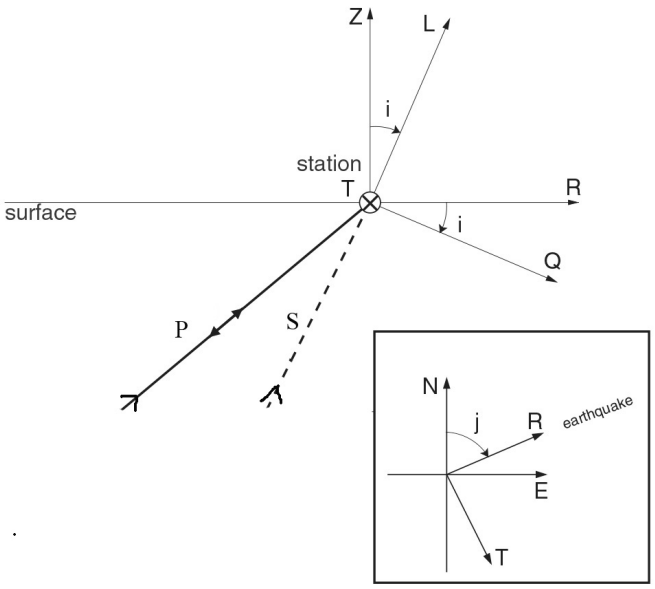

Figure 2.4: The diagram shows two horizontal components: N (North) and E (East). The component labelled "R" points to the earthquake's epicentre, while "T" is perpendicular to R. Angle "j" represents the back azimuth, and "i" is the angle of incidence for the S wave. The ZR system is transformed into the LQ system by rotating around angle "i." In the LQ system, the particle motion of the S wave is perpendicular to the L direction, while the Sp converted waves are polarized roughly along the L direction (modified from Kind et al., 2012).

2.2.3 Deconvolution

Deconvolution technique was initially introduced by Clayton and Wiggins (1976) and later refined by Owens et al. (1984) and Ammon et al. (1990). It is a critical process in seismic analysis, aiming to remove unwanted effects, such as contributions from seismic sources and propagation paths, from recorded seismic signals. By doing so, deconvolution allows for the isolation and study of specific characteristics of the Earth's subsurface structure without interference from these undesired components. The deconvolution process involves recognizing that the recorded seismic signal is the result of convolving the source wavelet (the seismic wave generated by an earthquake or other energy source) with the impulse response of the Earth's subsurface and recording instruments. The impulse response captures the combined effects of the seismic wave propagating through different layers of the Earth and instruments' response to these waves.

To eliminate the effects of the source wavelet and propagation paths, deconvolution (Figure 2.5) employs the concept of inverse filtering. This is achieved by dividing the recorded

seismic signal by the estimated source wavelet, which can be determined through various methods, such as the deconvolution process. To mitigate challenges due to noise, measurement errors, and uncertainties in estimating the source wavelet, we have applied the WLD algorithms (e.g., Langston, 1979; Owens and Zandt, 1985) (Figure 2.5). It involves dividing the vertical component of the seismogram by radial or transverse components, depending on the desired receiver function type.

Displacement response

In the realm of RF teleseismic waveforms, signals (ranging from 30^o to 95^o) that are captured on a three-component seismometer are used to eliminate the effects of source and propagation path (Figure 3.2). As per Langston (1979), the receiver function is obtained through the deconvolution of vertical waveform from one of the horizontal seismograms (Figure 2.5) (Last et al., 1997). In the time domain, the theoretical displacement response of a P-wave that strikes an under-horizontal interface can be presented as:

$$Disp_V(t) = Inst(t) * Srs(t) * Erth_V(t) \tag{2.1}$$

$$Disp_R(t) = Inst(t) * Srs(t) * Erth_R(t) \tag{2.2}$$

$$Disp_T(t) = Inst(t) * Srs(t) * Erth_T(t) \tag{2.3}$$

Equation 2.1 describes the vertical displacement response $Disp_V(t)$ as a convolution of the seismic source wavelet $Srs(t)$, the instrument response $Inst(t)$, and the vertical earth response $Erth_V(t)$. Similarly, Equation 2.2 describes the radial displacement response $Disp_R(t)$ and Equation 2.3 describes the transverse displacement response $Disp_T(t)$ (Langston, 1979).

If we assume that the Z component of the ground motion shows negligible conversion and reverberation energy of the seismic wave, it can be approximated as:

$$Disp_V(t) = Inst(t) * Srs(t) \tag{2.4}$$

Equation 2.4 simplifies the vertical displacement response to a convolution of only the seismic source wavelet and the instrument response, since the vertical earth response is assumed to be negligible. The deconvolution process is described using equations 2.1, 2.2, and 2.3, which represent the convolution of the seismic source wavelet, the instrument response, and the earth response for the vertical ($Disp_V$), radial ($Disp_R$), and transverse

($Disp_T$) displacement components, respectively. Equation 2.4 simplifies the vertical response to a convolution of the seismic source wavelet and the instrument response, assuming negligible vertical earth response (Cassidy, 1992).

Gaussian filter (GF)

While we apply deconvolution in our RFs analysis, we used a Gaussian filter (GF). The primary purpose of the Gaussian filter (Figure 2.6) in this context is to enhance the signal-to-noise ratio and improve the quality of RFs (Langston, 1979). The GF is a smoothing filter that modifies the frequency content of the signal by attenuating high-frequency noise while preserving the lower-frequency components. Overall, the application of a Gaussian filter in the deconvolution step of receiver function analysis helps to improve the signal quality, reduce noise interference, and enhance the visibility of important features like the P-to-S converted wave. It is a common technique employed to enhance the interpretability and accuracy of our receiver function results.

However, it is essential for us to eliminate instrument response to obtain an accurate representation of the ground motion. Assuming matched instrument responses between components, the deconvolution of $Inst(t) * Srs(t)$ from $Disp_R(t)$ and $Disp_T(t)$ will result in the discovery of $Erth_s(t)$ and $Erth_r(t)$. This process can be described in the frequency domain by Equation 2.5 (Langston, 1979):

$$\begin{aligned} Erth_R(\omega) &= \frac{Disp_R(\omega)}{Inst(\omega)Srs(\omega)} \approx \frac{Disp_R(\omega)}{Disp_V(\omega)} \\ Erth_T(\omega) &= \frac{Disp_T(\omega)}{Inst(\omega)Srs(\omega)} \approx \frac{Disp_T(\omega)}{Disp_V(\omega)} \end{aligned} \tag{2.5}$$

Equation 2.5 explains how to obtain the radial $Erth_R(\omega)$ and transverse $Erth_T(\omega)$ earth responses from the recorded radial $Disp_R(\omega)$ and transverse $Disp_T(\omega)$ displacement responses in the frequency domain. The approximations are based on the assumption that the seismic source wavelet and instrument response are matched between components and that the vertical displacement response $Disp_V(\omega)$ dominates over the radial and transverse displacement responses.

The source equalization approach (Ammon, 1991; Ammon et al., 1990; Dugda et al., 2005; Langston, 1979) is employed to calculate the RRF and TRF. In this method, the radial $Disp_R(\omega)$ and tangential component (Figure 2.4) $Disp_T(\omega)$ receiver

$$Erth_R(\omega) = \frac{Disp_R(\omega) Disp_V^*(\omega)}{AutCor_{SS}(\omega)} . G(\omega) \tag{2.6}$$

The above equation is the expression for deconvolved radial earth response $Erth_R(\omega)$ in the frequency domain, which is obtained by dividing the Fourier transform of the radial receiver function $Disp_R(\omega)$ by the Fourier transform of the vertical seismogram $Disp_V(\omega)$, and multiplying by the complex conjugate of the Fourier transform of the vertical seismogram $Disp_V^*(\omega)$. The function $AutCor_{SS}(\omega)$ is the autocorrelation of a vertical seismogram $Disp_V(\omega)$, which is defined as:

$$AutCor_{SS}(\omega) = \max Disp_V(\omega)\overline{Disp}_V(\omega), c \cdot \max[Disp_V(\omega)\overline{Disp}_V(\omega)] \tag{2.7}$$

Here, The bar over $\overline{Disp}_V(\omega)$ shows the complex conjugate (Langston, 1979). The resulting product's maximum value across all frequencies is scaled by a fraction c. The water level parameter, c is determined through trial and error, is typically used to attenuate frequencies where the vertical component's amplitude is small by using a larger denominator in the spectral division. To filter out high-frequency noise that may have been introduced during the deconvolution process, a Gaussian function called GF_ω is applied (Figure 2.6).

$$GF_\omega = e^{\frac{-\omega^2}{4\alpha^2}} \tag{2.8}$$

where α is a parameter that determines bandwidth of the filter (as shown in Figure 2.5). After obtaining the deconvolved radial earth response $Erth_R(\omega)$, the next step is to apply a Gaussian filter to limit the final frequency band and filter out high-frequency noise, which can be caused by noise in the data or by inaccuracies in the deconvolution process. The choice of α depends on the specific characteristics of data and the desired bandwidth of the final result. Once the Gaussian filter is applied, the resulting estimate can be considered the radial component of the seismic wavefield (Langston, 1979).

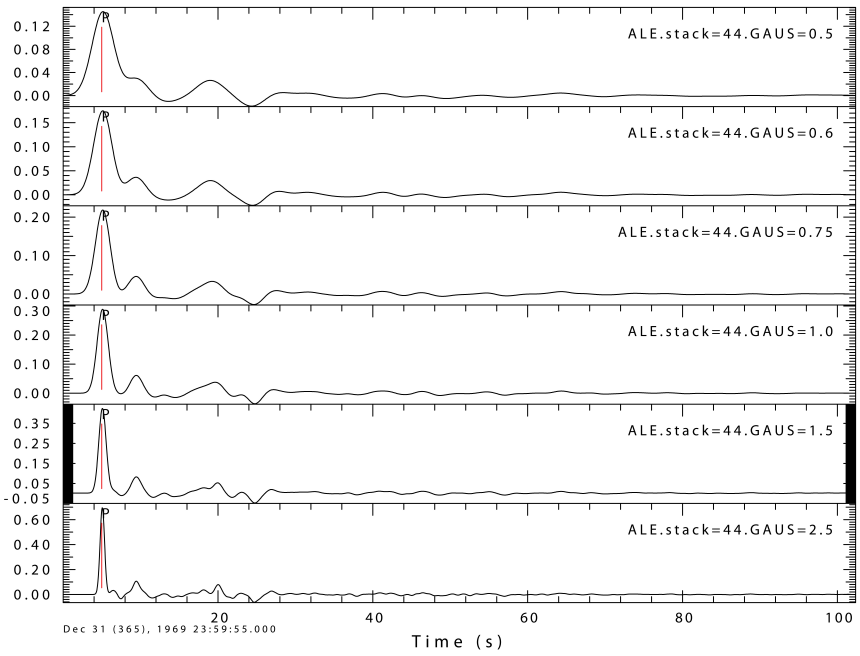

Figure 2.5: RFs is acquired by deconvolving the vertical from horizontal component using various Gaussian parameters that includes 0.5, 0.6, 0.75, 1.0, 1.5, and 2.5.

Overall, deconvolution plays a crucial role in RF analysis as it allows for the extraction of RFs that reveal important information about the Earth's subsurface structure and composition. By removing effects of the seismic source and instrument response, seismologists can obtain more accurate representations of the ground motion and identify seismic wave conversions and boundaries between different layers of the Earth.

Stacking

In this study, we utilized the technique of receiver function stacking, which proved to be a valuable approach in seismology. It involved combining multiple RFs from different seismic events to create a single representative receiver function (Figure 2.5) (Ammon et al., 1990; Kibret et al., 2023; Owens and Zandt, 1985; Reed et al., 2014). The major procedure of RF stacking entailed the amalgamation of multiple RFs having similar features to improve the signal-to-noise ratio and mitigate the effects of local scattering (Ayele et al., 2004; Julia et al., 2000; Liu and Niu, 2012). Typically, we identified a cluster of seismic events with comparable properties, such as back azimuth and slowness for the corresponding RFs. Subsequently, these RFs were aligned in time and superimposed to create a composite waveform having a heightened signal-to-noise ratio.

Fundamentally, RF stacking helped us fortify signals originating from the Earth's interior

that might be too feeble to identify in isolated RFs. Furthermore, stacking RFs could homogenize disparities in arrival amplitude owing to minor changes in slowness, leading to a more accurate analysis (Julia et al., 2000; Ligorria and Ammon, 1999). In this study, we also applied the process of stacking to improve the quality of the RFs obtained from individual events (Liu and Niu, 2012). By combining multiple RFs into a single estimate, we were able to enhance the signal-to-noise ratio and highlight the features of interest (Last et al., 1997). The stacked RFs were then analysed to determine various properties of the subsurface structure, including the depth and velocity (Figure 2.9) of discontinuities. This analysis was accomplished using various techniques, such as waveform inversion, which allowed us to estimate the model parameters that best fit the stacked RF. Overall, the stacking process played a critical role in improving the quality of our RFs and allowed us to draw more accurate inferences about the subsurface structure (e.g., Owens and Zandt, 1985; Reed et al., 2014).

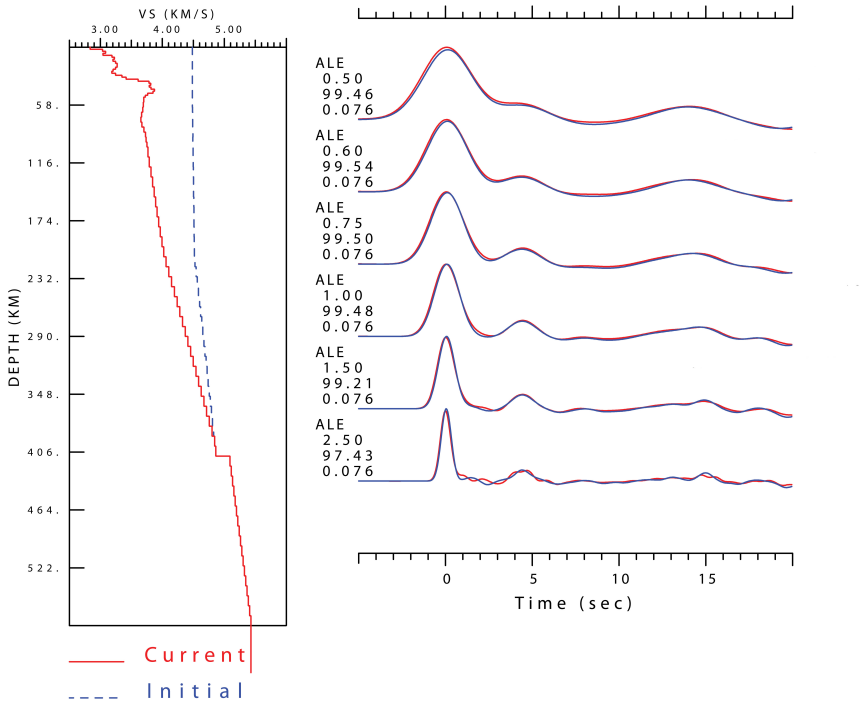

Figure 2.6: The stacked RFs and the corresponding fit synthetic RFs. The deconvolution is done for different Gaussian parameters which are 0.5,0.6,0.75,1.0,1.5 and 2.5.

2.2.4 Receiver Functions

While investigating crustal structures using seismic waveforms to obtain pertinent subsurface information, we implemented the widely employed receiver function (RF) (Figure 2.3) analysis stages. The implementation of RF, a widely employed method in seismology, al-

lowed us to scrutinize alterations in acoustic impedance beneath seismic stations deployed in Ethiopia. Seismometers recorded the seismic waveforms generated by a source at varying distances and azimuths (e.g., Eckhardt and Rabbel, 2011). By employing the transformation of P-to-S waves, we gained valuable insights into the different structures of the Earth's crust, mantle, and the underlying tectonic processes Ammon (1991); Cornwell et al. (2010); Langston (1979); Zhu and Kanamori (2000).

Once we calculate the RFs, we normalize them by dividing each frequency component of the receiver function by the amplitude of the corresponding frequency component in the input seismogram. This normalization process is carried out to eliminate the effects of the source and propagation path, allowing us to isolate the response of the Earth's structure (e.g., Owens and Zandt, 1985).

In the RFs data, we typically observe a direct P-wave arrival, followed by the P-to-S converted wave (Ps), and a sequence of reverberations. The arrival time and amplitude of the Ps wave provide us with valuable information about the thickness and properties of the underlying layer (Ammon et al., 1990; Langston, 1979; Ligorria and Ammon, 1999). By analysing the differences in arrival times and amplitudes of the seismic waves at different seismometers, we can infer boundaries between contrasting layers of the Earth's crust and mantle (Dugda and Nyblade, 2006; Hammond et al., 2011; Keranen et al., 2009).

Radial RFs

The radial receiver function (RRF) technique, as applied in this study (Dugda et al., 2007), focuses on analysing seismic waves that propagate through the Earth's crust and undergo reflection and conversion at interfaces between layers with different acoustic properties (Figure 2.3) (Ammon et al., 1990; Gurrola et al., 1995; Langston, 1979). The main emphasis is on the P-to-S conversions, where compressional waves (P-waves) transform into shear waves (S-waves) upon reflection at these interfaces (e.g., Reed et al., 2014).

In the process of RRF modelling, we begin by generating seismic waves from a source, which then propagate through the Earth's subsurface and are recorded by seismometers at varying distances and azimuths from the source. We analyse the recorded seismic waveforms to infer information about the structure and composition of the Earth's subsurface. To obtain the radial (R) as shown in Figure 2.7 and tangential component (T) of the seismic waves in RRF modelling, we rotate the north-south (N) and east-west (E) components. The R component aligns with the direction of the incoming wave and the P-to-S converted energy, while the T component comprises horizontally-polarized SH waves (Eckhardt and

Rabbel, 2011).

The Synthetic RFs

Each time iteratively we calculated the SRFs by applying Green's function for a chosen seismic VM and source time function (e.g., Aki and Richards, 2002). Once the Green's function is calculated, it is applied to calculate the SRFs by convolving it with the assumed source time function. As the inversion progresses, the VM (Figure 2.8) is continuously updated to improve the fit between ORFs and SRFs (Figure 2.7). This iterative cycle continues until a satisfactory match between the ORFs and SRFs is achieved or convergence criteria are met. The result is SRF, which can be compared to the ORF to estimate properties of Earth's interior. The resulting 1D Vs structure provides insights into the seismic wave velocities at different depths, allowing for a better understanding of the subsurface geology and tectonic processes.

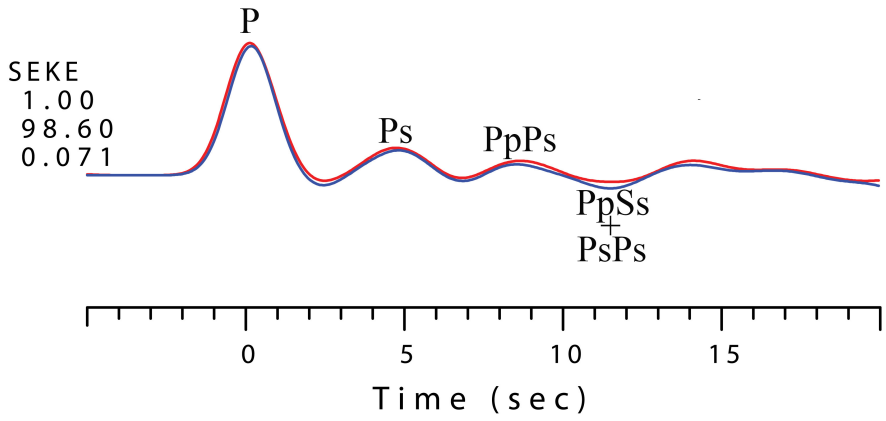

Figure 2.7: The SEKE station SRF and ORF model. In this model, the red-coloured RFs are the observed signals, whereas the blue colour shows the synthetic ones. The P is the direct seismic wave and the Ps is the inverted wave from direct P to S wave. The other conversions PpPs and the PpPs + PsPs are the reverberations

2.2.5 P-to-S wave conversion

When a direct P-wave encounters a layered interface with different properties, it exhibits conversions and reverberations that provide valuable information about subsurface structures. The key features involved in this process include the direct P-wave arrival, P-to-S converted wave (Ps), and reverberations (Ammon, 1991; Ammon et al., 1990; Dugda and Nyblade, 2006; Hammond, 2014; Langston, 1979; Owens and Zandt, 1985). The direct P-wave arrival is the first seismic wave to reach a receiver after being generated by a seismic source. P-waves are compressional waves that travel through the subsurface, and they

are the fastest seismic waves. They propagate by compressing and expanding the material they pass through. In seismic data, the direct P-wave arrival appears as the initial high-amplitude, short-duration wavelet (Ammon et al., 1990; Hammond, 2014). It carries information about the travel time and amplitude of the wave, which can be used to infer the depth and properties of the layered interface.

When P-waves encounter a subsurface boundary between two layers with different elastic properties, some of the energy can be converted into shear waves called S-waves (Ps). P-to-S converted waves (Ps) occur when a portion of the P-wave energy is transformed into a shear motion of the S-wave at the layered interface. The Ps waves travel slower than P-waves and have different polarization (e.g., Hammond, 2014). These conversions are significant as they allow us to detect and analyse the boundaries between different layers in the Earth's crust and mantle. By studying the timing and amplitude of the Ps arrivals, we can gain insights into the thickness, properties, and composition of the subsurface layers.

Reverberations in seismic data are multiple reflections of seismic waves that occur between subsurface interfaces. When a seismic wave encounters a reflector, part of the energy is reflected back towards the surface, while the remaining energy continues to propagate deeper. The reflected energy can then encounter another reflector and be reflected again, creating a series of reflections that can bounce back and forth between subsurface interfaces (Ammon, 1991; Ammon et al., 1990; Dugda and Nyblade, 2006; Dugda et al., 2005; Hammond, 2014; Langston, 1979; Owens and Zandt, 1985). Reverberations are secondary waves that occur due to multiple reflections and scattering within the layered structure (Dugda and Nyblade, 2006; Hammond, 2014). They result in a series of wave arrivals with decreasing amplitude and increasing travel time. Analysing the characteristics of reverberations helps in identifying layer boundaries and understanding the overall structure of the subsurface. The identification of layers, as well as the determination of Moho (the boundary between the crust and mantle), are crucial outcomes of studying seismic wave conversions at layer boundaries. These conversions provide valuable information for characterizing the crustal structure and gaining insights into the subsurface composition and properties (Dugda and Nyblade, 2006; Dugda et al., 2005; Hammond, 2014; Keranen et al., 2009; Kibret et al., 2022).

2.2.6 Iterative Inversion

The RFs were computed using the time domain iterative deconvolution method proposed by Ligorria and Ammon (1999). We performed an iterative inversion of the Earth's crustal

structure velocity (Figure 2.9) based on the corresponding SRFs (Figure 2.7) to estimate the seismic properties at discontinuities. The iterative inversion process entailed comparing the ORFs with a set of initial seismic parameters (e.g., Dugda et al., 2007).

The ak135 initial model

In our calculation of RFs, we utilize the ak135 initial velocity model (Figure 2.8) (aIVM) as a reference model to determine the seismic properties of the discontinuity, including the depth and velocity of the layers above and below it. The ak135 model (Kennett et al., 1995) is a widely accepted global reference model that provides a representative distribution of shear wave velocities (Vs) worldwide (see Figure 2.8 for the start.mod representation).

Once we calculate the RFs, the next step in our inversion process involves estimating the one-dimensional (1D) Vs structure of the Earth's crust and upper mantle. This process, known as inversion, entails iteratively adjusting the parameters of the velocity model (VM) to find the best-fitting model that reproduces the observed RFs (Figure 2.8) (Hammond et al., 2011). Initially, we assume the ak135 initial velocity model (aIVM), which is represented as a series of velocity-depth layers. We then compute the RFs using this initial model (Kibret et al., 2022, 2023).

During the inversion process, the present investigation compare the observed RFs to the synthetic RFs (Figure 2.7) generated from the aIVM. We calculate a misfit function to quantify the difference between the observed RFs (ORFs) and the synthetic RFs (SRFs) (Figure 2.7). We can use various measures, such as the root mean square (RMS) difference or a weighted sum of differences at individual time points, to define the misfit function (Julia et al., 2000; Ligorria and Ammon, 1999).

We adjust the VM parameters based on the calculated misfit (Figure 2.8). This adjustment usually involves perturbing the velocity values in our model. Our objective is to minimize the misfit by iteratively refining the VM (Ligorria and Ammon, 1999). We repeat the process, generating new SRFs using the updated VM, and recalculating the misfit function (Kibret et al., 2019) until the best fit model is achieved.

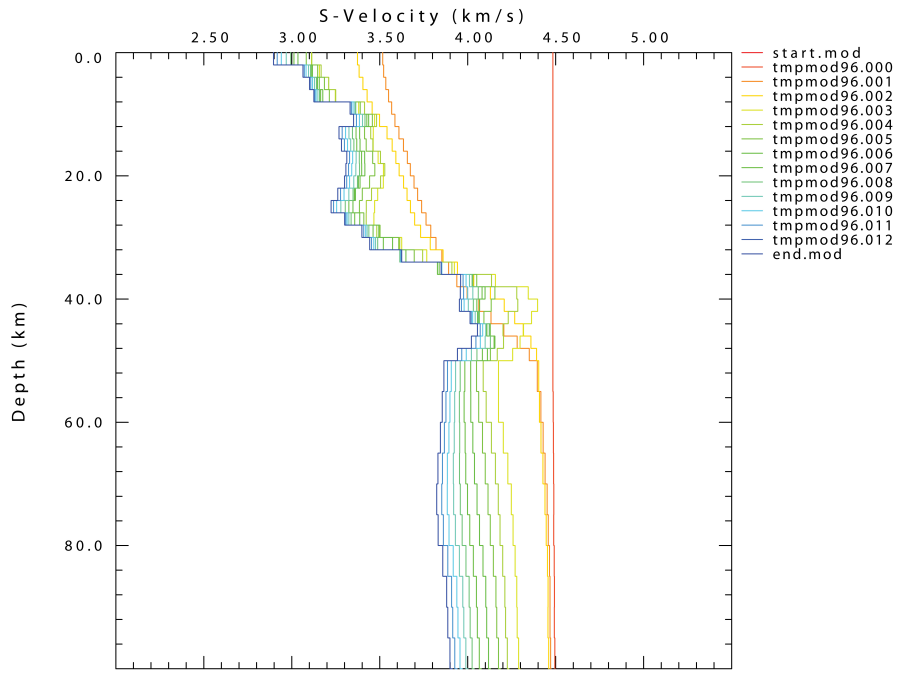

Figure 2.8: The VM calculated from the synthetics receiver function. The red line (start.mod) is the initial VM and the remaining models are calculated from the iteration started from the aIVM by generating the corresponding RF and checking fit of ORFs and SRFs. When the two RFs are matched the iteration halts.

The misfit calculation

In our study, we regarded the misfit value as a crucial indicator of accuracy in the RF calculation. Agreement degree of ORF with SRF was evaluated by quantifying the misfit, typically through statistical measures like root mean square error. A low misfit value indicated a satisfactory fit between the two functions, while a high misfit value indicated a less optimal agreement. This value was thus utilized to determine the accuracy of receiver function and was employed to guide the iterative inversion process for adjusting the model parameters and enhancing the fit (e.g., Kikuchi and Kanamori, 1982; Ligorria and Ammon, 1999).

In this study, we utilized the NLLS method to update the seismic parameters of the model based on the difference between the SRFs and ORFs. This approach involves iteratively adjusting the model parameters to minimize the misfit between two functions, by estimating the optimal parameters that result in the best fit (Ligorria and Ammon, 1999). The nonlinear least squares (NLLS) method is a widely-used approach for solving non-linear optimization problems, and is particularly suitable for problems with non-linear constraints and complex parameter spaces. By employing this method, we were able to improve the accuracy of the

receiver function and refine the seismic properties of the discontinuity, including the depth, velocity, and density of the layers above and below it.

Predicting Vs

In our study, we employ an iterative process to predict the Vs values at each 2 km depth. This is achieved using the nonlinear least squares misfit method (NLLS) (Dugda et al., 2007, 2005). The NLLS method allows us to adjust the model parameters iteratively, minimizing the misfit between ORFs and SRFs. The goal is to find the optimal parameters that provide the best fit (Ammon et al., 1990; Dugda and Nyblade, 2006; Dugda et al., 2007).

Through this iterative inversion, we update the seismic parameters of the model based on the difference between ORFs and SRFs. This process enhances the precision of our RF analysis, leading to a more accurate estimation of critical seismic properties, such as the depth and velocity (Dugda and Nyblade, 2006; Dugda et al., 2007; Keranen et al., 2009; Kibret et al., 2022) of subsurface layers. These refined seismic parameters are then used to improve the fidelity of Earth's response to seismic sources.

The inversion process is repeated until the disparity between the ORFs and SRFs is minimized (Dugda et al., 2007). Once this iterative procedure is completed, we obtain an appropriate model that allows us to compute various physical characteristics of the discontinuity, such as its thickness and shear wave velocity. This model facilitates the inference of valuable information regarding the structure and composition of the Earth's crust and upper mantle, including the identification of geological features like partial melting and mantle plumes (e.g., Chambers et al., 2019; Keranen et al., 2009; Kibret et al., 2022, 2023).

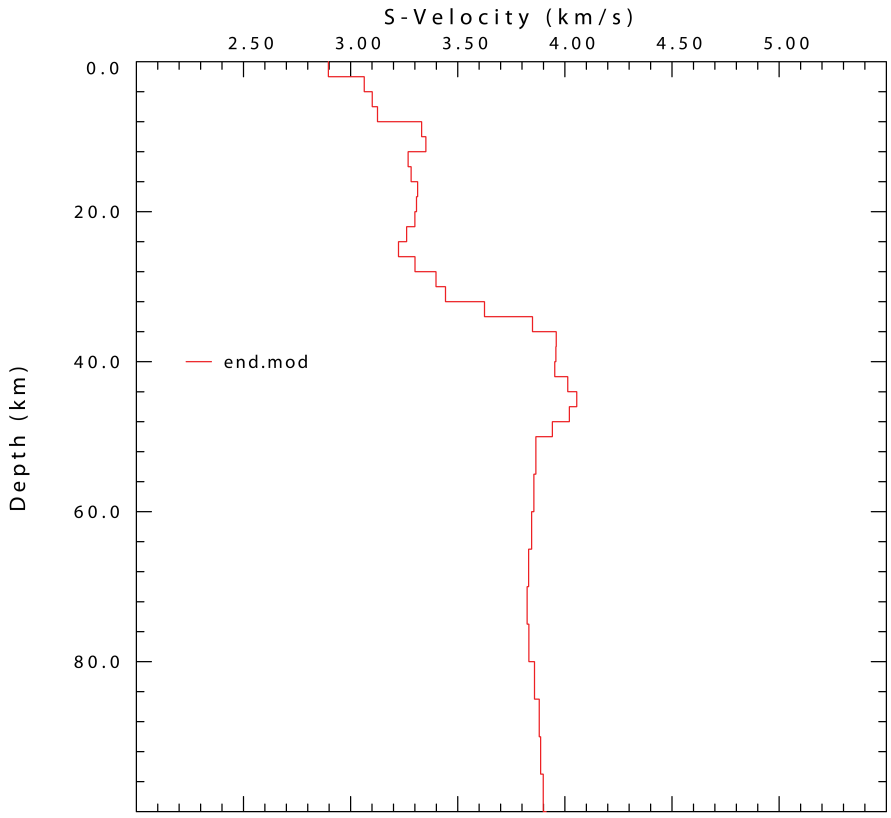

Figure 2.9: The final VM obtained from the inversion of the final and fit synthetic RF with the observed RF.

Inverse modelling typically involves an iterative process of adjusting model parameters and comparing the resulting predictions to observations. The goal is to find the set of parameters that best match the observed data. This is done by using a least-squares optimization methods.

2.2.7 2D Models from 1D Vs

Delaunay triangulation interpolation

The Delaunay triangulation interpolation method proved to be highly significant in our research for modelling the 2D Vs and Vp/Vs using the calculated values obtained through the complete RF analysis process. This interpolation method was employed to estimate unknown velocity values based on known ones (e.g., Kibret et al., 2022). The interpolation procedure consisted of dividing the region of interest into a network of triangles using the Delaunay triangulation technique (Ping et al., 2009). We assigned the calculated velocity values to the vertices of these triangles and performed interpolation across the entire region, taking into account the geometric relationships between neighbouring triangles. This in-

terpolation procedure yielded comprehensive 2D representations of Vs and Vp/Vs values, which enhanced our understanding of the crustal properties.

By incorporating the Delaunay triangulation interpolation method into our analysis of RFs, we spatially interpolated the calculated velocity values obtained from the RF analysis (Figure 2.9), resulting in continuous 2D Vs and Vp/Vs images. These models provided valuable insights into the spatial distribution of Vs and Vp/Vs across the study area. The integration of the Delaunay triangulation interpolation method into our overall RF analysis enabled the derivation of 2D Vs and Vp/Vs models that furnished essential information about subsurface properties, lithological variations, and tectonic processes within the study area. These models played a significant role in tasks such as seismic imaging, seismic hazard assessment, and geological investigations, thereby contributing to a comprehensive understanding of the lithosphere.

2.2.8 Statistical Analysis

One statistical technique utilized in this study is the computation of cumulative relative frequency. Specifically, the Vp/Vs model was analysed below a depth of 10 km, excluding the top 10 km associated with sediments. The cumulative relative frequency was calculated to quantify the proportion of the mid and lower crust with a Vp/Vs ratio greater than 1.9. This technique, based on the work of Ott and Longneckerv (2001) and Peck et al. (2008), involves dividing the frequency of each Vp/Vs value by the total number of observations and then multiplying the relative frequency by 100 to convert it to a percentage. This approach allows for the assessment of the distribution of Vp/Vs ratios in the crust and identifies regions with anomalous values, which can provide insights into geological structures and processes.

The percentage of cumulative frequency (PCF) derived from the Vp/Vs data below a depth of 10 km is a crucial parameter in this study. It represents the proportion of the mid and lower crust with a Vp/Vs ratio greater than 1.9. By computing the PCF, the study gains valuable information about the distribution of Vp/Vs ratios and can identify areas with significant deviations from the norm (Kibret et al., 2023). These anomalous values can offer insights into geological features, such as fault zones or magmatic intrusions, and provide important clues about the tectonic and geological processes occurring in the region.

The utilization of statistical techniques, such as the computation of cumulative relative frequency and the analysis of the PCF, enhances the robustness and significance of the findings in this study. These techniques allow for the quantification and assessment of the Vp/Vs ratios in the crust, enabling the identification of areas with distinct characteristics. By ap-

plying these statistical approaches, the study contributes to a better understanding of the lithospheric structure, providing valuable insights for geological and tectonic interpretations.

Generic Mapping Tool

The calculated values obtained through the Delaunay triangulation interpolation method play a crucial role in modelling the 2D Vs (shear wave velocity) and Vp/Vs (ratio of compressional wave to shear wave velocity) from the whole processes of RFs. These calculated values are then visualized and plotted using the Generic Mapping Tool (GMT) (Wessel et al., 2019), a widely used software package renowned for its powerful capabilities in geospatial data analysis and visualization. GMT enables the representation of interpolated 2D Vs and Vp/Vs models through various visualization techniques such as coloured contour maps. This allows researchers and geoscientists to effectively communicate and interpret the results, leading to a clearer and more comprehensive understanding of the characteristics of the lithosphere. The combined utilization of the Delaunay triangulation interpolation method and GMT greatly enhances the presentation and analysis of the calculated values, facilitating valuable insights into the geological features of the studied area.

2.2.9 Software and Tools Used

The primary software package utilized in this study was the Computer Programs in Seismology (Herrmann, 2013). This advanced package is specifically designed to facilitate the interpretation and understanding of seismic wave propagation in the Earth's crust and upper mantle. It offers a wide range of programs that enable diverse seismic data analyses. Within this package, synthetic seismograph codes are available, enabling the simulation of seismic waveforms for sources and receivers positioned in layered media. Additionally, the software includes dedicated programs for determining crustal structure through the inversion of teleseismic P-wave RFs. An interactive and script-based tool called GSAC is also integrated, providing the means to manipulate seismic traces.

In the Computer Programs in Seismology, various source codes were employed to conduct RF inversion and related analyses in this study. These codes, including rftn96, rftndr96, rftnpr96, rftnpv96, rftnvp, rdseed, saciterd, sacdecon, and pltsac, offer a wide array of functionalities. They encompass RF analysis, iterative time-domain deconvolution (Owens and Zandt, 1985) for RFs to determine the source time function, frequency domain WLD, and general utilities for plotting observed and predicted traces derived from source inversion.

By harnessing the capabilities of these software packages and codes, a comprehensive

framework was established for data processing, analysis, and visualization in the investigation of crustal structure. These tools provided the necessary resources to conduct RF inversion, manipulate seismic waves, compare observed and predicted traces, and visualize the results. The utilization of these software packages and codes ensured the accuracy and reliability of the analyses, ultimately contributing to an enhanced understanding of the upper-to-lower crust.

2.2.10 Validation and Quality Control

To establish the credibility of the results, extensive comparisons were conducted with existing research works that have investigated the same or similar areas within the NE African region. This involved a meticulous examination of findings from various studies, incorporating diverse geophysical methods such as gravity modelling (Cornwell et al., 2006; Lewi et al., 2016; Mammo, 2013), active source seismic tomography (Maguire et al., 2006), Magneto Telluric (MT) (Hübert et al., 2018; Johnson, 2012; Samrock et al., 2018, 2015), Interferometric Synthetic Aperture Radar(InSAR) (Albino and Biggs, 2021; Biggs et al., 2011; La Rosa et al., 2021) method, seismicity analysis (Keir et al., 2006a, 006b), and geodynamic modelling (Berhe et al., 1987; Rogers, 2006). By integrating and contrasting the outcomes of these different techniques, the reliability, consistency, and support of the RF analysis employed in this study were thoroughly assessed.

It is crucial to emphasize that the validation process in this study was characterized by meticulous comparisons and contrasts with independent datasets, previous research works, and the exploration of new areas. By demonstrating coherence and agreement between the findings of this study and the existing body of knowledge, the validation process served to strengthen the credibility and trustworthiness of the results. This rigorous validation approach instilled confidence in the inferred structure of the crust while simultaneously contributing fresh insights for previously unexplored areas.

2.2.11 Ethical Considerations

To acquire the necessary data, we requested seismic data from the Incorporated Research Institutions for Seismology (IRIS) through the Wilber II web page. This demonstrates our commitment to responsible data management by accessing data from a reputable and reliable source. By utilizing established platforms for data acquisition, we ensure transparency and ethical handling of the data.

In addition to data acquisition, we acknowledge and appreciate the contribution of the RiftVolc project and Derek Keir, one of the project's principal investigators. This recogni-

tion highlights the importance of collaboration, respect for intellectual contributions, and proper acknowledgement of others' work. By acknowledging the contributions of our colleagues and collaborators, we adhere to ethical practices within the scientific community.

Overall, the ethical considerations in this research work encompass responsible data management, proper acknowledgement of collaborators, and the potential societal implications of our findings. By upholding these ethical principles, we ensure the integrity and impact of our work, while contributing to the broader scientific community and the well-being of society.

CHAPTER 3

MODELLING S-WAVE VELOCITY STRUCTURE BENEATH THE CENTRAL MAIN ETHIOPIAN RIFT USING RECEIVER FUNCTIONS

Abstract

We applied the receiver function (RF) technique on high-quality teleseismic earthquake data recorded by the RiftVolc broadband network from February 2016 to October 2017. We calculate RFs at 17 stations, which are inverted to estimate Vs, and Vp/Vs structure beneath the Central Main Ethiopian Rift and the Eastern plateau. The observed slow S-wave velocity (Vs) in the uppermost crust (<6 km depth) is interpreted as sedimentary and/or volcanic layers. Beneath the rift valley, crustal Vs is heterogeneous both laterally and with depth. In particular, slow Vs (∼2–3 km/s) is localised beneath volcanic centres in the upper-mid crust but ubiquitously slow in the lower crust with Vs as low as ∼3.5 km/s common. The slow lower crust is associated with high Vp/Vs ratios of ∼1.9–2.0. The Vs and Vp are consistent with the observed seismic velocities, and interpreted the presence of the small fraction (<5%) of partial melt from previous seismic imaging studies of the lower crust. In addition, the velocity contrast is small between the lower crust and upper mantle. The results suggest that partial melt in the lower crust beneath magmatically active rifts might be more widespread than previously thought and an important component of the magma plumbing system. In contrast, Vs is far more homogeneous and faster beneath the Eastern Plateau, with a distinct velocity contrast between the crust and upper mantle suggesting less crustal deformation than what is observed beneath the central rift zone.

3.1 Introduction

The Main Ethiopian Rift (MER) is an active continental rift where magmatic intrusion is thought to play a key role by accommodating extension and thermally weakening the lithosphere (Daniels et al., 2014; Kendall et al., 2005).

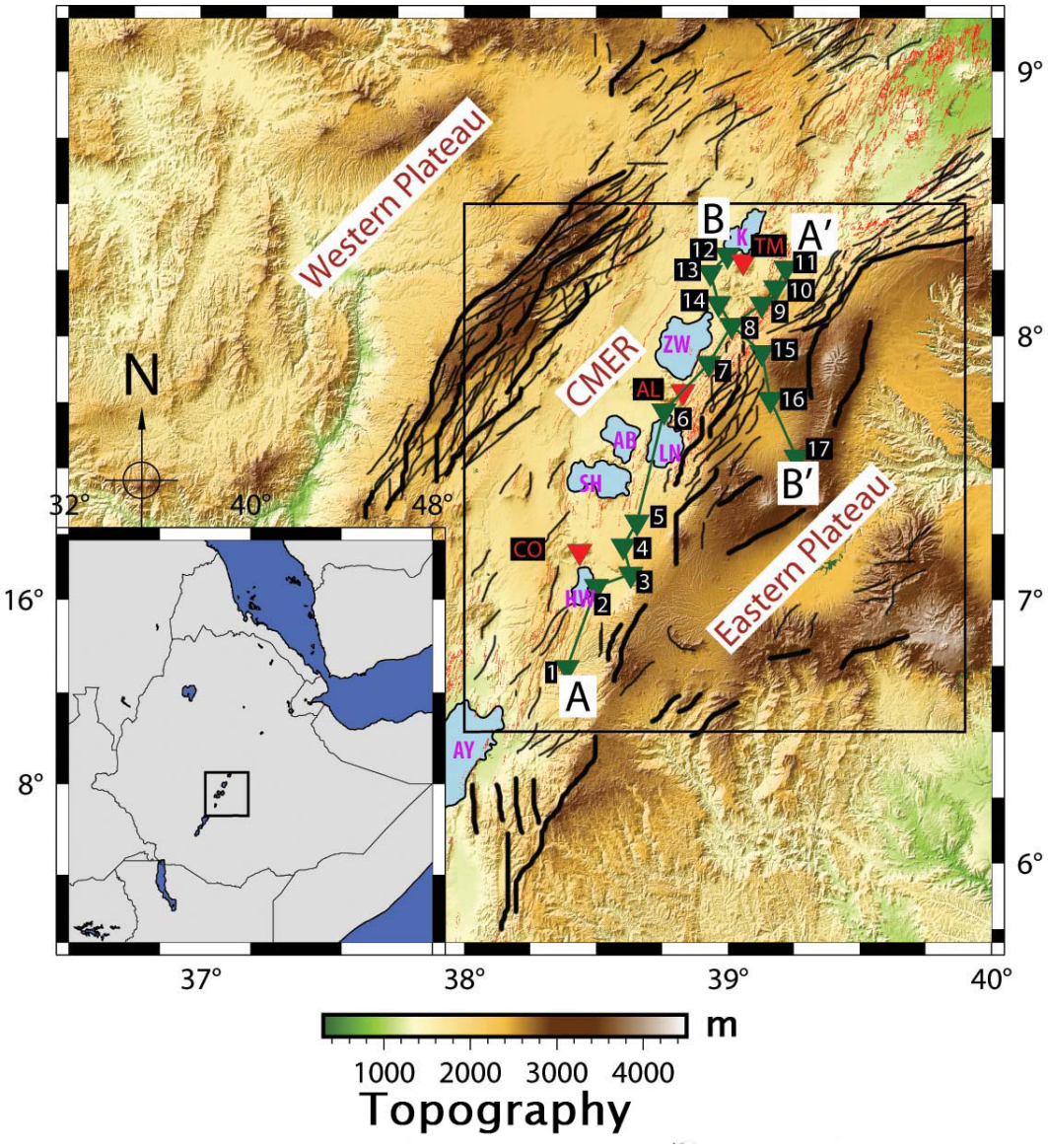

Figure 3.1: The black rectangle is the study area in the Central Main Ethiopian Rift. Profile AA'is along the eastern side of the Central Main Ethiopian Rift floor (alongrift) profile. Profile BB'is the across rift profile. Green reversed triangles represent the station location of 17 stations. Red-reversed triangles represent the locations of Corbetti (CO), Aluto (AL), and Tulu Moye (TM) calderas. The red thin and dense line represents the faults of the Main Ethiopian Rift (MER) (Corti et al., 2020). The bottom left corner inset shows the regional map, with a square for the area of our study. Names of the lakes are labelled by pink-coloured letters as AY (Abaya), HW (Hawasa), SH (Shala), AB (Abayata), LN (Langano), ZW (Ziway), and K (Koka).

Since the start of the Ethiopia-Afar Geoscientific Lithospheric Experiment (Bastow et al., 2011) in the early 2000s, consecutive and successful controlled and passive seismic deployments helped to delineate the seismic structure of the MER crust, especially the P-wave

velocity (V_p) structure and crustal thickness (e.g., Ebinger et al., 2017). A major finding of previous V_p images is that the V_p of the crust beneath the MER is faster than that of standard continental crust (Zandt and Ammon, 1995), a feature interpreted as caused by post-Miocene mafic intrusions that have accommodated extension (e.g., Keranen et al., 2004; Mackenzie et al., 2005).

More recently, however, the advent of ambient noise tomography at periods sufficiently short has facilitated imaging of shear-wave velocity (V_s) of the crust (e.g., Chambers et al., 2019; Kim et al., 2012). Results from these studies show that the MER crust has far slower V_s than the standard continental crust, with the absolute magnitude of the velocities in places interpreted to require the presence of partial melt (e.g., Chambers et al., 2019). The joint crustal seismic properties of relatively fast V_p and slow V_s are peculiar and poorly explored in previous literature. In addition, all previous constraints on the V_s structure of the MER come from models derived from surface wave imaging techniques, such as ambient noise tomography, with a lack of independent constraints provided by alternative methods. In order to address this and provide additional and independent constraints on the V_s structure of the MER crust, we applied the receiver function (RF) techniques using open-source codes from Computer Programs for Seismology (CPS) (Herrmann and Ammon, 2002) to estimate the velocity of the crust and upper mantle. To this effect, we have used 17 new seismic stations deployed as part of the 2016–2017 RiftVolc project (Greenfield et al., 2019a; Lavayssiere et al., 2019) to improve our understanding of the spatial variations of the crustal V_s structure within the central MER (CMER) and adjacent Eastern Plateau. In addition, we use the RF technique to constrain the V_p and V_p/V_s ratio. In investigating the heterogeneous structure, we have chosen two vertical cross-sections to represent the area of our study (Figure 3.1).

One profile (A-A') is along the rift, and the other profile is across the rift (B-B'). This study improves on the previous velocity models and Moho depth estimates of the CMER and Eastern Plateau (Dugda et al., 2005; Keranen et al., 2009) by using a relatively large number of broadband seismic stations compared with the previous studies.

3.2 Tectonic Setting and Crustal Structure

The CMER formed within the Oligocene Ethiopian flood basalt province and is thought to have initiated at between ∼20 and ∼10 Ma (Bonini et al., 2005; Corti, 2009; Wolfenden et al., 2004). The extension was initially localized to several ∼60-km long, NE-SW striking, high-angle (>60 °) border faults that bound the rift, such as the Boru-Toru and the Goba-Bonga structural lineament on the western side of the rift, and the Asela-Sire Border

Fault on the eastern side of the rift (Bonini et al., 2005; Corti et al., 2020). Since the Quaternary, the locus of tectonic and magmatic activity within the CMER is thought to have become focused to a ∼20-km-wide zone of small offset faults, aligned cones, and active volcanic centres within the rift valley floor known as the Wonji Fault Belt (WFB), and also at a few rift marginal magmatic systems, such as the Silti-Debre Zeyit Fault Zone (SDFZ) towards the western side of the rift (Chiasera et al., 2018; Rooney et al., 2014; Woldegabriel et al., 1990).

Constraints on the crustal structure in the CMER come from several geophysical techniques including seismology, magnetotellurics (MT), and inversion of gravity data. Constraints on crustal thickness come from sparse RF measurements (Dugda et al., 2005; Keranen et al., 2009; Kibret et al., 2019), the wide-angle controlled-source along-rift EAGLE project line, and the intra-crustal Vs structure using ambient noise tomography (Chambers et al., 2019; Kim et al., 2012).

Previous RF studies in the CMER using relatively sparse station spacing show that the crust is 27- to 40-km thick in the rift (Dugda et al., 2005; Keranen et al., 2009) and 33- to 44-km thick beneath the plateaus (Dugda et al., 2005; Kibret et al., 2019). The crustal structure beneath the Western Plateau is more heterogeneous (33- to 44-km thick) (Keranen et al., 2009) than that beneath the Eastern Plateau (38- to 41 km thick) (Dugda et al., 2005; Keranen et al., 2009; Kibret et al., 2019). Wide-angle controlled-source seismology provides further constraints in the CMER, and Western and Eastern Plateaus. The EAGLE across-rift line shows similar crustal thicknesses of 38–40 km beneath the CMER (Dugda et al., 2005; Maguire et al., 2006; Stuart et al., 2006), and 35–45 and 37–42 km beneath the Western and Eastern Plateaus, respectively (Cornwell et al., 2010; Dugda et al., 2005; Hammond et al., 2011; Kibret et al., 2019; Stuart et al., 2006).

The southern end of the EAGLE along-rift wide-angle controlled-source line is as far south as Lake Hawasa (near HAWA station) and shows a varied along-rift crustal structure in the CMER (Mackenzie et al., 2005; Maguire et al., 2006). The Vp structure, modelled by the wide-angle 2D profile studies, shows that the velocities of the upper crustal layers beneath the rift are 5%–10% higher than outside the rift, a feature interpreted to be caused by mafic intrusions associated with magmatic centres (Mackenzie et al., 2005; Maguire et al., 2006). Consistent with this, 3D controlled-source tomography of the upper crust by Keranen et al. (2004) imaged rift parallel high Vp (∼6.5–6.8 km/s) elongated bodies with a size of 20-km wide and 50-km long, and interpreted them as cooled mafic intrusions that are separated laterally from one another in a right-stepping enechelon pattern, which corresponds with the surface segmentation of the WFB. These fast Vp regions correlate to a region of distinct

positive Bouguer anomalies in gravity studies that are modelled as regions of dense rock (∼3,000 kg/m3) such a gabbro (e.g., Cornwell et al., 2006; Mahatsente et al., 1999).

In addition to the earliest studies revealing crustal structure in the MER based on Vp structure, later studies applied surface waves to render the Vs structure. Ambient noise tomography has been used to construct Rayleigh-wave group velocity maps covering the northern MER (NMER), CMER, and southern MER (SMER), and parts of the surrounding plateaus (Chambers et al., 2019; Kim et al., 2012). Chambers et al. (2019) also presented an absolute 3D Vs model of the crust and uppermost mantle of the region. An important feature of the Vs images is that the MER crust is mostly significantly slower than away from the rift, in contrast to the Vp, which is generally faster within the rift. The absolute Vs of less than 3.20 km/s + 0.03 in the lower crust are difficult to explain except with the presence of a fluid phase in the rock, such as partial melt (Chambers et al., 2019). In addition, slow Vs (<3.6 km/s) in the uppermost crust observed by Chambers et al. (2019) is consistent with the presence of sediments and/or partial melt (Diaferia and Cammarano, 2017).

Some studies reported that the anomalous high temperature is an important player on velocity structure in the case when it can trigger the transition of α–β quartz. In case of hydrated compositions (as one can presume about the current case study for the rift zone), the amphibole breakdown at increasing pressure and temperature produces a discontinuity that can be detected by RF or refraction studies (Diaferia and Cammarano, 2017; Guerri et al., 2015).

Similarly, several MT studies carried out in the CMER identify high conductivity anomalies associated with young surface volcanism (Whaler and Hautot, 2006). These conductive anomalies tend to be imaged in the uppermost crust at <1–2 km, in the upper crust at 3–6 km depth, and in the mid-lower crust at 20–25 km depth (Ebinger et al., 2017; Hübert et al., 2018). The shallowest anomaly is interpreted as being caused by hydrothermal fluids, whereas the other deeper high conductivity anomalies are interpreted to be caused by partial melt in the subvolcanic plumbing system (Ebinger et al., 2017; Hübert et al., 2018). Broadly speaking, there is a good correlation between the loci of slow Vs from seismology and high conductivities, giving additional remark to the idea that these anomalies are caused by partial melt (Chambers et al., 2019).

3.3 Data and methods

3.3.1 Data

The data were acquired from the RiftVolc temporary network project that was conducted from February 2016 to October 2017 and recorded by three-component broadband Guralp CMG-6TD and Guralp CMG-ESPCD seismometers with a 50-Hz sampling rate. We downloaded the teleseismic waveform data and instrument responses of the RiftVolc project data archived at the Incorporated Research Institutions for Seismology (IRIS) Data Management Center (DMC).

To constrain the V_s and V_p/V_s structure beneath 17 stations, which are deployed along and across the CMER 60 teleseismic earthquakes with magnitudes, $M_w \geq 6$ and source-to-receiver epicentral distances between 30° and 90° (Figure 3.2) were chosen. However, after calculating the RFs, only 8-38 signals were selected per station based on the percentage of signal power fit (Table 1).

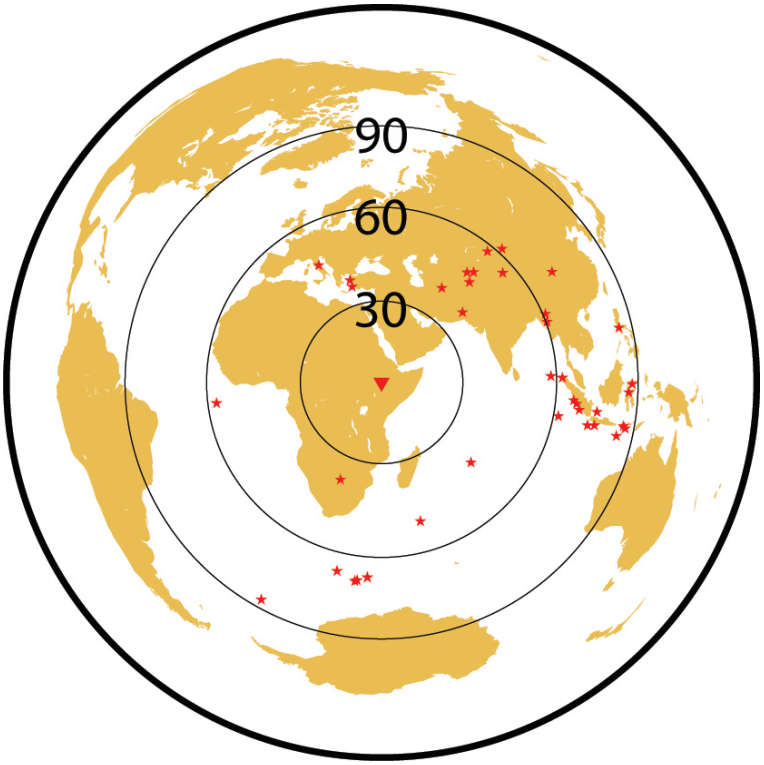

Figure 3.2: Red circles are locations of the teleseismic earthquakes used for the study. The data collected are in the distance ranging from 30° to 90°in the time range of February 2016 to October 2017. The dark blue triangle is the central location of the 17 seismic stations used in this study.

Data were processed in SAC format. We applied a cosine taper function for the P-waveform signal for a length of 50 s (10 s before and 40 s after the onset of the P-wave arrival) before computing the RFs. To reduce the influence of low-frequency noise on the RFs, all the signals were filtered with a Butterworth band pass filter of between 0.01 and 5 Hz to ensure the stability of the RFs and to avoid aliasing when decimating the data. Finally, each three-component signal was reviewed to remove signals that contained low signal-to-noise ratios and/or when any of the three components were not recorded properly due to instrument malfunction.

3.3.2 Methods

We applied a RF technique using time series teleseismic earthquakes to provide constraints on the local velocity structure of the crustal and upper mantle Ammon et al. (1990); Langston (1979). To extract the RF for each event, we first window the three-component seismograms starting from 10 s before and 40 s after the predicted P arrival. Selected teleseismic seismograms are rotated to radial (R), tangential (T), and vertical (Z) components from east–west, north–south, and vertical components, respectively. Each pair of horizontal-component signals (i.e., north–south and east–west components) was rotated to their corresponding radial and transverse directions.

A straightforward frequency domain deconvolution can be unstable due to spectral holes in the vertical component, and stabilization of this process can be obtained by either "prewhitening" (Robinson, 1982; Yilmaz and Doherty, 1987); or "water-level" algorithms. The former adds a small component of random noise to the vertical component, while the latter sets a lower bound on the magnitude of the denominator terms (the vertical seismogram spectral elements) in a frequency domain spectral division.

In this study, converted phases are isolated by iterative, time-domain spiking deconvolution (Gurrola et al., 1995; Ligorria and Ammon, 1999) with pre-whitening to stabilize the filtering. Iterative time domain deconvolution works well even with complex signals. However, regardless of a deconvolution algorithm, the response at the receiver depends on the complexity of structures. Simple structures generally lead to better RF images (Ligorria and Ammon, 1999). After deconvolving the vertical from the radial component, we removed the signature of source, travel path, and instrumental response effects (Ammon et al., 1990; Dugda et al., 2005; Kibret et al., 2019; Langston, 1979) employing the signals coming from four different back azimuths (Figure 3.3).

Table 3.1: The table shows the names of stations, the percent of signal power fit between observed and synthetic seismograms, and the number of receiver functions (RFs) used in the analysis during the model fit calculations.

NO	No. Stations	% fit	No. RFs	Average ray	Average Vp (km/s)
1	ASSE	92.3	38	0.058	6.7
2	SAGU	90.4	31	0.059	6.9
3	JIMA	88.2	8	0.057	6.4
4	BEKO	85.6	60	0.059	6.9
5	CHKA	85.3	11	0.069	6.7
6	ANOL	84.5	18	0.065	7.0
7	HURT	83.3	10	0.076	6.5
8	ODAS	81.1	28	0.067	6.7
9	OHIT	80.9	18	0.063	6.7
10	HAWA	79.4	35	0.063	7.0
11	KADO	79.2	27	0.064	7.3
12	WOND	79.0	34	0.065	6.3
13	JIRE	78.2	19	0.065	6.9
14	BESH	77.8	24	0.063	6.9
15	SHAS	77.6	14	0.058	6.8
16	YIRG	76.6	20	0.060	7.0
17	OGOL	76.6	25	0.061	6.7

The RF technique is a time series when the radial component trace is deconvolved from its vertical component seismogram, where the timing and amplitude of the RF phases are sensitive to the near receiver local Earth structure beneath the seismic station (Langston, 1979). The dominant signal in the first few seconds of the RF is the P_s conversion from the Moho and/or intracrustal velocity contrast followed by reverberated phases within the crust (e.g., Hammond, 2014; Last et al., 1997). In case of using a relatively dense array, RFs can show the fine crustal heterogeneity, anisotropy, and dipping structures (Eckhardt and Rabbel, 2011; Liu and Niu, 2012; Niu and James, 2002; Thybo et al., 2019; Youssof et al., 2013, 2015).

Each RF was deconvolved for 20 iterations with a limiting error of 0.001 by applying three different Gaussian width parameters of 0.5, 1.0, and 2.5. We applied an iterative deconvolution algorithm (**?**), which is calculated by the division of the denominator from the numerator (Herrmann and Ammon, 2002). Also, in each case, we allowed iteration to continue until the change in misfit resulting from the addition of a spike was 0.01%

(Ligorria and Ammon, 1999). The degree of fit between the synthetic and observed RFs is calculated from the three Gaussian width parameters. A sample of two RFs is selected from 17 stations based on their percent of fit to demonstrate the overall results throughout each step (Figures 3.4 and 3.5).

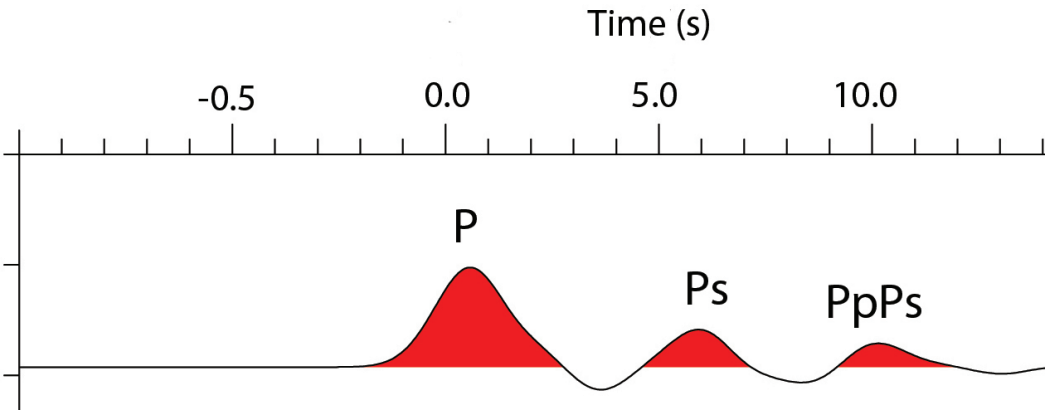

Figure 3.3: This is a sampled receiver function (RF), which is calculated from the deconvolution of the horizontal from the vertical component. The deconvolution is processed from the data collected by the ASSE station from an earthquake coming from a $\sim$178° azimuth.

Table 3.2: A summary of the findings of previous gravity and seismic methods studied in the SE plateau and the central main Ethiopian rift valley for the determination of Moho depth.

Geophysical methods	**Moho depth (km)**	**Study areas**	**Author/s**
Seismic refraction/ wide angle reflection	~39-40	SE MER	Mackenzie et al. (2005)
Gravity and topography data	~40	SE MER	Tiberi et al. (2005)
High-precision gravity data	~38-51	MER flanks	Cornwell et al. (2006)
RFs and Rayleigh wave group velocities	~38	CMER	Keranen et al. (2009)
RFs and Rayleigh wave group velocities	~38-41	Eastern shoulder	Keranen et al. (2009)
A 2D forward gravity model	~38	CMER	Emishaw et al. (2017)
Receiver function analysis	~33-44	Ethiopian plateau	Dugda et al. (2005)
Receiver function analysis	~27-38	MER	Dugda et al. (2005)
3D gravity modelling	~30-50	MER and Adjoining plateau	Mahatsente et al. (1999)

The study applies the ak135 velocity model (Kennett et al., 1995) as the initial velocity model to calculate the best fit velocity structure. Finally, we identified the level of the model fit of the observed and synthetic models by using both visual inspection and the calculated percentage of signal power fit. When the synthetic signals show a high degree of a misfit from the calculated RFs, both RFs and the synthetic models are automatically discarded.

The observed (red colour) and synthetic (blue colour) RFs (Figure 3.5) as well as the initial and the final velocity models (Figure 3.6) are calculated by using programs from Herrmann and Ammon (2002). The final velocity models are calculated from the global velocity model ak135. The calculated absolute velocity values at every 2-km depth are obtained from the inversions of the RFs. The uncertainties of the calculated RFs are estimated from the percentage of fit between the observed and the calculated RF. Subsequently, well-constrained Vs structures of the crust and upper mantle are provided in the 2D profiles.

We applied the Delaunay triangulation interpolation method to estimate unknown velocities based on several known calculated velocities (Ping et al., 2009). The method uses three

velocities at a time by assuming no points inside the circumference of any triangle. We applied this interpolation method as implemented in the GMT plotting software (Wessel et al., 2019) by triangulating and contouring the calculated velocity values to image the 2D velocity versus depth plots.

Crustal thickness and Vp/Vs ratio are estimated from the a priori known Vp value obtained from two-dimensional wide-angle seismic modelling from the EAGLE controlled-source survey (Mackenzie et al., 2005; Maguire et al., 2006) in the region. During our inversion, we calculated Vs values at 2-km depth intervals. Again, we employed the mathematical model by Last et al. (1997) and Zhu and Kanamori (2000) to get the Moho depth (H) at each station, where tPs-tP is the time interval between the arrival of the direct P wave and the Moho Ps converted phase, andpis the average ray parameter calculated from RFs.

3.4 Results

We computed observed and synthetic RFs at 17 stations where the degree of fit is between 77%–92% (at station OGOL and ASSE, respectively), as shown in Table 3.1. The range of degree of fit between observed and synthetic seismograms is similar to what is previously reported (70%–90%) in Ethiopia and Kenya by (Dugda et al., 2005).

The current RFs are obtained with two clusters of range of back-azimuths of 30°–110° and 185°–260° (Figure 3.4). The first arrival spike is the direct incident P wave at the surface; however, the subsequent arrivals correspond to the partition of converted and reverberated phases (Figures 3.3 and 5). For the two examples of observed RF in Figure 3.4, we present the RF of each event with the corresponding synthetic RF in Figure 3.5. In this model, the red-coloured RFs are the observed signals, whereas the blue colour shows the synthetic ones. The observed and synthetic RFs (Figure 3.5) show a high degree of fit for the Gaussian width parameters of $\alpha = 0.5$ and $\alpha = 1.0$.

Figure 3.6 indicates the 1D velocity models for the chosen two stations. These velocity models are calculated from the blue-coloured synthetic RFs shown in Figure 3.5. They are calculated in the depth range of 2-100 km. The blue-coloured nearly vertical line is the initial velocity model, which is assumed as a homogeneous half space with a Vs of ∼4.48 km/s, which is the value of most of the lithosphere in the ak135 velocity model (Kennett et al., 1995).

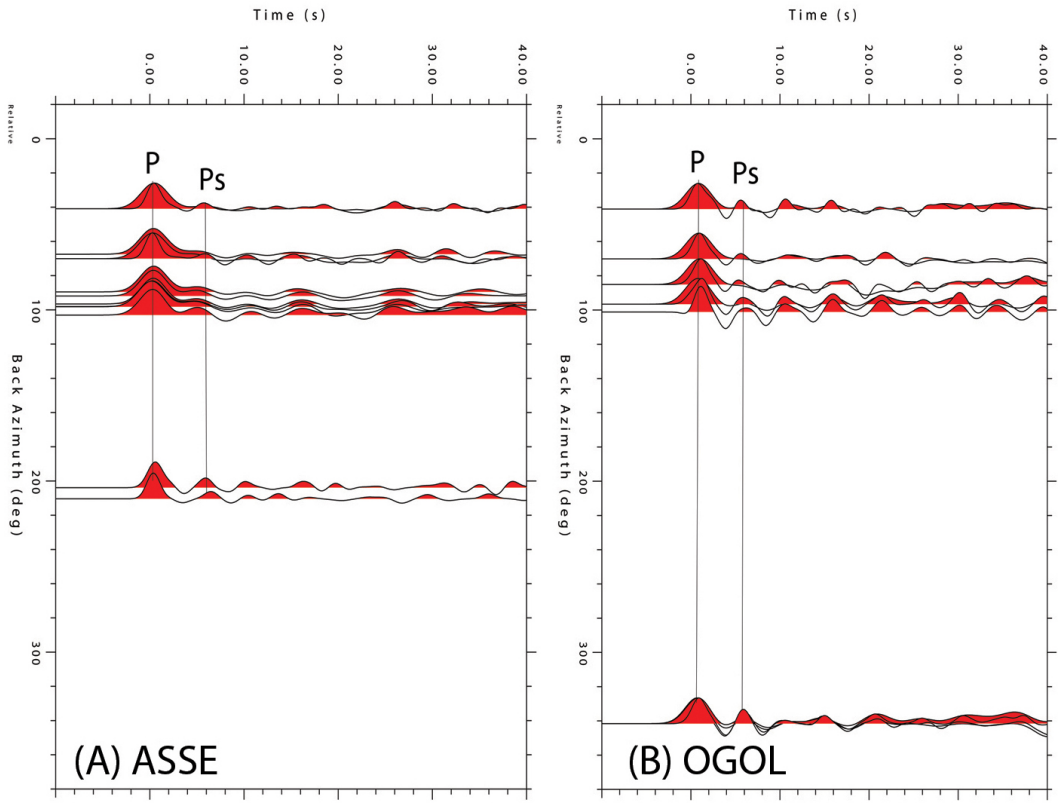

Figure 3.4: (A)and (B)are examples of RFs calculated for signals coming from different azimuths. Positive values were filled with red ink to emphasize prominent features, such as the direct P and the Ps phase, which is the P-to-S conversion.

From the calculated 1D Vs models shown in Figure 3.6, the red coloured 1D velocity value is the final and best fit calculated Vs model. From the models, the ASSE station, which is located on the Eastern Plateau shows very small heterogeneity in the upper and lower crust. However, station OGOL is located on the CMER floor and shows a heterogeneous velocity structure with a relatively high velocity of up to $\sim$4.6 $\pm$ 0.1 km/s in the upper crust and a relatively low velocity of as low as 3.4 $\pm$ 0.1 km/s in the lower crust.

For the remainder of the stations, we have shown the results in the form of the along- and across-rift profiles (Figure 3.7). Broadly speaking, the velocity models show a distinctive reduction in Vs in the mid to lower crust similar to that observed at OGOL (Figure 3.6), or a more regular increase in Vs with depth as observed at ASSE (Figure 3.6). Closer inspection for the stations along the rift shows that the velocity model varies considerably spatially with both styles of velocity structure observed in different places within the rift. In contrast, the across-rift profile shows that the stations on the Eastern Plateau have a velocity structure more similar to ASSE.

The upper to mid crustal high-velocity material (∼4-4.5 ± 0.1 km/s) observed in OGOL is also observed in the rift beneath YIRG, SHAS, KADO, and BESH stations for the depth range of 4-25 km (Figure 3.7). At these stations and beneath the observed high-velocity upper to mid crust, there is a relatively slow Vs (±3.5 ± 0.1 km/s) for the depth range of ∼24-45 km. The slow velocity deep crust is commonly beneath normal upper-to middle crust (4-4.3 km/s) such as beneath the JIMA station. In contrast, beneath JIRE, ODAS, ASSE, and SAGU stations (Figure 3.7), crustal Vs are relatively homogeneous.

Figure 3.8B1 shows the 2D Vs structure and Figure 3.8B2 the corresponding Vp/Vs ratio of the along-rift profile in the CMER obtained from the Delaunay triangulation interpolation method. Throughout the crust, the depth to particular velocity contours generally deepens with proximity to the major volcanic centres. This is especially pronounced in the 5- to 20-km depth range where the Vs increase significantly in regions in between the major volcanic centres. For example, beneath the two high topographic peaks (marked as Aluto and Tulumoye) observed in Figures 8A1 and A2, there are slow velocity (≤3.8 km/s) and high Vp/Vs ratio zones in the upper-mid crust. A similar slow velocity zone in the upper-mid crust is also observed beneath the Wondo Genet remnant Mega caldera rim. Vs is generally slow (±3.1-3.7 ± 0.1 km/s) in the lower crust beneath the CMER, with less spatial variation in velocities compared with that observed in the upper-mid crust. Generally, our findings are consistent with previous ambient noise tomography results showing the presence of slow S-velocity shallow crust beneath mega calderas, such as beneath Aluto and Tulu Moye, and slow Vs found more ubiquitously in the lower crust (Chambers et al., 2019).

Figures 9B1 and B2 show the variations in Vs and Vp/Vs structure across the rift, respectively. In a similar fashion to the along-rift profile, the topmost ∼5 km of the upper crust of the across-rift profile is a very low seismic velocity (2.0-3.2 km/s) material. The border fault of the eastern side of the CMER is marked by a topographic step from ∼1,700 m in the rift to ∼2,700 m on the rift margin (Figure 3.9).

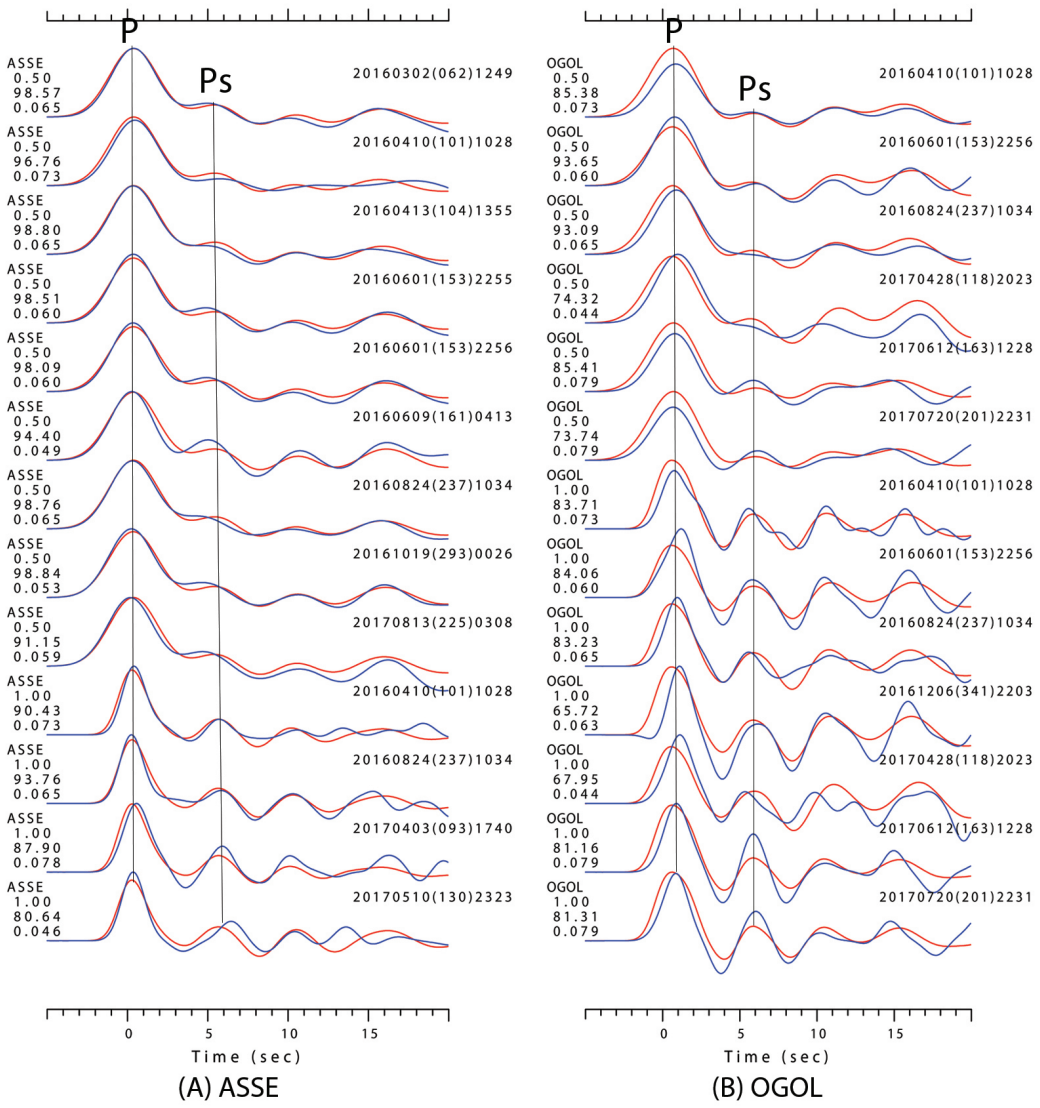

Figure 3.5: (A)and(B)are RFs of ASSE and OGOL stations. The ASSE station located on the eastern plateau, which is the best fit RF of this study, whereas station OGOL is located in the central MER (CMER) rift margin near the eastern plateau, which has the largest misfit of all the RFs. Blue-coloured RFs in the background are synthetic, whereas the red-coloured RFs on top are the observed RFs. P represents the direct primary wave, and Ps is the converted phase at the Moho. The numbers on the left show the station name, Gaussian width parameter, percentage of fit, and the applied ray parameters for the specified RF. The numbers to the right of the RFs are the occurrence time of the earthquakes. In(A), two signals and in (B) six signals are calculated twice for the Gaussian width parameters of 0.5 and 1.0.

Outside of the rift on the rift flank, we observe a fairly homogeneous crustal structure with a distinct lack of slow velocities in the lower crust. Instead, the seismic velocity

mostly increases with depth. In addition, there is a sharp increase in seismic velocity at ∼45 km depth, where previous studies based on different methods showed this change as Moho discontinuity (e.g., Cornwell et al., 2006; Mackenzie et al., 2005; Mahatsente et al., 1999), as shown in Table 3.2. However, similar to the along-rift profile, within the rift on the across rift profile, we see a more heterogenous velocity structure. At 20- to 35-km depths, particularly slow Vs and high Vp/Vs ratios are found beneath the eastern part of the across-rift profile beneath the JIMA and OGOL stations. In this depth interval, the lowest velocities are found beneath the eastern side of the CMER spatially associated with the surface position of the WFB volcanic centres.

3.5 Discussion

We discuss here the Vs and Vp/Vs structure of the rift obtained from our data analysis in the context of magmatic and tectonic extensional processes, and with the aid of a priori constraints of Vp ∼6.8 km/s (e.g., Dugda et al., 2005; Mackenzie et al., 2005; Maguire et al., 2006). We also compare our findings with constraints inferred from density and conductivity analysis conducted in the area. We use both one- and two-dimensional Vs profiles to interpret velocity variations in the lithosphere to answer basic questions about the nature of the crust and upper mantle when rifting modifies the lithosphere.

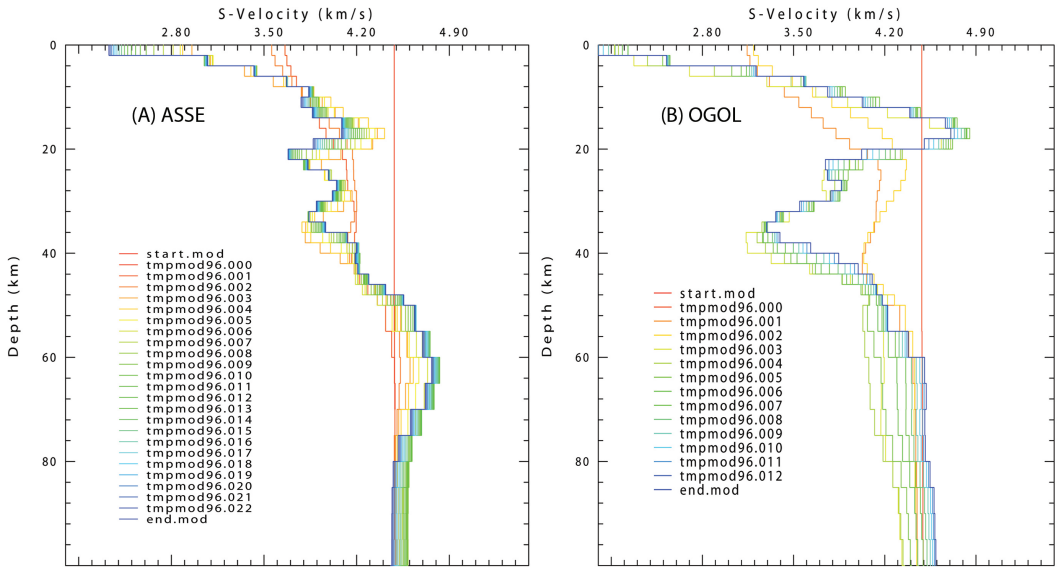

Figure 3.6: Panels(A)and(B)are the two representative velocity models for the ASSE and OGOL stations. The nearly vertical start. mod is an initial half space velocity model derived from the ak135 global velocity model (Kennett et al., 1995) and the end. mod is the final and best-fit velocity model. The tmpmod96. xxx are the calculated velocity models from the relatively less fit RFs during an inversion.

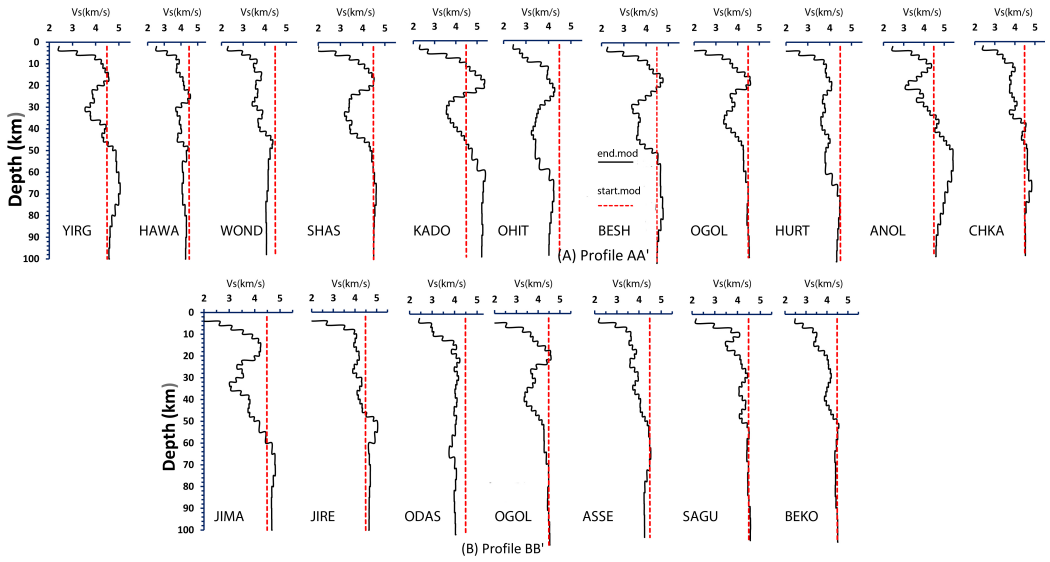

Figure 3.7: (A) shows the 1D velocity model for the along-rift profile AA', which is located along the eastern margin of the central main Ethiopian rift profile. (B) is the 1D velocity model for the across-rift profile, which includes the rift side (JIMA, JIRE, ODAS, and OGOL) and plateau side (ASSE, SAGU, and BEKO) stations.

3.5.1 S-wave Velocity Structure with in the Rift

The slow velocity (2–3 km/s) imaged at 2–6 km depth is similar to the proposed Vs of ∼1.9–2.8 km/s typical of layered sediments (Benoit et al., 006b). This is also in good agreement with the work of Chambers et al. (2019), which interprets a similarly low velocity at the topmost upper crust as sedimentary and/or volcanic layers. This result agrees with the interpretation of Cornwell et al. (2006), which interprets the existence of an upper crustal low-density (2,380 kg/m3) layer that represents interspersed volcaniclastics, lava flows, and lacustrine sediments within the rift valley (Wolfenden et al., 2004). In support of this interpretation, the low Vs of the uppermost crust extends to greatest depths within the rift valley than outside of it (Figure 3.9).

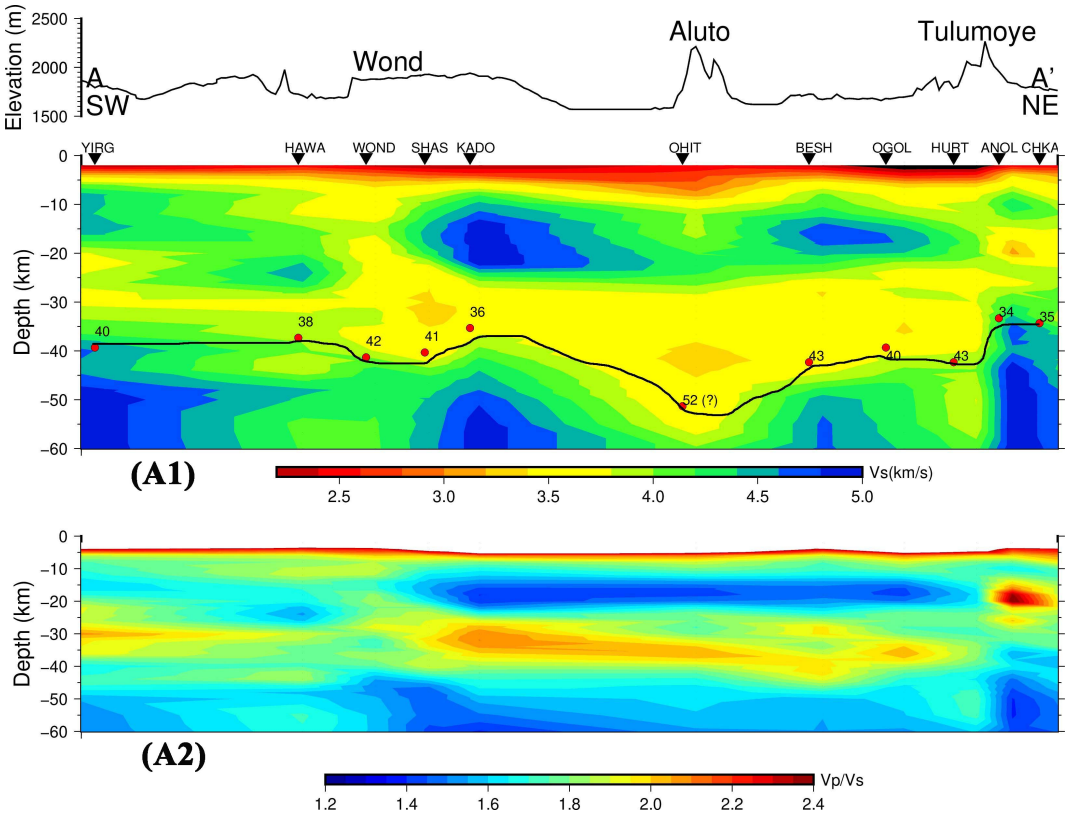

Figure 3.8: (A1)shows a 2D vertical slice along the eastern margin of the central Main Ethiopian Rift, which is obtained from profile AA' of Figure 3.1 covering from station YIRG (1,756 m) to CHKA (1,604 m).(A2)shows the Vp/Vs ratio values at various depth points. Red indicates slower velocity and blue faster velocity. B2 shows the values of Vp/Vs for the rift and the plateau side of the profile. Blue indicates low Vp/Vs, and red indicates high Vp/Vs ratio.

Both profiles shown in Figure 3.7 represent significant variations in the 1D velocity models. In particular, a number of the stations show elevated seismic velocity at 6–25 km, while others are less fast. When stations are organised spatially from NW to NE in Figure 3.8A1, the spatial variability of this is clearer. Typically, along rift, in-between the magmatic centres (such as beneath station YIRG, SHAS, KADO, BESH, and OGOL), the high Vs ($\sim$4–4.5 km/s) is present in the upper-to-mid crust. The across-rift profile in Figure 3.9 shows that these regions of higher Vs in the upper/mid crust are localised beneath the Wonji Fault Belt. The high seismic velocities coupled with their Wonji Fault belt position favours an interpretation of their origin being a solidified mafic intrusion, an interpretation in line with previous seismic imaging (Chambers et al., 2019), and spatially match high positive Bouguer anomalies constrained in gravity studies (Cornwell et al., 2006; Mahatsente et al., 1999; Tiberi et al., 2005). The average slow-velocity ($\sim 3.5 \pm 0.1$ km/s) regions at $\sim$24–45

km depth may represent a less mafic modification of a normal continental crust of Vp/Vs $<$ 1.85 (Zandt and Ammon, 1995), or a more complex modification from felsic intrusion, and/or presence of partial melt with a Vp/Vs value of $>$1.9.

Beneath 25-km depth in the lower crust, the 1D models show that the majority of seismic stations show a reduction in Vs in the lower crust to 3.1–3.7 $\pm$ 0.1 km/s (Figure 3.7). Figure 3.8 shows that this feature is spatially ubiquitous. There is some spatial variability in the magnitude of the velocity inversion (Figures 8A1, A2), with a hint that the most pronounced slow Vs regions in the lower crust are beneath the volcanic centres, such as Aluto, although this pattern is not particularly clear elsewhere. These regions of slow Vs correlate to high Vp/Vs of $\sim$1.9–2.1. The observation of slow Vs and high Vp/Vs in the lower crust in the rift valley is consistent with the ambient noise tomography by Chambers et al. (2019), which shows that the slowest velocities for all depths within the MER range from 3.28 $\pm$ 0.01 km/s at 10-km depth to 3.83 $\pm$ 0.01 km/s at 40-km depth. The magnitude of the slow Vs at this depth range, combined with the high Vp/Vs, is consistent with previous deep crustal imaging studies, which combined interpret between 0.5% and 5% partial melt (e.g. Chambers et al., 2019). More tightly constraining melt fraction from the seismic velocities alone is difficult since Vp and Vs measurements are potentially explainable by either lower melt fractions aligned vertically as dikes or more elevated melt fractions aligned as sills (Dvorkin, 2021; Paulatto et al., 2012, 2010, 2019). However, dominance of horizontal sill-like melt alignment is favoured by inversions for radial anisotropy derived from surface waves for the MER (e.g., Chambers et al., 2021), and petrological models of the deep crustal magma plumbing system globally (e.g., Annen et al., 2006). The interpretation of partial melt in the lower crust is also supported by high conductivities in the lower crust observed in crustal-scale MT studies at comparable depths (e.g., Whaler and Hautot, 2006).

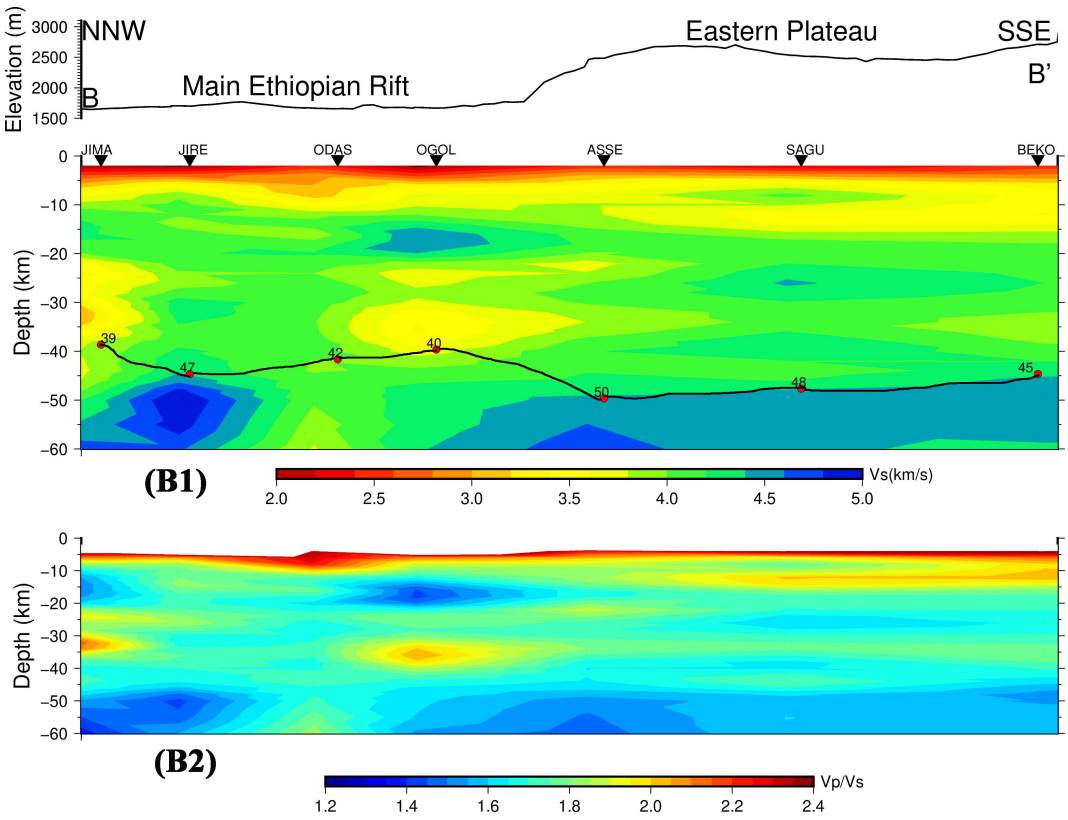

Figure 3.9: (B1) shows a 2D vertical slice across the rift profile BB' of Figure 1 ranging from JIMA (in Central WFB) with an altitude of 1,659 m to BEKO (Eastern Plateau) having an elevation of 2,848 m. Red indicates slower velocity and blue faster velocity. (B2) shows the values of Vp/Vs for the rift and the plateau side of the profile. Blue indicates low Vp/Vs, and red indicates high Vp/Vs ratio.

Profile AA' in Figure 8shows variations in the Vs structure, which provides insights into the crustal-scale magma plumbing system. The ubiquitous slow Vs suggests a diffuse interconnected melt-rich lower crust beneath most of the rift valley, with potentially higher melt concentration beneath the volcanic centres. In contrast, in the upper half of the crust, slower Vs beneath the volcanic centres, with anomalously fast Vs in between the volcanic centres, is consistent with volcanic segment-centred melt supply, in which subvolcanic melt reservoirs focus and store melt, which is delivered episodically mafic intrusion along the rift axis. Such an upper crustal plumbing system has been proposed in Afar on the basis of episodic segment-centred fed dyke intrusions observed with InSAR and seismicity (Barnie et al., 2016; Keir et al., 009b). Here in the MER, a similar subvolcanic plumbing system is consistent with the seismic velocity structure of the upper/mid crust. In addition, in the MER, observations of such rifting episodes are lacking, with geodetic observations of magma-related ground deformation being restricted to volcanic centres such as Aluto

and Tulu Moye (Albino and Biggs, 2021; Biggs et al., 2011). Similarly, localised subvolcanic pockets of melt beneath the volcanic centres (Gleeson et al., 2017) suggest localised longer-lived magma bodies in the shallow crust of the volcanic centres. However, our seismic imaging of the deeper crust suggests that the distribution of melt in the lower crust might well be widespread and enable significant melt transport along rift.

3.5.2 S-wave Velocity Structure of the Eastern Plateau

In contrast to the rift valley floor, the Vs structure beneath the Eastern Plateau is remarkably homogeneous (Figure 3.9B1). In addition, the distinctive increase in Vs at ∼45 km depth, is remarkably similar to constraints on the Moho depth computed in our study, consistent with a previous wide-angle active source, and passive source RF studies (Mackenzie et al., 2005; Maguire et al., 2006), and adds support observations that the Moho beneath the Eastern Plateau is a sharp and distinctive seismological boundary (Ogden et al., 2019). This profile shows a smooth transition toward the shoulder compared with the western plateau margin in which sharp lateral contrast between plateau and rift is observed (Chambers et al., 2019). Limited heterogeneity of the crustal and mantle structure beneath the Eastern Plateau is typical of regions of stable continental crust with limited history of deformation and modification by magmatism (Thompson et al., 2010; Youssof et al., 2013, 2015). The strong contrast in velocity structure from the Eastern Plateau into the rift (Figure 3.9) is in sharp contrast to the conjugate side of the rift valley, with the Western Plateau showing evidence for significant magmatic modification (Chambers et al., 2019; Mackenzie et al., 2005), indicating strong asymmetry to the rifting process. The lack of evidence for magmatic modification of the crust beneath the Eastern Plateau also favours a model of dynamic uplift from a deep-seated asthenospheric anomaly (Sembroni et al., 2016), as opposed to uplift being compensated by crustal magmatic additions (Chambers et al., 2019; Keranen et al., 2009).

Our study reveals new important insights regarding the variability in crustal structure and melt fraction on a local scale beneath the volcanic regions of the MER. The results demonstrate the continued need for more future efforts to understand crustal structure and distribution of partial melt in the wider sense beneath and near the East African rift. We would like to point out the need to have more international collaboration–although we would imagine that long-term and sustainable research in Ethiopia really needs local scientists to lead the way.

3.6 Conclusion

We use RF to delineate the V_s structure of the lithosphere beneath 17 stations in the CMER, which are arranged in two profiles along and across the rift valley. The observed low V_s ($\sim$2–3 km/s) uppermost crust ($<$6-km depth) is interpreted as sedimentary and/or volcanic layers. Beneath the rift valley crust, V_s is heterogeneous laterally and with depth. In particular, slow V_s and high V_p/V_s ratio is localised beneath volcanic centres in the upper-mid crust but ubiquitously slow in the lower crust. The V_s and V_p are consistent with the presence of the small fraction ($<5\%$) partial melt interpreted in previous seismic imaging studies of the lower crust. In addition, the velocity contrast is small between the lower crust and upper mantle in the rift. The results suggest that partial melt in the lower crust beneath magmatically active rifts might be more widespread than previously thought and is an important component of the magma plumbing system. In contrast, V_s is more homogeneous and faster beneath the Eastern Plateau, with a distinct and sharp velocity contrast observed between the crust and upper mantle at Moho, jointly indicative of very little crustal modification from magmatism.

CHAPTER 4

CRUSTAL STRUCTURE OF THE ETHIOPIAN NORTHWESTERN PLATEAU AND CENTRAL AFAR FROM RECEIVER FUNCTION ANALYSIS

Abstract

In magma-rich continental rifts extension by magma intrusion is thought to accommodate much of the extension. We aim to constrain major melt reservoirs in the crust during magma-rich rifting by applying P-to-S receiver functions (RFs) using legacy teleseismic data having magnitudes Mb $>$ 6.0 and epicentral distances ranging from 30° to 90° and collected between the years 2000 and 2013 in 17 temporary broadband stations in Ethiopia and Eritrea. The majority of the NW Plateau crust shows fast Vs of 4–4.7 km/s with localized slow Vs (3.2 km/s) and high Vp/Vs (1.85–2.0) in the mid-crust (10–25 km depth). The seismic velocity beneath the Afar crust is fairly homogeneous except beneath the current locus of strain at the magmatic segments, which have a relatively fast Vs. (4.5 km/s) at a shallow (6–14 km) depth underlain by slower Vs. ($<$3.2 km/s) and high Vp/Vs (2.0) at lower crustal depths (20–25 km). The Moho is sharp beneath most of the plateau stations and more gradational beneath Afar with estimated values of 36–44 km in the NW plateau and 26–30 km in Afar. The results point towards the presence of partial melt in localized places in the mid-crust beneath the NW plateau, and in the lower crust beneath the west of Afar, and particularly focused in the lower crust beneath the magmatic segments in Afar. The results suggest that the lower crust is an important melt reservoir for rift-related magmatic processes. The presence of melt in the NW plateau crust is more difficult to explain but is potentially linked to the broad extension of the plateau, or lateral migration of melt from the rift.

4.1 Introduction

The northern part of the East African rift system has extensive dike and sill intrusions beneath the rift, which have modified the compositional, thermal, and mechanical properties

of the lithosphere (Bialas et al., 2010; Buck et al., 2006). However, observations are also increasingly showing that magmatic processes beneath the Northwestern (NW) plateau may impact the region's distribution of extension and geological evolution (Chambers et al., 2021; Cornwell et al., 2006; Mackenzie et al., 2005). The magmatic processes can potentially be offset by tens to hundreds of kilometres from the centre of the rift and similarly offset from the magma source deep below the surface (Maccaferri et al., 2014). Most previous studies were focused near the centre of the rift mainly around the magmatic segments of the Main Ethiopian Rift (MER) and Afar (Corti, 2009), and as a result, magmatic and tectonic processes away from the rift valley are poorly understood.

The geology of both regions within and outboard of the MER and Afar show strong evidence of Recent magmatic activity (Corti et al., 2018). This observation is strengthened by the presence of significant geothermal activity both within the rift and around the NW plateau (Chambers et al., 2021; Keir et al., 009b; Wolfenden et al., 2005) which is visible at the Galema range and Yerer-Tullu Wellel Volcano lineament (Chambers et al., 2019; Keranen and Klemperer, 2008; Kieffer et al., 2004). Furthermore, low Vp and Vs have been imaged away from the rift valley in various locales in the region and interpreted as being affected by off-rift magmatism (Hammond et al., 2013). Beneath the NW plateau as far north as Lake Tana, slow seismic wave velocity anomalies have been interpreted as melt stored in stacked sills in the mid-to-lower crust (Chambers et al., 2019; Hammond, 2014; Maguire et al., 2006). Therefore, off-rift magmatic activity may significantly impact the locus and evolution of extension (Chiasera et al., 2018). This observation is also demonstrated in places other than the MER, Afar, and NW plateau, such as at the Baikal Rift Zone where the Vitim volcanic field lies more than 200 km away from the rift centre (Yang et al., 2018). However, more studies on the Afar rift margin and adjacent plateaus are still required.

We used the P-to-S receiver function (RF) technique applied to broadband teleseismic data from seismic stations that were temporarily deployed between 2000 and 2013. Our study area includes the Afar rift and the NW plateau regions, where broadband seismic investigations have produced an abundance of seismic data (Figure 4.1). We aim to better understand how and where magmatic processes and mechanical rifting have taken place by determining the thickness, internal structure, and composition of the crust inside and outside the rift valley. Given that RF techniques are particularly sensitive to bulk crustal features, we created new 2D profiles to constrain first-order estimation of Vs, Vp, and Vp/Vs versus depth beneath the study areas to determine the extent to which the crust has been modified by magmatic processes (Christensen and Mooney, 1995; Stuart et al., 2006; Zandt and Am-

mon, 1995). This effort will enhance knowledge of regional tectonics and the relationships between plate stretching, thinning, and magma intrusion during a continental breakup by analysing the crustal structure along the two profiles (Figure 4.1).

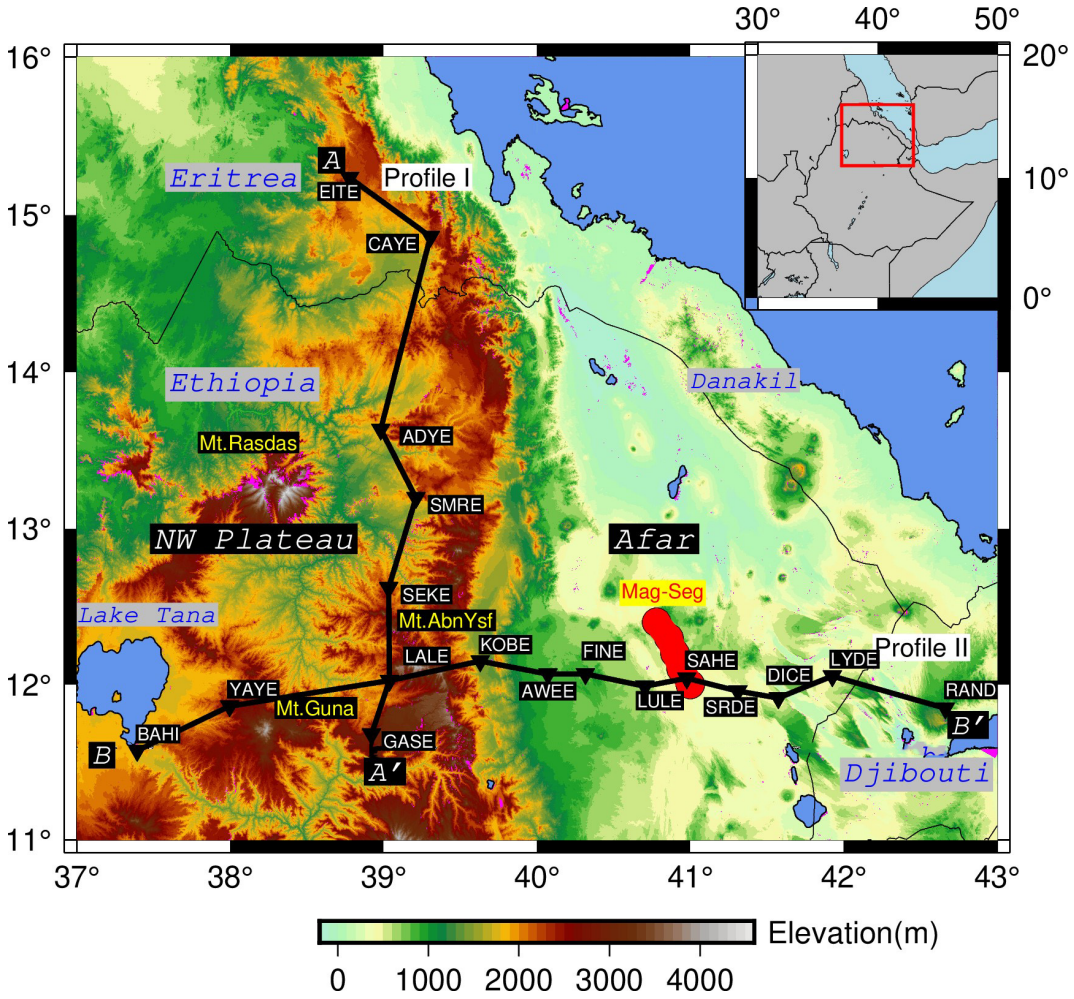

Figure 4.1: The figure displays a topographical map of Afar and the adjoining NW plateau. MER represents the Main Ethiopian Rift. Lakes appear as deep blue polygons. Mt. Rasdas, Mt. AbnYsf, Mt. Guna, Mt. Choke and Mt. Guguftu are to represent Ras-Dashen Mountain, Abune-Yosef Mountain, Guna Mountain, Choke Mountain and Guguftu Mountain respectively. The black inverted triangles show the temporary broadband seismic stations that were installed in the Afar andNW plateaus between 2007 and 2012. Profile I is oriented north-south from A to A', while Profile II is oriented east-west from B to B'. The red polygon in Afar (Mag-Seg) represents the magmatic segment. The red rectangle in the inset map represents the study area.

4.2 Tectonic Setting and Crustal Structure

The Afar region is a unique locale since it is here that the transition from continental plateaus to imminent seafloor spreading within the rift takes place (Ahmed et al., 2022; Bastow et al., 2010; Hayward and Ebinger, 1996). The rifting in Afar is thought to have started soon after the impact of the Afar mantle plume at around 30 Ma (Beccaluva et al., 2009; Hofmann et al., 1997; Pik et al., 1998, 1999, 2008), with the extension thought to have been initiated on the border faults mainly by mechanical faulting (Hayward and Ebinger, 1996; Wolfenden et al., 2005). However, with continued rifting, the extension progressively migrated into the rift valley floor and is also thought to have increasingly included magma intrusion (Wolfenden et al., 2005). The rifting in Afar occurs between the Nubian, Somalian, and Arabian plates and the Danakil microplate. In the central and northern parts of Afar that are the focus of this study, the counterclockwise rotation of the Danakil microplate relative to the Nubian plate controls the extension. This motion causes $\sim$NE directed extension that increases from $<$1 cm/yr in the Danakil Depression of northern Afar to $\sim$2 cm/yr across central Afar (Viltres et al., 2020). The spatial localization of the strain is debated. InSAR data has revealed localized extension from episodic crustal dike intrusion in the $\sim$20 km-wide, $\sim$70 km long magmatic segments (Barnie et al., 2016; Pagli et al., 2015; Wright et al., 2006, 2012), whereas in regions linking the magmatic segments, strain occurs by a combination of normal and oblique slip faulting (La Rosa et al., 2021; Pagli et al., 2019). However, regional strain analysis that includes regional GPS data shows that this localized strain is set within an extension distributed across the whole rift (Doubre et al., 2017), and includes distributed extension across the Northwestern Plateau (Birhanu et al., 2016).

Previous seismic studies such as RF studies (Dugda et al., 2005; Hammond et al., 2011; Kibret et al., 2019; Rooney et al., 2018; Stuart et al., 2006; Wang et al., 2021) and joint inversion of RFs and surface wave analysis (Dugda and Nyblade, 2006; Dugda et al., 2007) estimated the crustal thickness beneath most of Afar to be in the range of $\sim$20–26 km and shallowing to $\sim$16 km northward to the Danakil Depression (Ahmed et al., 2022; Hammond, 2014). Central east Afar near the Djibouti border has a crustal thickness of $\sim$30 km (Hammond et al., 2011). These studies also constrain bulk crustal Vp/Vs, which are commonly very high ($<$1.9) beneath the rift, especially in proximity to the magmatic segments, an observation explained by both solidified mafic intrusion and the presence of partial melt in the crust (Ahmed et al., 2022; Desissa et al., 2013). The interpretation of thinned and intruded continental crust including localized melt pockets is supported by the modeling of both gravity and magnetotelluric (MT) datasets (Desissa et al., 2013; Lewi et al., 2016;

Mammo, 2013). S-p RFs have been used to try to understand deeper lithosphere structures (Lavayssiere et al., 2018; Rychert et al., 2012). A common observation is that the lithosphere-asthenosphere boundary (LAB) is difficult to image seismically, interpreted to be due to melting percolation into the lithosphere masking the expected seismic discontinuity (Lavayssiere et al., 2018). These findings are consistent with deeper seismic tomography revealing a low-velocity anomaly in the upper mantle beneath Afar, interpreted as the asthenospheric melt zone (Chambers et al., 2021; Hammond et al., 2011).

Several geophysical studies have also constrained the crust and lithosphere structures beneath the NW plateau. Many P-s RF studies show crustal thickness ranges of (38–44 km; Ahmed et al., 2022; Cornwell et al., 2010; Dugda et al., 2005; Hammond et al., 2011; Kibret et al., 2019; Stuart et al., 2006; Wang et al., 2021). This result is consistent with estimates of the thickness of the crust derived from seismic refraction profiles (40–45 km; Mackenzie et al., 2005; Maguire et al., 2006; Makris and Ginzburg, 1987), gravity inversion analysis (>40 km; Mammo, 2013; Tiberi et al., 2005), and joint inversion of surface waves and P-s RFs (40 km; Dugda et al., 2007). The crust of the NW plateau is significantly more mafic (Vp/Vs >1.85) than the SE plateau because of the distinct pre-rift crustal magmatic compositions (Bastow et al., 2011). According to magnetotelluric research, seismic anisotropy, and receiver function analysis, the high Vp/Vs values on the NW plateau are often associated with the presence of crustal melt in the crust from ongoing magmatism (Hammond et al., 2011; Whaler and Hautot, 2006). Similarly, S-p RFs detect the lithosphere-asthenosphere boundary (LAB) as a velocity drop 65–75 km beneath the NW plateau (Lavayssiere et al., 2018; Rychert et al., 2012).

4.3 Data and Methods

4.3.1 Description of Data Sources and Instrumentation

The data used for this study are from the IRIS Data Management Center (DMC) archive. This legacy data was gathered by six projects that installed temporary seismic stations between 2000 and 2013. Out of a large number of stations that were installed as part of these temporary projects, we only selected 17 stations that fit our two profiles and produced clear RFs with the direct P and converted phases.

This study employs 39 teleseismic events that occurred between March 2007 and March 2012 at 10 broadband seismic stations (ADYE, DICE, GASE, KOBE, LALE, LYDE, SEKE, SMRE, SRDE, YAYE) that are acquired from Afar Consortium project operated by Universities of Bristol, Leeds, and Addis Ababa. We also used 15 teleseismic events

that occurred at BAHI station during 2000–2002 from the Seismic Investigation of Deep Structure Beneath the Ethiopian Plateau and Afar Depression (Ethiopia) project operated by IRIS/PASSCAL (Nyblade et al., 2000), as well as 54 teleseismic events recorded by two stations (FINE, AWEE) during 2007–2009 from the AFAR07 project operated by the University of Rochester (Ebinger, 2007).

Similarly, we utilized 35 teleseismic events recorded by two stations (LULE, SAHE) during 2009–2013 from the AFAR0911 project operated by the University of Southampton, and 22 teleseismic events recorded by two stations (EITE & CAYE) during 2010–2011 from Eritrea Seismic Project (ESP) operated by Birkbeck University of London. Likewise, 15 teleseismic events were recorded by RAND station during 2009–2012 from the DORA project operated by Ecole et Observatoire des Sciences de la Terre (EOST). The instruments used were Guralp CMG-3T (120 s natural period), CMG-ESP (60 s natural period), and CMG-40T (30 s natural period) (Hammond et al., 2011), and STS-2 sensor for RAND stations that continuously collected the data with a sample rate of 50 Hz. The selected earthquakes have magnitudes $M_b > 6.0$ and epicentral distances between 30° and 90° (Figure 3.2). All the events were requested from the IRIS Data Management Center (DMC)[1].

[1] https://ds.iris.edu/ds/nodes/dmc/

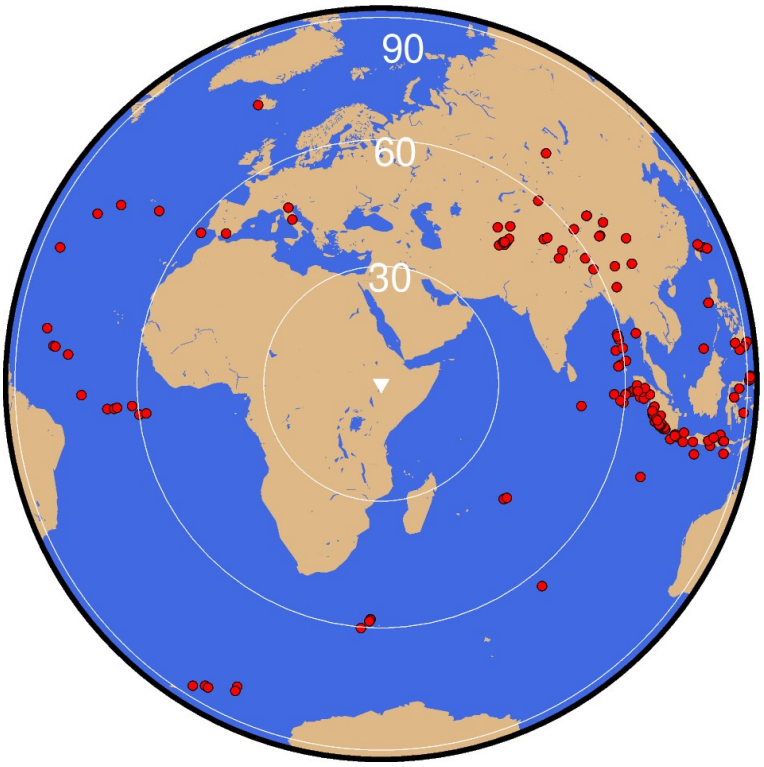

Figure 4.2: The locations of teleseismic earthquakes. Red circles are epicentre of individual earthquakes used for the analysis with Mb >6.0 and epicentral distance between 30 to 90 degrees. The narrowest white circle denotes a distance of 30 degrees, while the medium and larger white circles denote distances of 60 and 90 degrees, respectively.

4.3.2 The RFs analysis steps for imaging crust and upper mantle

In our study, we focused on investigating the regional velocity structure of the crust and upper mantle using high-quality seismic data from temporarily deployed stations in Ethiopia, Eritrea, and Djibouti. Our analysis was based on the receiver function (RF) approach (Ammon et al., 1990; Langston, 1979), which is a well-established technique for locating P- to S-wave conversions and their reverberations from interfaces in the crust and mantle (Langston, 1979). Specifically, we applied the RF technique to identify the discontinuities of the crust and upper mantle, as well as to map their depths and characteristics.

The raw data are processed using the Herrmann software (Herrmann and Ammon, 2002). In order to ensure the accuracy and reliability of the data, various pre-processing steps and corrections are employed in SAC formatted data. Firstly, a trend removal technique is applied to eliminate long-term variations. This is followed by a tapering procedure, which smooths the signal and minimizes abrupt changes that may cause distortion. Mean removal is also used to eliminate the average value of the signal from the raw seismic data (Ahmed et al., 2022). Subsequently, the instrumental frequency response is corrected by

implementing a pole-zero function, which preserves the amplitude and phase alteration of the recorded waveform.

We truncate the three component seismograms using a time window from 10 s before, to 40 s after the P arrivals and apply a Butterworth bandpass filter between 0.01 and 5 Hz to decrease the impact of low-frequency noise on the RFs (e.g., Kibret et al., 2022). Selected teleseismic seismograms are rotated to produce the radial (R), tangential (T), and vertical (Z) components from the east-west, north-south, and vertical components, respectively. A Gaussian parameter of 1.0 and a water level of 0.01 are used in computing all RFs (Dugda et al., 2007; Langston, 1979). Each P-to-S RF is calculated from the frequency domain deconvolution method (Ammon, 1991). We selected good signal-to-noise ratio seismograms using the visual inspection method in which the radial component of the seismogram obtained from the deconvolution of the vertical from the horizontal is clear and where the direct P and the converted phases are found. The Ps conversion, which is normally from the Moho is typically the dominating signal in the first few seconds of the RF, followed by converted P-wave multiples inside the crust (e.g., Hammond et al., 2011; Zandt and Ammon, 1995). Following the deconvolution, we stacked events as a vital part of the RF process to increase the signal-to-noise ratio and decrease the need for damping (e.g., Gurrola et al., 1995). The number of individual RFs for each stacked trace ranges from 8 to 40.

4.3.3 Velocity Modelling from Stacked RF

We aimed to determine the 1D velocity model for each station from their calculated stacked RF. To enhance the resolution of the images and improve the signal-to-noise ratio, we employ a technique of stacking multiple RFs. This involves combining various RFs obtained from different back azimuths, as demonstrated in Supplementary Figure 4.5. We employed an approach known as iterative deconvolution to reduce the variance between the observed and the synthetic RF (e.g., Ligorria and Ammon, 1999). Synthetic seismograms were calculated using the method of Randall (1989), which is based on the reflection-matrix technique of Kennett (1983) and Ligorria and Ammon (1999). The ak135 initial velocity model which depicts a close-to-constant velocity layer for the lithosphere is utilized to get Vp and Vs during the inversion (Kennett et al., 1995; Kibret et al., 2022). The ak135 model was selected for the purposes of comparing the findings of this investigation with those of prior studies conducted by authors in different areas (e.g., Kibret et al., 2022), as well as for its facile usability with the CPS software. To calculate the appropriate final synthetic RF and the corresponding 1D velocity model, we checked to see if the RF obtained from the global initial ak135 velocity model (Kennett et al., 1995) matched the stacked RF (Supplementary

Figure 4.3). We move on to the next iteration if the corresponding RF obtained from the global starting ak135 velocity model and the stacked RF do not resemble one another. If the mismatch between the stacking RF and the synthetic RF is bigger, then the derived 1D velocity model obtained from this synthetic RF is rejected. Following the initial inversion, starting with the initial model, all subsequent inversions are performed iteratively until the misfit (the root mean square difference) between the stacked RF and the synthetic RF is within the range of 0.01 to 0.05% (Gurrola et al., 1995; Ligorria and Ammon, 1999). This process is repeated until we have the final 1D velocity model with a corresponding synthetic RF that appears to be the best fit for the stacked RF. Finally, the best fit RF and its corresponding 1D velocity models are automatically selected by comparing the percentage of fit and visual inspection (Figure 4.3).

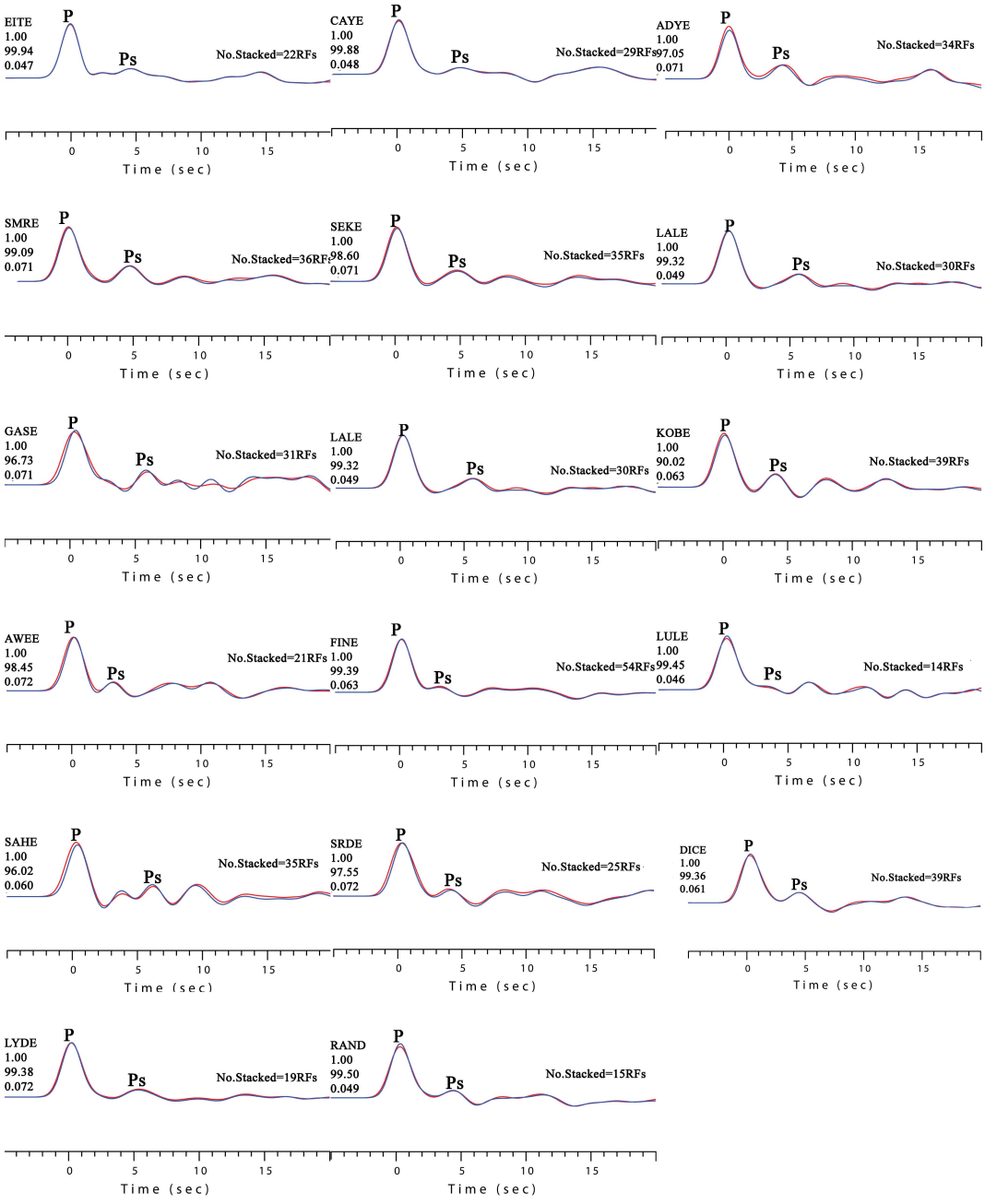

Figure 4.3: Comparison of the observed RFs in blue with the synthetic RF in red for 17 seismic stations. P shows the direct phase, while Ps represent the converted phase, likely from the Moho. The text to the left of the plots lists the name of the station, the Gaussian width parameter, the percentage of model fit between the estimated and observed value, and the applied ray parameters.

The 1D velocity models of Vp and Vs are also produced for each station by inverting best fit synthetic RFs over a range of lower frequencies and ray parameters (Cassidy, 1992; Dugda et al., 2007) (Figure 4.4). Velocities in the 1D models were solved at a depth interval of

2km, and we plot and interpret the top 60km of the models. To interpret the crustal composition, we also calculated the Vp/Vs ratio at each 2km depth interval in the Vs model, (Ligorria and Ammon, 1999) and using the average Vp (6.5 km/s) computed for the same station (Hammond, 2014; Zhu and Kanamori, 2000). For this study, a variety of ray parameters between 0.04–0.069 and Gaussian width factors 1.0 were used. To help interpret the deep crustal structure in 1D velocity models we plot the crustal thickness derived from previous H-k stacking of RFs (e.g., Ahmed et al., 2022; Hammond et al., 2011; Wang et al., 2021). We then re-interpreted the Moho in our 1D models by identifying the largest velocity step within a similar depth range to the previous Moho estimates.

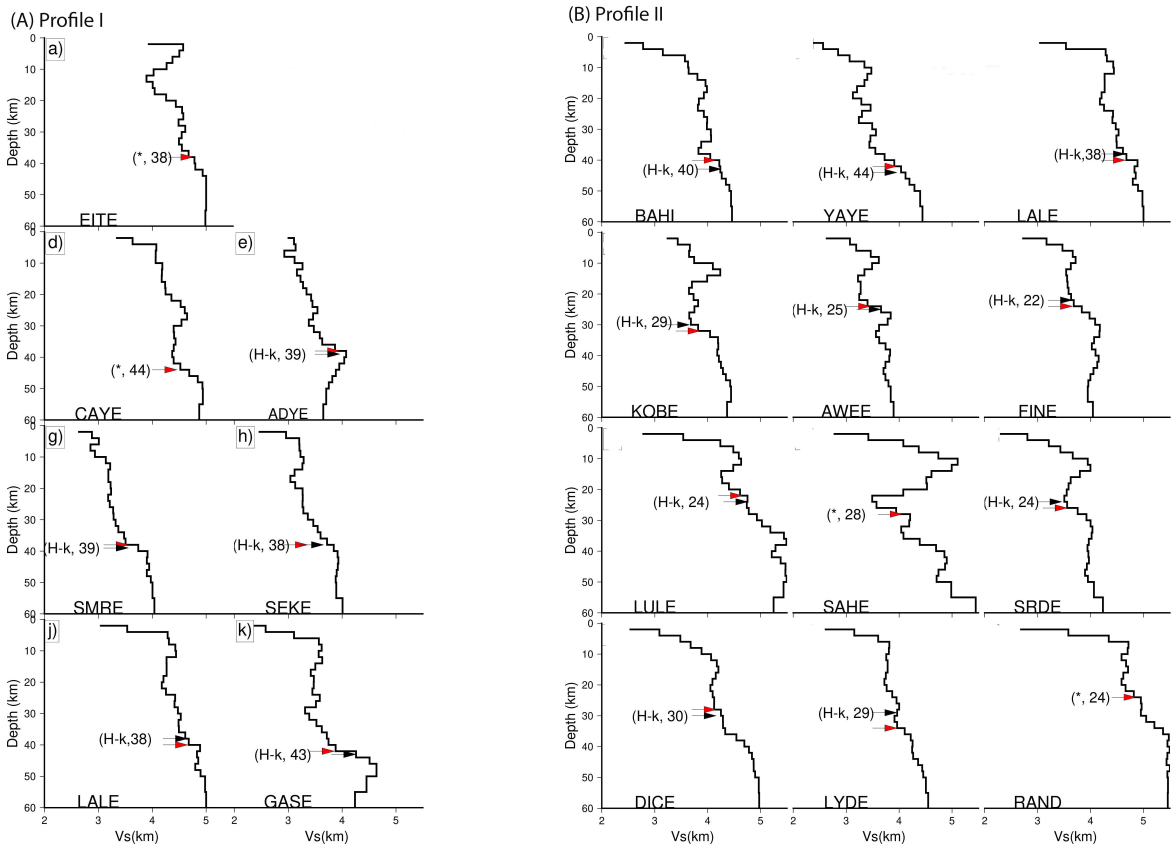

(A) Profile I represent the AA' axis' north-south direction.

(B) Profile II represent the BB' axis' east-west direction.

Figure 4.4: 1D models resulted from RF inversion. The red arrows in Figures (A) and (B) correspond to Moho discontinuities obtained from the inversion. The black arrows in these figures represent the Moho depth calculated in the previous H-k RFs stacking technique (Hammond et al., 2011). The black stars is used to show the stations do not have previously calculated Moho depth values. Profile I represent the AA' axis' north-south direction, whereas profile II displays the BB' axis' east-west direction.

4.3.4 2D Velocity and Vp/Vs Ratios Models

Additionally, we employed the Delaunay triangulation interpolation method to estimate unknown velocities based on several calculated velocities and created a 2D velocity model (Kibret et al., 2022; Ping et al., 2009). The technique assumes there are no points inside any triangle's perimeter and works with three velocities at once. By triangulating and contouring the estimated velocity data we imaged the 2D velocity versus depth plots. we used this interpolation technique as implemented in the GMT plotting software (Kibret et al., 2022; Wessel et al., 2019).

Geophysicists routinely use Vp/Vs data to interpret the presence of partial melt in the crust and typically use Vp/Vs values of >1.9 as evidence (Ahmed et al., 2022; Ebinger et al., 2017; Hammond, 2014; Kibret et al., 2022; Wang et al., 2021). We compute the cumulative relative frequency (Ott and Longneckerv, 2001; Peck et al., 2008) of our Vp/Vs model below a depth of 10 km to quantify the proportion of the mid and lower crust with a Vp/Vs of $>$1.9. We remove the top 10 km from the analysis since high Vp/Vs ratios are more likely associated with sediments. We use the Vp/Vs model acquired at 2km intervals on profiles I and II (9 stations on the NW plateau and 9 stations in Afar) by dividing the frequency of each value by the total number of observations and then multiplying the relative frequency by 100 to convert it to a percent (%) (e.g., Abdulla et al., 2014) (Table 4.1). The percentage of cumulative frequency (PCF) is computed using the Vp/Vs data and its frequency below a depth of 10 km. PCF represents the proportion of the mid and lower crust with a Vp/Vs of $>$1.9, which is an important parameter in our study. Specifically, it provides valuable information on the distribution of Vp/Vs ratios in the crust and can be used to identify areas with anomalous values, which could be indicative of geological structures and processes.

Table 4.1: The table shows the names of stations, the percent of signal power fit between observed and synthetic seismograms, and the number of receiver functions (RFs) used in the analysis during the model fit calculations.

NW Plateau stations	NW Plateau stations	Afar stations	Afar stations
Range of Vs	PCF	Range of Vs	PCF
<1.5	14.29%	<1.5	18.18%
1.5–1.6	19.39%	1.5–1.6	14.14%
1.6–1.7	30.10%	1.6–1.7	25.25%
1.7–1.8	19.90%	1.7–1.8	27.78%
1.8–1.9	15.31%	1.8–1.9	12.63%
>1.9	1.02%	>1.9	2.02%

4.4 Results

4.4.1 Receiver Function

Figure 4.3 shows our observed RFs in blue compared to the synthetic RFs in red. Overall, we detected a clear Ps conversion in both Profiles I and II at delay times from 3 to 6 s, with the arrival time of the Ps discontinuity in the observed stacked RF signal increasing towards the NW plateau. Additionally, our synthetic RFs are very well matched to the observed RFs, with a misfit score ranging from 97.05 to 99.88.

4.4.2 Velocity Models of the NW Plateau

The 1D models of the station on the NW plateau generally show a fairly simple velocity structure with increasing seismic velocity with depth. The profiles fall into 2 distinct classes of characteristic S-wave velocities. Most of the stations (ADYE, SMRE, SEKE, GASE. YAYE) show S-wave velocities of between ∼3–4 km/s for the majority of the crust. Slower velocities than this are in the top ∼5 km for some of the stations. The second class of stations shows somewhat faster velocities through most of the crust. Specifically, stations EITE, CAYE, LALE, and BAHI show seismic velocities between ∼4–4.7 km/s through most of the crust. Again, slower velocities than this are commonly modelled for the uppermost crust at these stations. The 1D models for most of the NW plateau stations also demonstrate a relatively large velocity discontinuity seen at depths between 36 and 44 km (Figure 4.4A).

The 2D profiles provide a means to identify the spatial variability of the major variations in Vs structure, and also to identify finer scale patterns. A significant area of anomalously slow crustal Vs (<3.2km/s) is observed from ADYE, SMRE, and SEKE (Figure 4.5A1). This region is the slowest in the middle of the feature beneath SMRE. While the magnitude of the velocities varies in the anomaly, it generally shows a slightly slowest Vs in the mid-crust at ∼10–25 km depth. This region is flanked on either side by the faster crust (4–4.7 km/s). Vs at mantle depths of more than 40 km is slowest (<4.0 km/s) beneath regions of the slower crust, while the higher Vs crust beneath EITE, CAYE, and LALE is underlain by a faster mantle of >4.0 km/s.

The 2D Vp/Vs profiles for the NW plateau show that most of the crust has a Vp/Vs of 1.7 to 1.8 (Figure 4.5A2). The exceptions are regions in the mid-crust at ∼10–25 km where Vp/Vs is generally 1.8–1.9. This depth range of the high Vp/Vs is similar to the depth range across which Vs is commonly slower, causing the local Vs inversion described above. In addition, in the middle portion of the profile, Vp/Vs in the uppermost crust is locally as

high as 2.0.

4.4.3 Velocity Models of Afar

The broad characteristics and pattern of variabilities in Vs in the Afar stations are quite different from the NW plateau. Firstly, the overall Vs is generally relatively faster at the majority of stations compared to the NW plateau (Figure 4.4). Except for the top 5km under station AWEE, all stations have crustal Vs that are mostly between 3.5 and 4.5 km/s (Figure 4.4B). However, set within this simpler framework, far more dramatic local spatial and depth variability is observed. For example, a noticeable feature common in the profiles is that relatively fast velocities of ∼4 km/s are reached at relatively shallow depths, resulting in fairly minimal increases in velocity with depth through the crust (e.g. stations FINE, LYDE, RAND). Some stations also show a very noticeable decrease in velocity at mid-lower crustal depths (e.g. SAHE, LULE, SRDE).

Profile II displays the 2D Vs model that is under Afar and allows us to explore the spatial variations of Vs characteristics identified in the 1D models above. As a reference point geologically and in terms of variability in the Vs structure, the current locus of extension (magmatic segment) is positioned between LULE and SAHE stations. Both these stations have a similar seismic structure with a relatively fast (∼4.5 km /s) Vs at a shallow (∼6–14 km) depth range, underlain by slower velocities at lower crustal depths (∼15–25 km). On either side of the current locus of strain within the rift, the Vs is generally slower, particularly in the lower crust.

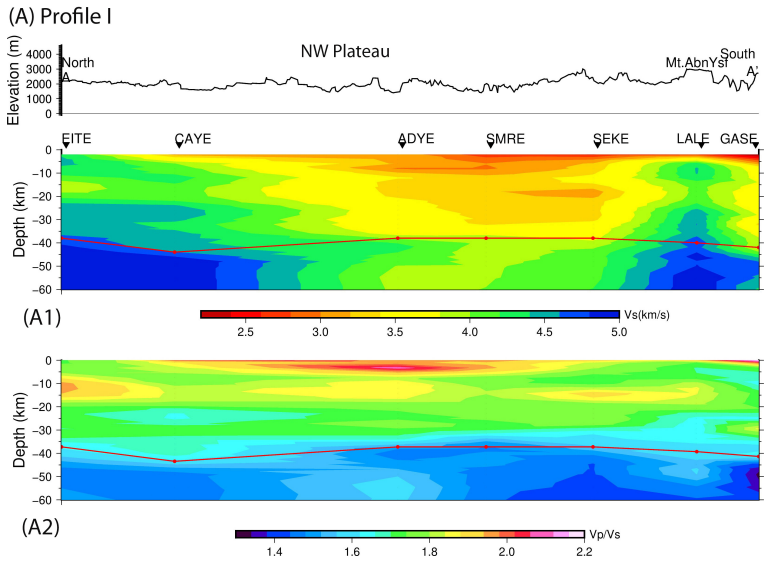

(A) displays a 2D vertical slice taken from profile I of Figure 4.1 spanning the area from station EITE (in Eritrea) to GASE along the NW plateau (from north to south).

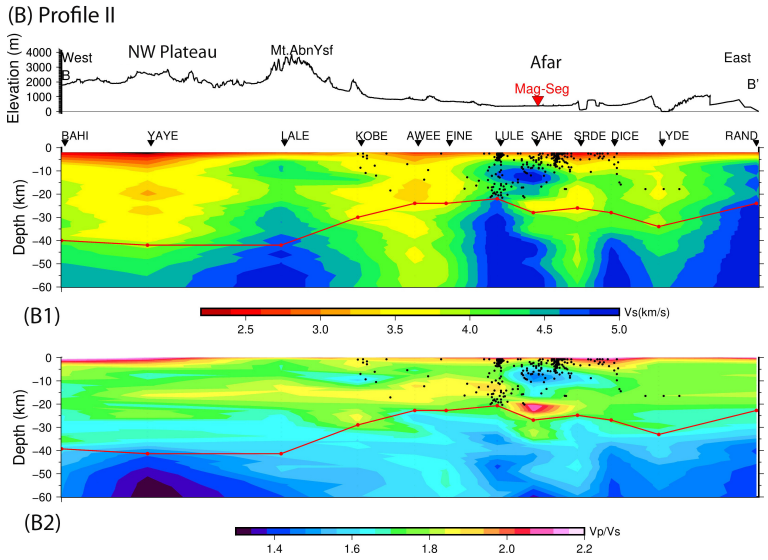

(B) displays a 2D vertical slice across the Afar profile II of Figure 4.1 from BAHI (at Bahir Dar near Lake Tana) to RAND in Djibouti.

Figure 4.5: Blue denotes faster shear wave velocity, whereas red denotes slower shear wave velocity. However, red denotes a high Vp/Vs ratio, whereas blue denotes a low Vp/Vs ratio. The red inverted triangle represents the location of the magmatic segment in central Afar. The 2D Vs and Vp/Vs models shown in Figure 4.5B1 and B2 were produced by inverting RFs with an east-west alignment (profile II). Under profile II, the earthquake hypocentres from Zwaan et al. (2020) are shown as black circles. The red solid line depicts the shear wave velocity discontinuity shown in the 2D models. The solid black line above profiles I and II may be seen as a 1D topographical map of those two profiles.

Vp/Vs of the Afar crust is mostly in the 1.7–1.8 range (Figure 4.5B2). In particular, the east of Afar shows a distinct lack of variability in Vp/Vs from these values. In contrast beneath the magmatic segment, the Vp/Vs at ∼20–25 km depth is locally and markedly high at over 2.0. Beneath the west of Afar, the Vp/Vs shows elevated values of up to ∼1.9 at ∼10–20 km depth. Vp/Vs is also locally elevated in the uppermost ∼5 km in places.

4.4.4 Moho Depth of the NW Plateau

The Moho depth of the NW plateau is first calculated from the 1D Vs model and compared with the Vp/Vs model from the 1D and 2D Vs models. The 1D Vs model and the 2D model both show that the Moho is both an abrupt (ADYE:38km, SMRE:38km, LALE:40km, GASE:42km, and BAHI:38km) and a gradational (EITE:38km, CAYE:44km, SEKE:38km, and YAYE:42km) discontinuity (Figure 4.4A). The Moho is sharp beneath most of the NW plateau stations. These strong velocity discontinuities are found beneath the bulk of NW plateau stations at depths where they were previously thought to be Moho (Hammond et al., 2011). The thickest crust (about 44 km) is seen at Eritrea's furthest station, CAYE (Figure 4.4). The deepest Moho, 44 km, is imaged at the NW plateau border beneath the CAYE and YAYE stations (Figure 4.5A). However, the NW plateau's crustal thickness varies from 36 to 44 km.

4.4.5 Moho Depth of Afar

Both the 1D Vs and the 2D Vp/Vs models show the Moho depth beneath Afar. However, compared to the NW plateau, only about four Afar stations have strong velocity discontinuities (KOBE:32, AWEE:25km, SRDE:26km, and SAHE:28km). Instead, beneath most of the Afar stations (FINE:24km, LULE:22km, DICE:28km, LYDE:43km, and RAND:24km), a more gradational Moho is observed (Figure 4.4B). In Afar, the crustal thickness ranges from 26 to 30 km (Figure 4.4B). Afar has a thinner crust than the NW plateau (Figure 4.5B), with the AWEE station at the Tendaho graben in Central Afar having the thinnest crust (26 km) in our region.

4.4.6 The Percentage of Cumulative Frequency

The percentage of cumulative frequency (PCF) is computed using the Vp/Vs data and its frequency below a depth of 10km. The analysis shows that 2% and 1% of the Afar and NW plateau crust, respectively, have Vp/Vs of >1.9 (Table 4.11).

4.5 Discussion

4.5.1 Velocity Models of the NW plateau

We provide new independent constraints on crustal Vs and Vp/Vs structure beneath the NW Plateau that build on previous S-wave imaging and RFs studies (Chambers et al., 2019; Hammond et al., 2011) (Figure 4.5A). Our result shows that the regions of slow Vs ($<$3.2 km/s) lie beneath the broader area of the NW plateau. In particular in profile I the region between SMRE and SEKE is characterized by such velocities at 10–25 km depth. These velocities are slower than expected. For example, silicic and intermediate rocks that are most typical of continental crust have Vs at these depths in the range of 3.6 to 3.8 km/s Birch (1960); Simmons (1964), with mafic rocks having typical Vs of $>$3.8 km/s at crustal temperatures of 600^{o}C (Chambers et al., 2019; Hacker and Abers, 2004). The velocities we observe are significantly slower and require alternative explanations than simply variation in rock types, such as warmer temperatures or the presence of a fluid phase.

Uniquely constraining the slow Vs as being from high temperature or the presence of fluids is difficult without independent constraints. However, broadly speaking the reduction in Vs with an increase in temperature in a range believable for the crust is insufficient to explain the observations. For example, intermediate rocks at 600^{o}C, more typical of lower crustal conditions have Vs of $\sim$3.7 km/s. We, therefore, turn to the presence of a fluid phase, such as partial melt to explain the regions of especially slow Vs (e.g., Artemieva et al., 2004). Direct support for our interpretation comes from our own computed Vp/Vs. In general, regions with slow Vs (3.2 km/s) have a high Vp/Vs (1.85–2.1). Vp/Vs of typical continental crust is $<$1.8 (Christensen, 1996; Hammond et al., 2011), while for mafic rock it is 1.7–1.9 (Hammond et al., 2011). However, in localized places (1% of the NW Plateau crust as shown by the PCF analysis (Table 4.1) we observe Vp/Vs of $>$1.9, which can only really be explained by the presence of a fluid phase such as partial melt.

Independent constraints on the presence of partial melt at this mid-crustal depth range beneath the NW plateau are also supported by other studies (Chambers et al., 2019; Eshetu et al., 2021; Hammond et al., 2011). For example, seismic imaging from ambient noise and surface waves show slow Vs ($\sim$3.2 km/s) at 10 km depth beneath localized regions of the NW plateau, which are interpreted as regions including partial melt (e.g., Chambers et al., 2019). The presence of localized regions of partial melt beneath the NW plateau is further supported by Ahmed et al. (2022) who observed bulk crustal Vp/Vs of $>$1.85 beneath limited stations in the area. Additionally, scattered deep crustal earthquakes and high electrical conductivities below 10km beneath the NW plateau have been previously inter-

preted as being magma or fluid-related Keir et al. (2009); Whaler and Hautot (2006). The presence of melt in the NW plateau crust is somewhat unexpected, with potential explanations for the melt source being from decompression melting of the asthenosphere directly beneath a broadly extending plateau (Birhanu et al., 2016), or from lateral migration of magma from beneath the rift (e.g., Ebinger et al., 2017).

4.5.2 Velocity Models of Afar

The uppermost crustal velocity structure beneath Afar is very variable (Figure 4.5B). Thickest regions of slow Vs (<3.2 km/s) and high Vp/Vs at depths of <6 km commonly correlate well with the position of sedimentary and volcanic material which agrees with previous findings (Chambers et al., 2021; Hammond et al., 2011; Kibret et al., 2019). Below the uppermost crust, the seismic velocity beneath Afar is fairly homogeneous except beneath the current locus of strain at the magmatic segments. East of the magmatic segment, Vs is fairly high (>4.0 km/s) and Vp/Vs is mostly 1.75–1.8, consistent with continental crust intruded with now solidified mafic rock. West of the magmatic segment however, Vs is slightly slow (∼3.2–4.0 km/s) but with distinctively high Vp/Vs of ∼1.8–1.9, more suggestive of mafic crust including limited partial melt. This suggests asymmetry in present-day magmatic modification of the crust beneath Afar, with ongoing processes more focused between the magmatic segment and the western Afar margin. Beneath the magmatic segment, a distinctive feature is slow Vs combined with especially high Vp/Vs (2.0) at depths of ∼20–25 km (i.e. lower crust), which is best explained by the presence of partial melt. The PCF analysis shows that this region constitutes 2% of the crust (Table 4.1), and strongly points towards the lower crust being a major and long-lived magma storage zone. In the upper crust beneath the magmatic segment, we observe high Vs (>4.5 km/s) but anomalously low Vp/Vs. This combination is difficult to explain without the presence of a gas phase (Whittington et al., 2009), which is consistent with vigorous magmatic degassing from solidifying intrusions, and also a vigorous hydrothermal system (Ebinger et al., 2017; Lee et al., 2016; Roecker et al., 2017).

While the study of seismic wave velocities beneath EITE revealed a well-defined velocity discontinuity at the Moho, with a noticeable difference between the velocities of the crust and the mantle, the Vs at the Moho beneath KOBE and SRDE were found to be smaller than those of the upper-to-mid crust. This may be due to high-velocity materials intruding and solidifying in the region, or the Moho's material properties may have been altered by partial melting caused by the surrounding nature of the interface (e.g., Chambers et al., 2019). Furthermore, the Vs distribution beneath the SAHE station, situated on the rift axis where magmatic activity is observed, is scattered, indicating potential crustal heterogeneity

resulting from repeated magmatic intrusion and solidification at different times as a similar crustal property is observed beneath the Central Main Ethiopian Rift (MER) axis (e.g., Kibret et al., 2022). These observations provide further insight into the complex geological processes occurring in the Afar region and suggest that future studies may benefit from a more detailed investigation of the local geological features and their effects on seismic wave velocities.

4.5.3 Moho depth and nature

We have derived a new, continuous Moho map by interpolating the RF constraints to characterize the Vs and Moho variability for the NW plateau and Afar stations. To first-order, the crustal thickness in our interpretation assumes the Moho depth at the base of the relatively large velocity gradient (e.g., Bello et al., 2021; Clitheroe et al., 2000; Collins, 1999; Collins et al., 2003; Fontaine and Kennett, 2013), and our Moho depths are consistent with previous studies (e.g., Ahmed et al., 2022; Hammond et al., 2011). However, beneath most of our stations in the NW plateau, the Moho is characterized by a sharp velocity contrast, whereas in Afar, the velocity contrasts are more commonly gradational. The gradational velocity gradient across the Afar Moho as compared to the NW plateau might be due to the increasing lower crustal mafic intrusion, which reduces the velocity contrast between crust and mantle. This agrees with previous findings that mafic intrusions in the lower crust can alter the nature of the Moho to become more gradational (e.g., Hodgson et al., 2017; Thybo and Artemieva, 2019). A similar observation is inferred beneath the southern Tanganyika Rift of Ufifipa (e.g. Hodgson et al., 2017). The generally sharper Moho beneath the NW plateau suggests magma modification of the lower crust is less common, pointing towards spatially isolated supply from depth.

4.6 Conclusions

This study utilized teleseismic data collected from 17 broadband stations in Ethiopia and Eritrea between 2000 and 2013 to investigate the crustal structure of the region. The results revealed that the majority of the crust has faster Vs (4–4.7 km/s) with a regionally slower Vs (3.2 km/s) and a high ratio of Vp/Vs (1.85–2.0) in the mid-crust of the NW Plateau at a depth of 10–25 km. The analysis also identified homogeneous crust beneath most of the Afar stations, except for faster material (4.5 km/s) observed in the upper-mid crust beneath the magmatic segment, which is the current locus of extension. Conversely, the magmatic segment of Afar revealed slower Vs (3.2 km/s) and a high Vp/Vs (2.0) at deeper crustal depths (20–25 km). Furthermore, slow Vs (sim3.2 km/s) and a high Vp/Vs ($>$1.9) were inferred beneath the NW Plateau, indicating the presence of partial melt. These results

suggest the presence of mafic crust with fluid phases, such as partial melt, beneath Afar and the NW Plateau. They have important implications for our understanding of the tectonic processes and geodynamic evolution of the region. The study provides valuable insights into the crustal structure and composition of the area and could pave the way for further research.

CHAPTER 5

CRUSTAL THICKNESS ESTIMATES BENEATH THE ETHIOPIAN PLATEAUS AND NORTHERN MAIN ETHIOPIAN RIFT

Abstract

This study explores the lithospheric structure in the Northwest (NW) plateau, Northern Main Ethiopian Rift (NMER), and Southeast (SE) plateau using Receiver Functions (RFs) derived from teleseismic waveform data $30^{\circ} - 30^{\circ}$. Both plateaus experienced uplift from plume activity and flood basalt volcanism. The Nubian Plate on the western plateau has a more mafic composition ($Vp/Vs \sim 1.6$) compared to the Somalian Plate ($Vp/Vs \sim 1.6$ to 1.8). High shear wave velocities (Vs) exceeding 4.5 km/s at depths of $7-30$ km beneath the NMER suggest intruded material, solidified mafic intrusions, or cooled magmatic intrusion. The crust beneath the NMER also shows high Vp/Vs values exceeding 1.9 below 35 km, indicating potential partial melt from the upper mantle due to magmatic activity or different crustal compositions. To the northwest of the NMER, regions with high Vs exceeding 4.5 km/s are underlain by lower Vs values of $3.0 - 3.3$ km/s, while a high Vp/Vs ratio of $1.9 - 2.0$ is observed at depths of $25 - 35$ km. On the southeast side, high Vs values of 4.4 km/s at 15 km depth suggest intrusive material, accompanied by low Vs values and high Vp/Vs ratios exceeding 1.9, indicating partial melting or magmatic fluid release. Across the rift axis, the crust thickness varies from $36 - 44$ km in the NW plateau to $38 - 42$ km in the SE plateau. These variations in crustal thinning and lithospheric composition support the hypothesis of magma-assisted rifting as the region transitions from continental to oceanic rift.

5.1 Introduction

The East African rift architecture is an ideal place to study the evolution of continental extension, lithospheric rupture, and focused continental deformation (Corti, 2009; Ebinger, 2005). Lithospheric Extension from continental rifting to sea-floor spreading due to the

rise of magma and axial dyking (e.g., Ebinger and Casey, 2001) appear to cause comparable amount of strain than normal faults (Rowland et al., 2007). Subsequently, however, magma injection replaced mechanical failure as the dominant strain accommodation mechanism (Cornwell et al., 2010; Ebinger and Casey, 2001). The Nubian and Somalian plate extension is driven by a combination of mechanical (Hayward and Ebinger, 1996); Hopper et al., 2004) and magmatic (Buck, 1991) extension. Furthermore, it is still unknown how much of the Ethiopian rift extension is occupied by magma intrusion and where the magma is kept in the crust below the rift. Geophysical observations such as MT (Whaler and Hautot, 2006), seismicity investigations (Keir et al., 006b), and geochemical studies (Rooney et al., 2005, 2007) indicate dyke intrusion largely facilitates extension in the MER without marked crustal thinning (Bastow et al., 2010; Cornwell et al., 2010; Dugda et al., 2005; Stuart et al., 2006). However, according to GPS data, 80 percent (Bilham et al., 1999) of the current extension is concentrated in the magmatic segments where the locus of extension is mainly focused due to dike intrusion (Ebinger and Casey, 2001; Keranen et al., 2009). When tectonic forces are required to generate extension via faulting or ductile stretching, the presence of melt-filled fractures caused by magma injection that weakens the lithosphere allowing rifting (Bastow et al., 2010; Buck, 2004). This study constrains a P to S wave receiver function analysis in one profile from 10 temporary seismic stations. Therefore, the purpose of this work is to estimate the crustal structure of the NW plateau, the NMER, and the SE plateau (Figure 1) using teleseismic data collected from 2000–2003 and 2008–2009.

Previous research has shown that the extension of the Nubian and Somalian plates is the result of both mechanical and magmatic processes. However, the specific extent and location of magma intrusion beneath the rift remain uncertain (Agostini et al., 2011; Corti, 2009, 2012; Ebinger et al., 2017). To address this knowledge gap, this study aims to provide insight into the crustal structure of the Northwestern plateau, the North MER, and the Southeastern plateau by analysing teleseismic data collected from 2000 to 2002 and 2008 to 2009. Specifically, we employed a P to S wave receiver function analysis using signals from teleseismic earthquakes with magnitudes greater than 6 mb and epicentral distances between 30^o and 95^o (Figure 5.3). By using purely passive sources seismic signals, we can analyse the crustal thickness and internal structure of the NMER and neighbouring plateaus (Ahmed et al., 2022; Chambers et al., 2019; Hammond, 2014; Hammond et al., 2011). Our primary focus is to understand how magma has influenced the mid- to lower crustal structure of the study area located beneath the rift and plateaus. We constructed 2D Vs and 2D Vp/Vs profiles to illustrate the solidified and melted regions of the rift and plateaus (Kibret et al., 2022, 2023). It is worth noting that although similar receiver function studies

have been conducted in the rift and adjacent plateaus using a different alignment profile, this study specifically emphasizes the study area along a single profile (Figure 5.1).

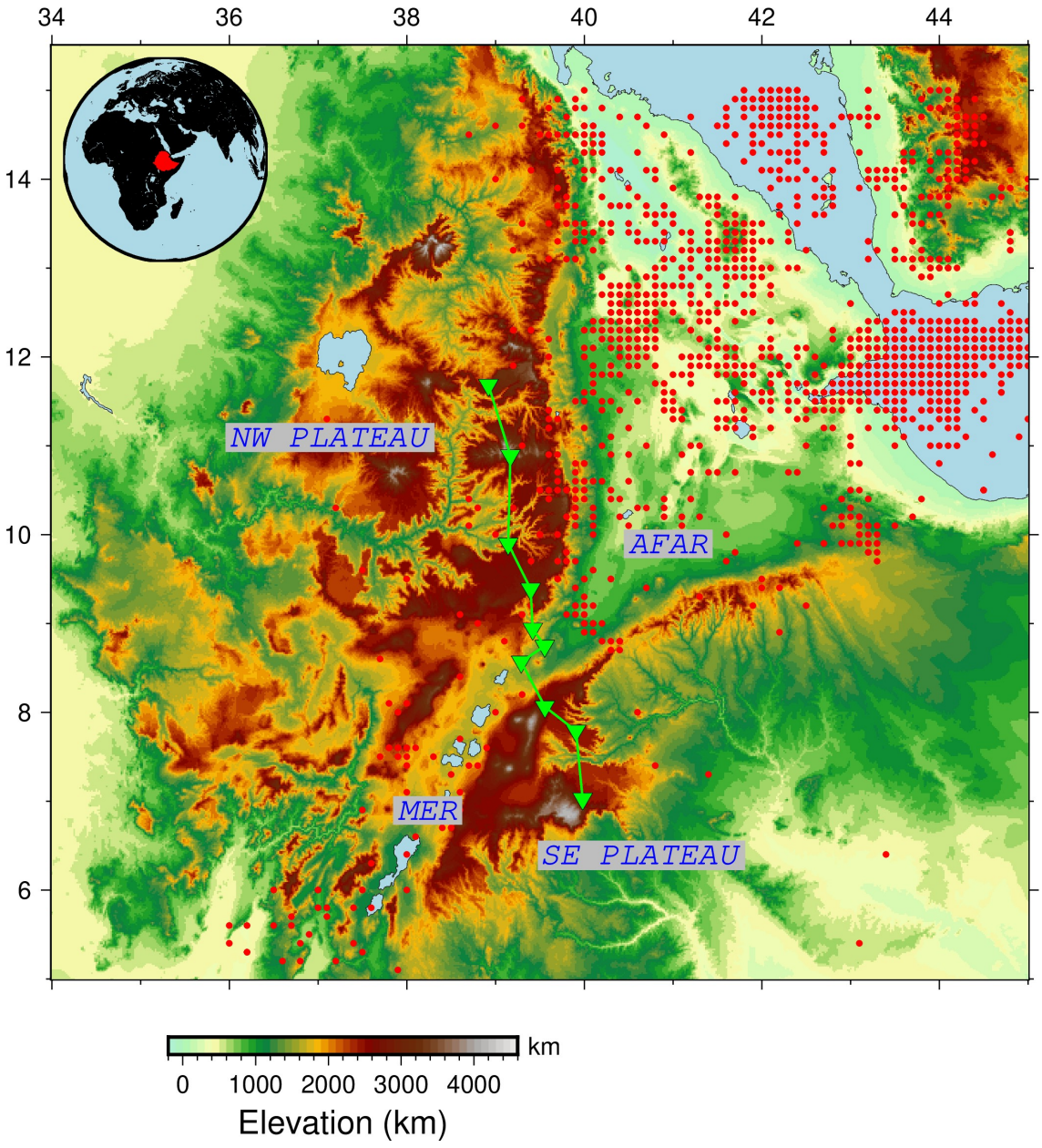

Figure 5.1: Location map of the temporary seismic stations in the MER, Northwestern and Southeastern plateau. The green inverted triangles are stations locations. The red polygon in the inset map to the top left is the study area. The MER refers to the Main Ethiopian rift. The seismic data from these white stations are obtained from the Ethiopia Afar Geoscientific Lithospheric Experiment (EAGLE) and Afar Consortium Network (AFAR) projects. Small red circles are locations of earthquakes for the time period 1960 to end of 2022 are downloaded from http://www.iris.washington.edu

The results of our analysis will provide insight into the distribution and extent of magmatic intrusion in the region and how it may be affecting the lithosphere's ability to accommodate strain. By understanding the crustal structure, we can also gain a better understanding of the tectonic processes that are driving the extension in the East African Rift system. Our study is a valuable contribution to the ongoing efforts to unravel the complex geological history and evolution of the region.

5.2 Previous constraints on crustal structure and seismicity

5.2.1 Previous crustal structure studies

Constraints on the crustal structure observed solidified materials beneath parts of the NW plateau from several geophysical techniques including ambient noise (Chambers et al., 2019; Eshetu et al., 2021), radial seismic anisotropy (Chambers et al., 2021; Kendall et al., 2006), H-k stacking of receiver functions (Ahmed et al., 2022; Dugda and Nyblade, 2006; Hammond, 2014; Hammond et al., 2011; Wang et al., 2021), magnetotellurics (e.g., Samrock et al., 2018, 2015), and gravity modelling (Cornwell et al., 2006; Lewi et al., 2016; Mahatsente et al., 1999; Mammo, 2013; Mickus et al., 2007; Tessema and Antoine, 2004; Woldetinsae and Gotze, 2005). The high seismic velocities in the seismic studies and the high positive Bouguer anomalies in the gravity studies favours an interpretation of their origin being a solidified mafic intrusion (Chambers et al., 2019; Cornwell et al., 2006; Mahatsente et al., 1999; Tiberi et al., 2005). Likewise, some research found high Vp/Vs ratios and high seismic velocity zones along the rift axis, which were interpreted as signs of the presence of a molten fraction in fractures within solidified mafic intrusions (e.g., Daly et al., 2008). Moreover, the EAGLE active source experiment also observed a fast Vp layer in the lower crust coupled with a dense lower crust beneath the northwestern plateau (Chambers et al., 2019; Cornwell et al., 2006; Mackenzie et al., 2005; Maguire et al., 2006). In contrast, ongoing magmatism and partial melt in the lower crust are also observed from the different geophysical studies such as magnetotelluric (Whaler and Hautot, 2006) and seismic anisotropy (Bastow et al., 2010; Kendall et al., 2005; Paulatto et al., 2010). The western rift boundary (Nubian plate), which has a crust that is thicker (40–43 km) than the eastern flank (Somalian plate) (38–40 km), is thought to have a mafic crust with partial melt and Vp/Vs $>$2.0. In general, there is a strong association between the locations of slow Vs from seismology and high conductivities, providing more evidence that these anomalies are produced by partial melt (Chambers et al., 2019; Whaler and Hautot, 2006). However, the deeper high conductivity anomalies are thought to be formed by partial melt in the sub-volcanic plumbing system, whereas the shallowest anomaly is thought to be created by

hydrothermal fluids (Ebinger et al., 2017; Hübert et al., 2018).

In Table 5.1, we provide a summary of earlier discoveries of the crustal thickness determined from the seismic and gravity methods.

Table 5.1: A Summary of the findings of previous receiver function studies and gravity modeling to calculate the Moho depth in MER, Southeastern and Northwestern plateau.

Location	Moho (km) RFs	Source	Moho (km) Gravity	Source
MER	27–40	Dugda et al. (2005); Keranen et al. (2009); Mackenzie et al. (2005)	∼32–38	Cornwell et al. (2006); Emishaw et al. (2017); Mickus et al. (2007); Tiberi et al. (2005); Mahatsente et al. (1999); Mammo (2013)
E plateau	32-44	Dugda et al. (2005); Stuart et al. (2006); Cornwell et al. (2010); Hammond et al. (2011); Hammond (2014); Mackenzie et al. (2005)	34-38	Mahatsente et al. (1999); Tessema and Antoine (2004); Cornwell et al. (2006); Mickus et al. (2007)
W plateau	38–48	Hammond et al. (2011); Stuart et al. (2006); Wang et al. (2021)	38-51	Mahatsente et al. (1999); Mammo (2013); Tessema and Antoine (2004); Cornwell et al. (2006); Woldetinsae and Gotze (2005); Mickus et al. (2007)

Compared to the NW plateaus, the MER has a typically thinner crust and a greater Vp/Vs ratio (Ahmed et al., 2022; Chambers et al., 2019; Hammond et al., 2011). Beneath the rift valley crust, Vs is heterogeneous laterally and with depth. In particular, slow Vs and high Vp/Vs ratio is localized beneath volcanic centres in the upper-mid crust but ubiquitously slow in the lower crust. In particular, slow Vs and high Vp/Vs ratio are restricted to the upper-mid crust beneath volcanic centres but are pervasively sluggish in the lower crust (Chambers et al., 2019; Hammond et al., 2011; Kibret et al., 2022). Prior seismic and gravity investigations have increased our understanding of a wide zone of heavily intruded mafic crustal underplate and/or frozen magmatic segment in the axis of the MER south of Fentale Volcano with seismic velocities similar to oceanic crust (Daly et al., 2008; Dugda

et al., 2005; Ebinger and Casey, 2001; Keranen et al., 2004; Mackenzie et al., 2005; Stuart et al., 2006; Tiberi et al., 2005). Additional magnetotelluric (MT) investigations in the CMER have revealed high conductivity anomalies linked with hydrothermal fluids and young surface volcanism in the topmost crust at ∼1–2 km and the upper crust at ∼3–6 km depth (e.g., Whaler and Hautot, 2006). Similar deep high conductivity anomalies, interpreted as evidence of partial melt in the subvolcanic plumbing system, were found in the mid-to-lower crust at depths of 15–25 km beneath the rift axis (Desissa et al., 2013; Ebinger et al., 2017; Hammond, 2014; Hübert et al., 2018; Johnson, 2012; Kibret et al., 2022, 2023). Generally speaking, there is a good correlation between the areas of slow Vs from seismology, low-density material from gravity measurements, and high conductivities from MT, providing credence to the idea that these anomalies are caused by partial melt.

This study analyses data from a single profile aligned 10 temporary broadband seismic stations along the North-South direction in order to provide crustal thickness and Vp/Vs result using station-specific mean crustal Vp. Using these values, we then constrain the distribution of melting to investigate the nature of the crust underlying the plateaus and the MER. By evaluating the crustal composition and melt characteristic of the MER and the adjacent plateaus, we then try to provide the typical rifting characteristic of the region. This work tries to characterize additional constraints on the hypothesis that the rifting of the MER is highly facilitated by the solidified intrusion and localized melt.

5.2.2 *Previous Seismicity Studies*

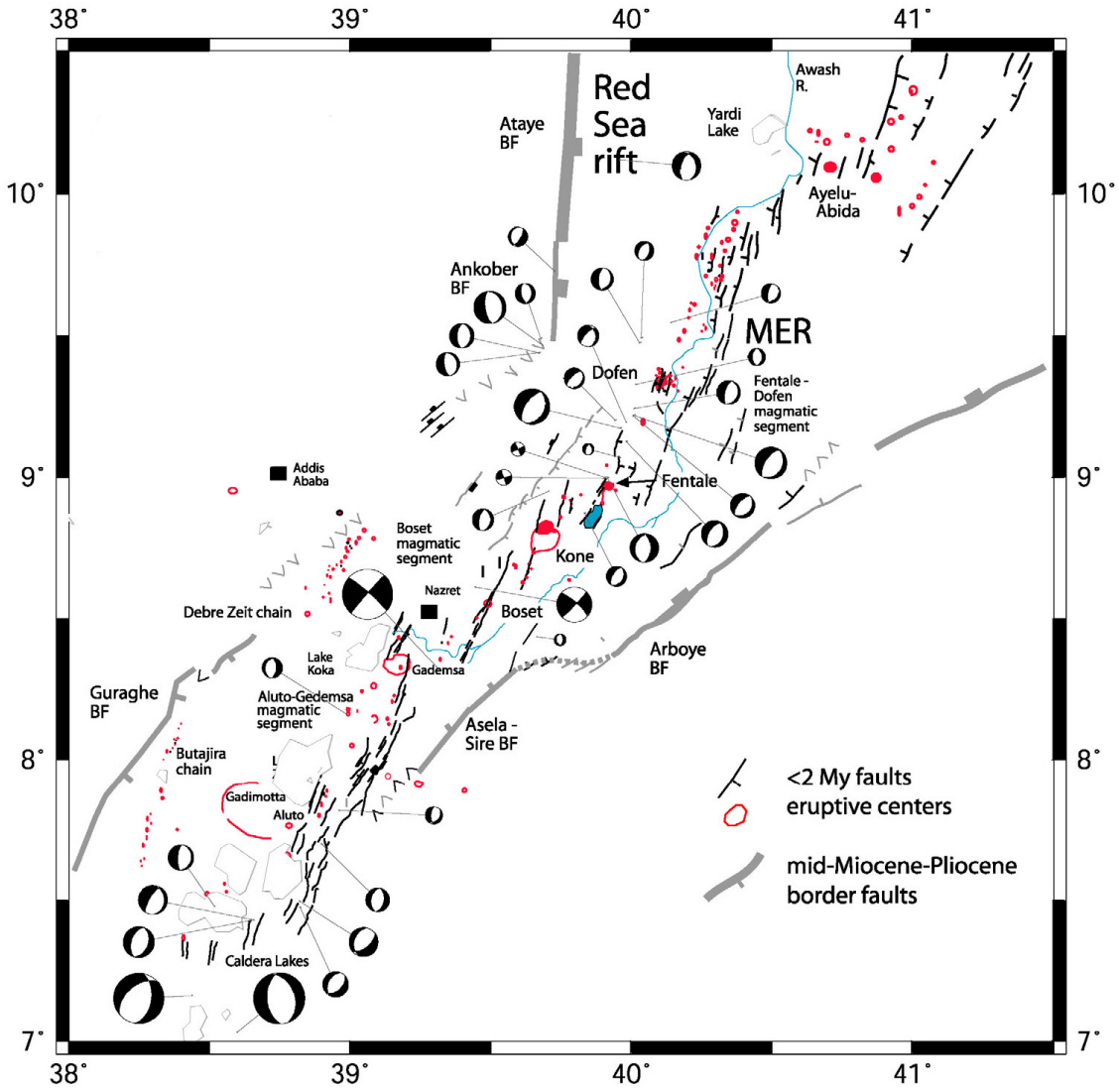

Figure 5.2: The faults which cut lavas, magmatic segments in the Miocene border faults around MER. Fault plane solutions scaled to local magnitude of 1.17–5.3 (adapted from Keir et al., 2006a).

The evidence presented in Figure 5.2 strongly supports the notion that faults exhibiting a normal dip-slip mechanism are prevalent in the earthquake focal mechanisms studied in Ethiopia. These faults predominantly align in a north-to-northeast (NNE) direction. Through detailed analysis of these focal mechanisms, it is consistently observed that the orientation of the minimum compressive stress corresponds closely to an eastward azimuth of approximately 103 degrees from North. This alignment is further supported by the convergence of geodetic data and global plate kinematic constraints, providing substantial

reinforcement to the correlation between them (Keir et al., 2006a).

5.3 Data and Methods

5.3.1 Data

We use data from temporary seismic deployments in the Main Ethiopian Rift (MER) and surrounding plateaus. The data were acquired from the legacy temporary network project that was conducted from 2000 to 2002 and 2008 to 2009 recorded by three-component broadband Guralp CMG-6TD and Guralp CMG-ESPCD seismometers with a 50-Hz sampling rate. The data were collected from the Ethiopian Broadband Seismic Experiment (Nyblade, 2002), the Ethiopia Afar Geoscientific Lithospheric Experiment (EAGLE) (Bastow et al., 2005). We downloaded the teleseismic waveform data from the Incorporated Research Institutions for Seismology (IRIS) Data Management Center (DMC) archive.

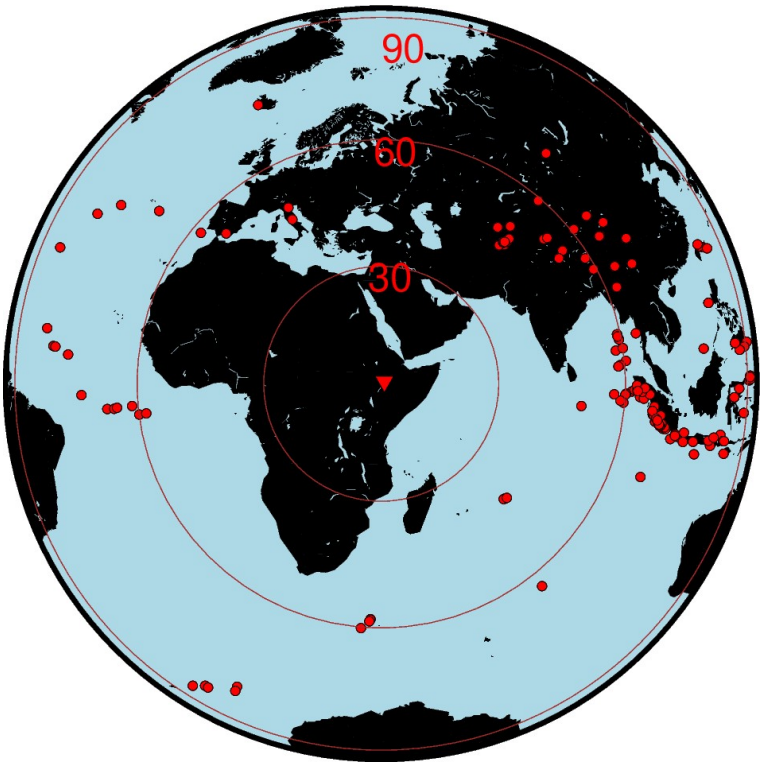

Figure 5.3: The red circular symbols represent the locations of teleseismic earthquakes that occurred between 2000–2002 and 2008–2009 with a magnitude greater than or equal to 6 mb and within epicentral distances between 30^o and 95^o which is denoted by brown circles. The red triangle in the centre of brown circles represent the study area. These earthquake data were recorded by the Ethiopia Afar Geoscientific Lithospheric Experiment (EAGLE) and Afar Consortium Network (AFAR) projects.

5.3.2 Method

Receiver function (RF) technique, a popular time-series method to image the crust and upper mantle and seismic velocity (Ammon, 1991; Ammon et al., 1990; Dugda et al., 2005; Kibret et al., 2019, 2022; Langston, 1979). When a seismic wave strike an interface between two layers the have possible case of being converted from the direct P to S wave. The RF is calculated by the deconvolution of the radial or transverse component of the seismogram from the vertical component. Therefore, the method makes use of the amplitude and timing of the P to S wave conversions (Ps) and reverberation from discontinuities underneath a seismic station (Figure 6-2) (Ammon, 1991; Langston, 1979) to get interpretable results that constrain the underlying geology. We show the schematic diagram of the direct P phase and the converted wave forms in the radial receiver function calculation obtained from the deconvolution of vertical with radial component at a seismic station (Figure 6-2).

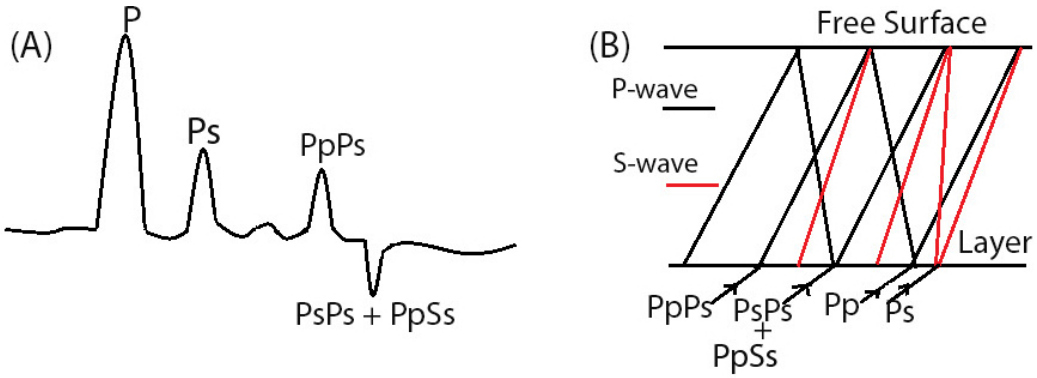

Figure 5.4: (A) is a receiver function that shows the direct P-wave and the reverberations (Ps, PpPs, PsPs + PpSs) and (B) is a graphical representation ray diagram of receiver functions identifying the major P- to S converted phases that illustrates the direct P, Ps, PpPs and PpSs phases that comprises the receiver function for a single half-space.

The study applied RFs technique which utilized teleseismic earthquake with a magnitude of > 6.0 and epicentral distance of 30^o to 90^o Ammon (1991); Langston (1979). The range of epicentral distance helps to avoid triplication caused by multiple arrivals in the direct P-wave occurring at distances $<30^o$ and multiplication from core mantle boundary for signals with epicentral distances $>90^o$ (Figure 5.3). The signals used in the study are those which show clean P arrival and is cut with a cosine taper function for a length of 50 s (10 s before and 40 s after onset of the P-wave arrival).

The parameter determining width of the Gaussian filter was set to $\alpha = 1.0$ for each deconvolution. Then, a low-pass Gaussian filter removes high-frequency noises that are not filtered by the deconvolution to acquire better P onset arrival time. To get better quality of

P-to-S converted phases and its multiples all selected and pre-processed RFs in one station are stacked before the beginning of 1D velocity inversion.

During the inversion, the study applies ak135 VM (Kennett et al., 1995) as the initial VM to calculate the best fit velocity structure. By using the initial VM and the Gaussian width parameter of ∼1.0 (Ammon, 1991; Ammon et al., 1990; Randall, 1989; Zandt and Ammon, 1995) the synthetic RFs and the corresponding 1D velocity values are iteratively calculated from the stacked RFs using the open-source code from Computer Programs for Seismology (CPS) (Herrmann and Ammon, 2002; Kibret et al., 2022; Stuart et al., 2006). The iteration halts when the synthetic receiver function (blue colour) begins to repeat itself without having significant modification during fitting process with the observed receiver function (red colour) (Kibret et al., 2019; Ligorria and Ammon, 1999). The final level of best fit calculated RF is checked by using both visual inspection and the calculated percentage of signal power fit. Accurate calculations of the crustal thicknesses from Vs and Vp/Vs are made using synthetic RF from all ten stations under the MER and the surrounding NW and SE plateaus (Figure 6-6).

The 1 D VM for each station is changed to the 2 D VM for the profile using the Delaunay triangulation interpolation method. This technique uses a number of known calculated velocities to predict a number of unknown velocities (Kibret et al., 2022; Ping et al., 2009). The 2 D velocity versus depth plot and interpolation are estimated and modelled using the GMT plotting tool (Wessel et al., 2019).

The Moho depth, crustal thickness, and the Vp/Vs ratio are all significantly influenced by the average crustal Vp values (Youssof et al., 2013). The average Vp values for each station are applied to identify the crustal material properties and Moho discontinuities at the P-to-S wave conversions point. The topography of the Moho along the profile is evident as the line drawn through the 2 D Vp/Vs and 2 D Vs strong contrast at the bottom of the lower crust (Figure 6-6).

5.4 Results and Discussions

5.4.1 Results

Observed and Synthetic Receiver Functions

Figure 5.5 plots the observed and synthetic receiver function with degree of fit >90%. Crustal thicknesses, Vs and Vp/Vs at every 2 km depth are calculated from synthetic RFs of the ten stations under the MER and the surrounding NW and SE plateaus (Figure 5.7). The

first results which are calculated in the inversion processes are the simple stack observed RF models that contains the arrival times of the Ps and the remaining multiple phases. Hence, the synthetic RF models are iteratively generated with the corresponding VM until we obtain the best fit model that take the possible highest percentage of fit, which are >90% (Figure 5.5 and Table 5.2). The red RF models are the observed waveform and the blue ones represents the synthetic models. The observed RFs models are obtained from the deconvolution of the radial component from the horizontal component of the teleseismic earthquakes.

Figure 5.5 shows a relatively excellent fit between observed and calculated RFs. The inverted VM shows normal crustal properties beneath the NW plateaus station, but high-velocity values (>4.0km/s) are recorded beneath INEE station. A very slow Vs value was obtained below the high-velocity zone at depths of 26–40 km, which is unusual compared to previous studies in the area. The slow Vs material reaching a depth of ∼40 km suggests the possible presence of free fluid phase in the continent.

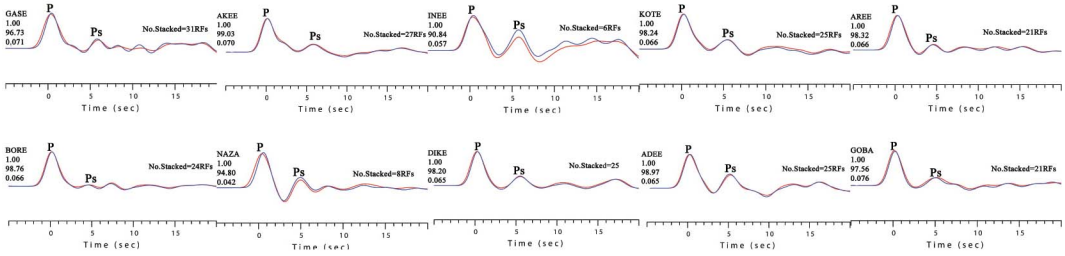

Figure 5.5: Receiver functions of 10 stations which were deployed in the NW plateau, MER and SE plateau. The red RF models represent the observed while the blue RF in the background are the synthetic waveforms. The delay time contrast given for the P wave for all stations is ∼10 s. The direct P arrival with the largest amplitude is denoted by the letter P, and the converted form of P to S is the letter Ps. The station name is represented by the four alphabetic words to the left of each RF, and the three numbers, from top to bottom, stand for the Gaussian parameter, the percentage of fitness, and the ray parameter of the receiver functions.

Table 5.2: Values of Vs at various depths beneath four permanent broadband Stations which are deployed at various geological structures such as rifting and uplifted plateaus. Locations of the stations and resulting values for Moho and the Vp/Vs ratio.

Station	Lat. N^o	Long. E^o	Elevation (m)	Number of RFs	Percentage of fit (%)	Moho depth (km)
GASE	11.68	38.99	2933	31	96.7	42
AKEE	10.89	39.20	3253	27	99.0	36
INEE	9.895	39.24	2647	6	90.8	44
KOTE	9.387	39.50	2932	25	98.2	36
AREE	8.990	39.51	1776	21	98.3	36
BORE	8.845	39.65	1182	24	98.7	38
NAZA	8.568	39.40	1701	8	94.8	46
DIKE	8.262	39.70	2712	25	98.2	40
ADEE	7.791	39.99	2470	25	98.9	44
GOBA	7.027	40.00	2640	21	97.5	42

The 2D velocity model (VM)

Figure 5.6 shows the 1 D Vs models of each station. We built one profile that spans the MER from the NW plateau to the SE plateau. Then, the 2D profiles in Figure 5.6 are plotted using the Delaunay triangulation technique. The blue synthetic RFs in Figure 5.5 are used to compute the 1D VM for the depth range of 2 to 60 km. The blue-colour nearly vertical line is the ak135 initial VM (Kennett et al., 1995) in a homogeneous half-space medium. The ak135 initial VM represents a Vs of $\sim$4.48 km/s is an approximate average velocity of global VM (Kennett et al., 1995).

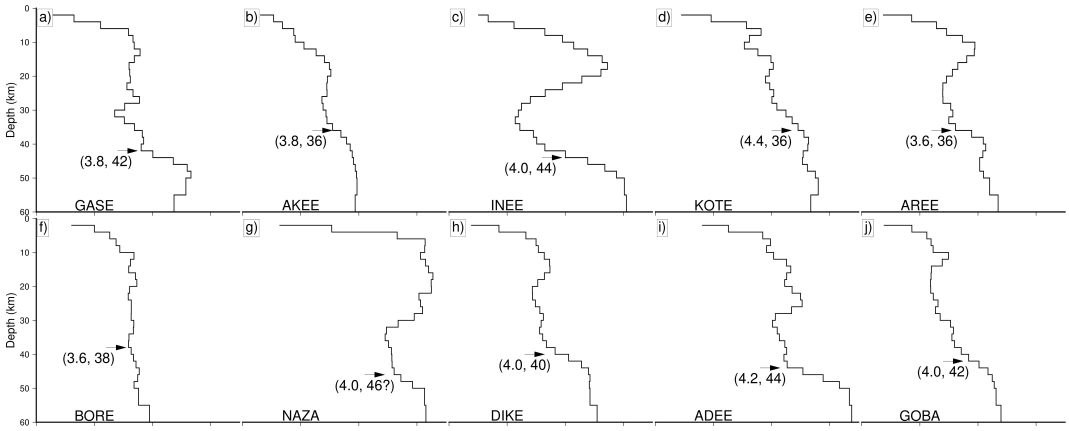

Figure 5.6: The Vs models obtained by inverting receiver functions for the 12 seismic stations. The inversion results in these plots were obtained using programs by Ammon (1991). The Moho is interpreted as the depth at which there is a sharp increase in Vs. The black arrow displays the estimated Moho obtained from the Vs velocity gradient. The Moho depth is indicated by the second number in the bracket, while the first number in the bracket denotes the Vs value at the Moho discontinuity.

At the GASE station, the Moho depth was estimated to be 42 km, and the corresponding Vs value was ∼3.8 km/s. Whereas, the relatively shallower Moho depth of ∼36 km observed beneath AKEE station, with a similar Vs value of 3.8 km/s. At the INEE station, a deep Moho depth of ∼44 km was observed, with a very high velocity discontinuity. At the KOTE station, a very small velocity discontinuity was observed at an estimated Moho depth of around 4.4 km/s. In contrast, a remarkable velocity discontinuity was observed beneath the AREE station, where the velocity jumps from 3.6 km/s to approximately 4.0 km/s. Beneath the BORE station, the velocity was observed to be homogeneous, without any remarkable velocity discontinuity. However, a small discontinuity was observed at a depth of around 38 km, with a value of approximately 3.6 km/s. Next to the BORE station, beneath the NAZA station, a high velocity material was observed at the most shallow depth, from 5 to 20 km, which was underlain by a low velocity material to a depth of around 46 km. However, beneath NAZA, a high velocity discontinuity was observed at the deepest depth. Finally, relative high velocity discontinuities were observed beneath the DIKE, ADEE, and GOBA stations at depths of 40 km, 44 km, and 42 km, respectively, with corresponding Vs values of 4.0 km/s, 4.2 km/s, and 4.0 km/s.

The Two Dimensional Vs and Vp/Vs Models

The 2D Vs and Vp/Vs models (Figure 5.7) displays interesting geological features of the Northwestern (NW) plateau and the Main Ethiopian Rift (MER) region. In the NW plateau,

a high-velocity material is observed at a depth of 12 to 22 km $\pm$ 2 km from the surface, with a velocity of >4.3 km/s, in contrast to the lower-velocity materials beneath the INEE station, which is a relatively low-elevation area. Below this high-velocity material, a low-velocity material of <3.4 km/s covers a vast area ranging from the location of INEE station to the AKEE station. However, in this area the Moho interface is observed beneath this low-velocity material.

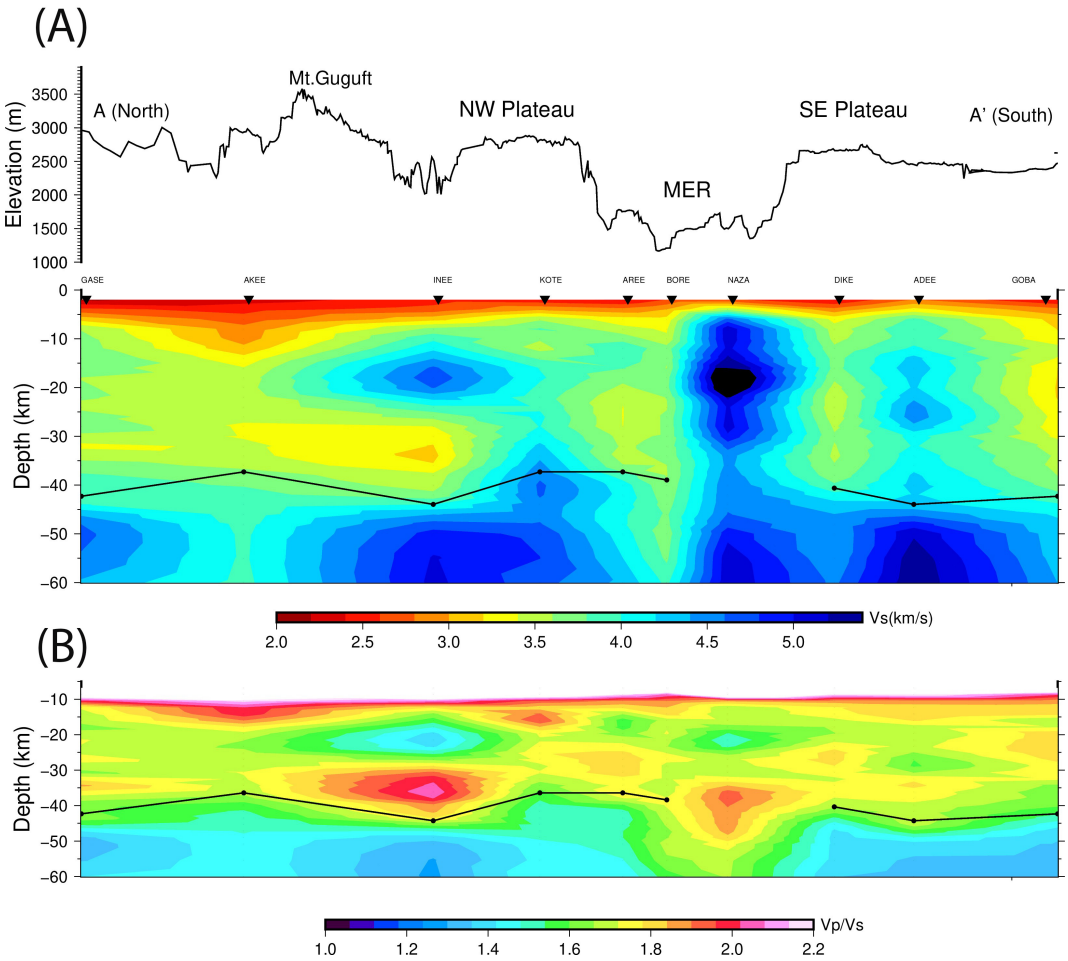

Figure 5.7: (A) shows the 2D Vs model drawn from the 1D Vs result using the Delaunay triangulation technique. The black line above Figure A represents the topography of the region on which the profile passes. (B) indicates the 2 D Vp/Vs plot. The black line in the 2 D plot of both models show the Moho interface indicated in the 1D models of the Vs model.

On the other hand, in the MER region, a very high-velocity material is localized beneath the topmost crustal layer, ranging from the AREE, BORE, and NAZA stations, for the entire depth range. This high-velocity material of >4.6 km/s is observed without any discontinuity throughout the upper-to-mid and lower crusts (Maguire et al., 2006; Mahatsente et al.,

1999), except at the interface where the Moho interface is observed on the NW and SE plateaus.

The study indicates that the low-velocity material observed beneath the INEE and AKEE stations to be high Vp/Vs material. Furthermore, a high Vp/Vs material was observed in the deepest layer of the lower crust, beneath the NMER, with a discontinuity observed at the interface between this material and the high Vs material. The Moho layer, which lies underneath the rift zone, is identified as high Vp/Vs material in the region. Additionally, the Vs at depths shallower than 30km beneath the NMER is >4.6km/s, which is toward the higher end of globally prevalent velocities. However, beneath the NMER, there is a slow Vs body at a deeper depth beneath the high Vs material in the study (Figure 5.6).

The Moho Interface

The results show significant variations in the Moho depth and velocity structure in the study area. The deeper Moho depth observed at the INEE station, along with the sharp velocity discontinuity. The KOTE station, on the other hand, showed a relatively homogeneous lithospheric structure, with a small velocity discontinuity observed at a shallow Moho depth.

5.4.2 Discussion

The Moho Interface

The deeper Moho depth observation at the INEE station, along with the sharp velocity discontinuity, suggests a significant change in the composition and/or temperature of the lithosphere at this location (Chambers et al., 2019; Cornwell et al., 2010; Stuart et al., 2006). This could be indicative of a complex tectonic history or the presence of a deep-seated geological feature in the area. The relatively shallower Moho depth observed at the AKEE station, despite having a similar Vs value to the GASE station, could be attributed to differences in the crustal composition and tectonic history between the two locations. Homogeneous lithospheric structure, beneath the KOTE station with a small velocity discontinuity observed at a shallow Moho depth could be indicative of a more stable and uniform tectonic setting in the area (Kibret et al., 2022).

Lithospheric structure and Compositions

The results obtained from the iterative inversion technique show significant variations in the lithospheric structure and composition at different depths in the study area Ebinger and Sleep (1998); Stuart et al. (2006). The remarkable velocity discontinuity observed

beneath the AREE station indicates a significant change in the lithospheric composition or structure at this depth, which could be related to tectonic activity or the presence of a geological feature. The absence of a significant velocity contrast at the BORE station suggests a more uniform composition and structure of the lithosphere in this region, which could be attributed to a stable tectonic setting. However, the small discontinuity observed at a depth of around 38 km could indicate some heterogeneity in the lithospheric structure at this location, possibly related to the Northern Main Ethiopian rift, where melting and intrusion are usually observed (Cornwell et al., 2006, 2010; Keranen et al., 2009).

The High Vs Materials

The high velocity material observed at the most shallow depth beneath the NAZA station, which was underlain by a low velocity material at a depth of around 46 km, suggests a layer of denser intruded material at the shallowest depths (e.g., Stuart et al., 2006), which is then underlain by less dense material at greater depths. The high velocity discontinuity observed at the deepest depth beneath NAZA indicates a significant change in the lithospheric composition or structure at this depth, which could be related to a deep-seated geological feature or tectonic activity. This observation may be attributed to frozen mafic rock in a high Vs through the lower crust could be due to recent magmatic activity beneath the NMER and the Northwestern plateau (Kibret et al., 2019; Mackenzie et al., 2005).

Specifically, our observation to the NW side of the MER might support previous findings that the magma-driven modification of the crust (Bastow et al., 2008; Chambers et al., 2019; Eshetu et al., 2021; Keranen et al., 2009). Our finding of high Vs beneath the MER and the plateau region might strengthen the previous understanding of extensive extent of intrusion into the upper crust along the NW plateau and NMER (Bastow et al., 2008; Chambers et al., 2019). The crustal intrusion beneath the MER is mainly composed of solidified mafic intrusions beneath the magmatic segments, which is consistent with previous beliefs (Cornwell et al., 2010; Kibret et al., 2023). The slow Vs body beneath the high Vs material in Figure 5.6 is interpreted as evidence for the presence of partial melt. The observed crustal structure beneath NW plateau is consistent with the interpretation that the crust beneath the northwestern side of Afar and the MER has been significantly modified by magmatism (Bastow et al., 2011, 2008; Kendall et al., 2005; Keranen and Klemperer, 2008; Kibret et al., 2022, 2023). However, the intrusion into the upper crust along the western side of the NMER might be more significant than previously thought. The high-velocity zone beneath INEE station could be due to the presence of cooled magmatic intrusion or deep-seated magma reservoirs.

The high Vs materials beneath the NMER (>4.2km/s) are consistent with the presence of upper-lower crustal mafic intrusion . The cause for the existence of the intrusion under the rift floor could be partial melting in the lithosphere. The observed Vs beneath the MER shows that the crust is continental, with mainly solidified mafic intrusions beneath the magmatic segments. The low Vp/Vs material in Figure 5.6 is also observed in light of independent constraints of high conductivities observed in MT studies and gives new insights into the storage of melt under an on-axis volcano like previous observation in the CMER (Chambers et al., 2019; Hübert et al., 2018; Samrock et al., 2018, 2015).

The high-velocity material in the MER could be due to the availability of high-velocity intruded material. Most Vs and depth H beneath the NW plateau are similar to the global average crustal structure, suggesting that the crust on the Southeastern side of the MER has not been significantly modified by plate thinning and intrusion supporting previous studies in which the crustal thickness beneath the SE plateau seems to be homogeneous at about 42 km $\pm$ 2 km, with Vs of $\sim$4.5 km/s. The result strengthens previous geophysical studies (Dugda et al., 2005; Hammond et al., 2011; Mahatsente et al., 1999; Mammo, 2013; Stuart et al., 2006) contrasting the crustal material of the NMER >4.6 km/s.

The Low Vs Materials

The slow Vs material beneath the NW plateau could be due to low Vs partial melting or the release of magmatic fluid from the mantle. The high availability of magmatic material beneath the NW plateau compared to the MER is indicated by the existence of melt and/or fluid beneath AKEE and INEE stations . The source of the low velocity beneath these stations could be the accumulation of hot H2O-rich fluid composition in the lower crust or the induction of partial melting of suitable composition (e.g., Reed et al., 2014). Likewise, beneath INEE and AKEE stations the observation of a low Vs and a high Vp/Vs materials might be due to the availability of partial melting (Kibret et al., 2019; Maguire et al., 2006). This discovery is consistent with prior research that has identified partial melting beneath the Northwestern plateau (Chambers et al., 2019; Keranen et al., 2009; Kibret et al., 2023). Furthermore, at the deepest layer in the lower crust, beneath the NMER, high Vp/Vs material has been observed, and a discontinuity has been noted at the interface between the high Vs material and this layer. Seismic velocities beneath the NMER (>4.2km/s) are consistent with the presence of upper-lower crustal mafic intrusion. This matches with our 1D velocity model (Figure 5.6). The cause for the existence of the intrusion under the rift floor could be partial melting in the lithosphere (Jentzsch et al., 2000). This shows that the crust beneath the MER is continental, with mainly solidified mafic intrusions beneath the mag-

matic segments as previously believed in the MER (Keranen et al., 2009). Beneath the high Vs material, there is a slow Vs body at the deeper depth.

This low Vp/Vs material in Figure 5.6 is also observed in light of independent constraints of high conductivities observed in MT studies and gives new insights into the storage of melt under an on-axis volcano like previous observation in the CMER (Hübert et al., 2018). A similar low Vs and high Vp/Vs is observed in Afar, Semera and interpreted as evidence for the presence of partial melt (Ahmed et al., 2022; Desissa et al., 2013; Kibret et al., 2019; Lewi et al., 2016). This interpretation is strengthened by InSAR analysis beneath the MER and shows a broad zone of significant volcanism, and the mantle beneath is characterized by high temperatures and partial melt (Biggs et al., 2011). In light of previous results, the observed crustal structure beneath NW plateau is consistent with the interpretation that the crust beneath the northwestern side of Afar and the MER has been significantly modified by magmatism. Our results suggest that intrusion into the upper crust along the western NMER might be more significant than previously thought.

Our two-dimensional image (Figure 5.7) provides valuable insights into the subsurface structure beneath the axial volcanic systems of the Northern Main Ethiopian Rift (NMER). Notably, at a depth of approximately 35 km, we observe a distinct region characterized by low shear wave velocities (Vs) and high Vp/Vs ratios exceeding 1.9. This observation suggests the presence of partial melt in this depth range, which may have a direct connection to the uppermost crust. The existence of such partial melt supports previous models proposing the coexistence of high and low Vs materials at various depths throughout the rift (Chambers et al., 2019; Kibret et al., 2022; Stuart et al., 2006). This finding further reinforces the notion that the upper and lower crust beneath the rift flanks, where volcanic and hydrothermal activities are ongoing at the surface (Korostelev et al., 2015), are influenced by these variations.

Additionally, our study reveals the presence of a substantial body of material with high Vs values exceeding 4.6 km/s within the depth range of 7-30 km. This finding aligns with previous models and indicates the occurrence of high Vs materials throughout the rift, although the exact depth range remains undefined (Chambers et al., 2019; Kibret et al., 2022; Stuart et al., 2006). This high Vs material likely contributes to the strengthening of both the upper and lower crust. We propose that the low Vs material observed beneath this high Vs region represents a solidified magmatic intrusion in the actively developing rift valleys. It is widely believed that the initial extension in the region is primarily accommodated by border faulting, gradually localizing to narrower segments of axial volcanism as the rift valley widens (e.g., Ebinger and Casey, 2001; Korostelev et al., 2015).

The Moho depth

The relative high velocity discontinuities observed at depths of 40 km, 44 km, and 42 km beneath the DIKE, ADEE, and GOBA stations, respectively, suggest significant changes in the lithospheric composition and/or structure at these depths. The change in lithospheric composition in turn could be related to tectonic activity or the presence of geological features. Moreover, our empirical findings have divulged that the Moho depth in the study areas ranges between 38 and 44 $\pm$ 2km (Dugda and Nyblade, 2006; Eshetu et al., 2021; Keranen et al., 2009; Kibret et al., 2022; Mahatsente et al., 1999; Stuart et al., 2006), a close approximation to prior estimates. The Moho layer, which is present beneath the rift zone, is supported by the observation of high Vp/Vs material in this region. Furthermore, our analytical investigations have unearthed some notable anomalies in the crustal structure. For instance, the Moho depth beneath the NMER (BORE and NAZA) displays an anomalously high Vs value of >4.5km/s (Keranen and Klemperer, 2008; Kibret et al., 2022) which could be mafic intrusion clearly evident in the upper crust (Keranen and Klemperer, 2008), enveloping the entire crust except for the uppermost layer. Additionally, our findings reveal that the seismic velocity structure of BORE is markedly disparate from the global average continental crust and from other stations in the profile. This finding alludes to the existence of unique geological processes occurring in this area, signifying a focal point for further research.

Overall, these results provide valuable insights into the crustal structure and composition in the Northwestern plateau and the Main Ethiopian Rift region, and can help advance our understanding of the geological processes that have shaped these regions.

5.5 Conclusion

P-to-S Receiver Functions (RFs) were computed using teleseismic data (magnitude >6.0 and epicentral distance between 30 and 90 degrees) collected between 2000–2003 and 2008–2009 in 10 transient broadband stations in the NW plateau and the NMER. The study explores the lithospheric structure of the Northwest (NW) plateau, Northern Main Ethiopian Rift (NMER), and Southeast (SE) plateau using advanced techniques. The plateaus have experienced uplift from plume activity and flood basalt volcanism. The crust thickness on the Somalian plate is about 42 km, while the western plateau has a thicker crust ranging from 38 to 42 km. The Nubian Plate on the western plateau has a more mafic composition ($Vp/Vs \sim 1.6$) compared to the Somalian Plate ($Vp/Vs \sim 1.6$ to 1.8). Beneath the NMER, high shear wave velocities (Vs) exceeding 4.5 km/s at depths of $7 - 30$ km may originate from various sources such as intruded material or cooled magmatic intru-

sion. The crust beneath the NMER also exhibits high Vp/Vs values exceeding 1.9 below 35 km, suggesting partial melt connected to the upper mantle. These observations indicate ongoing magmatic activity or distinct pre-rift crustal compositions. Moving northwest of the NMER, regions with high Vs exceeding 4.5 km/s are underlain by lower Vs values ranging from 3.0 to 3.3 km/s, while a high Vp/Vs ratio of $1.9 - 2.0$ is observed at depths of $25 - 35$ km. On the southeast side, the crust demonstrates elevated Vs values of approximately 4.4 km/s at a depth of 15 km, suggesting possible intrusive material. Low Vs values and high Vp/Vs ratios exceeding 1.9 in this area may be associated with partial melting or magmatic fluid release. Across the rift axis, the crust thickness varies from $36 - 44$ km in the NW plateau to $38 - 42$ km in the SE plateau. These findings highlight substantial variations in crustal thinning and lithospheric composition, indicating a connection to ongoing tectonic activity. The results support the hypothesis of magma-assisted rifting as a plausible explanation for the transition from a continental to an oceanic rift in this region.

CHAPTER 6

GENERAL DISCUSSION

The tectonically active region of Ethiopia and its surrounding areas have been a subject of interest for geologists and geophysicists due to the intraplate volcanism, magmatism, intrusion, partial melting, and crustal heterogeneity that have been observed in the Afar and the MER rift systems (Dugda and Nyblade, 2006; Keranen and Klemperer, 2008; Kibret et al., 2022; Pik et al., 2003). Although much of the plateau in the study area is covered by widespread flood basalt volcanism that started around 30 million years ago, the complex interplay between tectonic, magmatic, and geological processes makes these regions fascinating for research. Therefore, Geoscientists combine data from various sources to gain a better understanding of the underlying processes that are shaping these dynamic and rapidly evolving regions.

6.1 Plume-Related Influences

From a plume-related perspective, our research has discovered unusual features characterized by high-velocity materials ($Vs > 4.5$ km/s). These findings indicate the presence of solidified magma that has played a significant role in facilitating the process of rifting. In particular, we have observed a magmatic plume aligned with the rift axis in active rifted areas like the Main Ethiopian Rift (MER) and Afar, where rifting, faulting, and volcanic activity are prominent. These regions undergo continental rifting and weakening of the Earth's outer layer, which result from a combination of seismic activity and geological processes such as the stretching and erosion of the Earth's crust, intrusion of magma, and the influence of a mantle plume (Bastow et al., 2011, 2008; Chambers et al., 2019; Dugda and Nyblade, 2006; Keranen et al., 2009). However, our knowledge of the specific locations and magnitudes of plume-related effects, including the distribution of solidified magma and thermal erosion, is still limited. Therefore, further investigation is essential to enhance our understanding of these plume-related phenomena in these regions.

In our previous chapters, particularly in Chapter 3, 4, and 5, we have conducted a thorough examination of how the plume influences faulting, tectonic extension, crustal heterogeneity, and deformation. We have drawn insights from previous studies and made careful comparisons to ensure the accuracy of our findings. Our study incorporates existing knowledge of key parameters like V_p and density, and we have conducted detailed analyses of conductivity within the study area (Dugda et al., 2005; Hübert et al., 2018; Johnson, 2012; Lewi et al., 2016; Mackenzie et al., 2005; Maguire et al., 2006; Mahatsente et al., 1999; Mammo, 2013; Samrock et al., 2018, 2015). By studying the underlying materials beneath each observation point and interpreting the overall geological profile, we aim to uncover the powerful internal forces that shape the Earth's surface. This research helps us deepen our understanding of these dynamic processes and unravel the intricate mechanisms that drive the initiation and progression of rift development (Rogers et al., 2000; Woldegabriel et al., 1990; Wolfenden et al., 2004).

In Chapters 3, 4, and 5, we have conducted detailed analyses of unusual features that we call anomalous bodies. These bodies have unique characteristics related to the location of magmatic plumes and their effects. We have also found that these anomalies are associated with continuous geological processes, such as faulting, volcanism, and dyking. By studying seismic velocity measurements, we have been able to identify structures in the crust of the Main Ethiopian Rift (MER) and Afar with both high and low velocities (Ahmed et al., 2022; Dugda et al., 2007; Keranen et al., 2009; Kibret et al., 2022, 2023). This analysis has provided valuable insights into how these structures contribute to the development of rifts (Ahmed et al., 2022; Chambers et al., 2019; Keranen et al., 2009).

Our investigation has primarily focused on the Afar and MER rift systems, as they are closely associated with mantle upwellings and the process of continental break-up (Bastow et al., 2010, 2005; Chambers et al., 2019; Keir et al., 2006b). By carefully analyzing velocity contrasts using parameters such as Vs and Vp/Vs, we have uncovered the influence of magmatic materials on the complex evolution of rifting (Keir et al., 2009, 2006a). Moreover, our study has not only identified these remarkable anomalies but has also provided valuable insights into their specific distribution in space. We have observed that these anomalies are predominantly concentrated along the rift axis, as shown in Figure 3.8 in Chapter 3, where intense geological activities are visible on the Earth's surface (Hammond et al., 2013). It is important to recognize that these geological activities have implications beyond just the development of rifts. They intersect with various aspects, including geohazards, geothermal phenomena, and volcanic eruptions, which have significant implications for governmental plans and decision-making in terms of development (Hübert et al.,

2018; Samrock et al., 2018, 2015). Therefore, our findings not only provide insight into the complex nature of these phenomena but also offer valuable guidance for making informed decisions in these domains.

6.2 Magmatic Intrusion & Partial Melting

The creation and development of rift systems like the Afar and MER are greatly influenced by the presence of molten rock and the melting of rocks in the Earth's crust (Hammond, 2014; Hammond et al., 2011; Hodgson et al., 2017; Hutchison et al., 0501). This process occurs when magma from deep within the Earth interacts with the crust, causing certain parts of the crust to partially melt. As the magma rises to the surface, it forms volcanoes in regions like the Afar and MER (Ahmed et al., 2022; Chambers et al., 2019; Ferguson et al., 2013; Rooney et al., 2014, 2011). By understanding these processes and how different layers of the Earth's crust interact, we gain valuable insights into the formation and characteristics of these unique geological features. It also helps us better grasp the powerful forces that shape our planet and contribute to its ongoing transformation.

In the Afar and MER rift systems, we observe an asymmetrical pattern of partial melting, with more frequent melting occurring in the southwestern plateau compared to the NW plateau (Chambers et al., 2019; Keranen et al., 2009; Rooney, 2017). This asymmetry highlights the strong link between magmatic activity and the tectonic processes driving the formation and evolution of these rift systems. By studying these interactions and processes, we can improve our understanding of the complex forces at play, which shape our world and contribute to ongoing changes. This knowledge is essential for preparing and mitigating risks associated with volcanic and tectonic activity. It allows us to implement effective safety measures and build resilience in communities located near volcanic regions.

6.3 Fault-Magmatic Interplay

The interaction between solid rock and magma has important implications for the Earth's surface. It can create new faults, reactivate existing faults, and change the paths of magma underground. This interplay affects the physical and chemical properties of the Earth's crust, as well as volcanic activity and seismic events related to the movement of magma near the surface (Greenfield et al., 2019a,b; Ogden et al., 2021).

Understanding how faults and magma interact is crucial for gaining insights into the complex processes that shape our planet's surface and drive its evolution. In rifted areas like Afar and MER, especially on the NW side of the rift, dense faults and intrusions are closely

linked to magmatic activity (Ahmed et al., 2022; Chambers et al., 2021; Keir et al., 2009). Observing magmatic intrusions in the form of sills and other intrusive bodies is a crucial indicator of active magmatic processes in these areas (Ferguson et al., 2013; Hamling et al., 2009; Wright et al., 2012). Geophysical techniques such as gravity surveys, seismic reflection surveys, and passive-source seismological mapping help us observe these intrusive bodies and gain a better understanding of their characteristics (Ahmed et al., 2022; Bastow et al., 2008, 2005; Hammond, 2014; Hammond et al., 2011; Kibret et al., 2019, 2022; Lewi et al., 2016; Mackenzie et al., 2005; Maguire et al., 2006; Mahatsente et al., 1999; Mammo, 2013).

The magmatic intrusions in rifts and plateaus not only shape the physical features of the region but also play a significant role in seismic activity. As strain builds up in the Earth's crust across the MER, magma intrudes at depths of around 10 kilometers, while faulting or dike intrusion occurs in the brittle seismogenic zone (Keir et al., 2006b). Exploring the intricate connection between magmatic processes and tectonic activity provides valuable insights into the forces that shape the different lithospheric zones of the NEARS (North East African Rift System) and how they interact.

In the remarkable landscapes of Afar and MER, we have made incredible discoveries about the magmatic plumbing system in the upper crust. By comparing cutting-edge techniques like InSAR and seismicity analysis, we have found that anomalous bodies tend to align with active areas where episodic intrusions have been detected, particularly around volcanic segments. This provides valuable insight into the complex processes driving these rift systems. What's even more fascinating is that this magmatic system is not confined to one region but also extends to the MER, suggesting that magma bodies exist in the shallow crust of volcanic centers and have longer lifespans than previously believed. These groundbreaking discoveries, supported by the seminal work of Gleeson et al. (2017), provide a new understanding of the dynamic processes that shape the interaction between rifts and plateaus.

6.4 Crustal Low Vs: A Causal Connection

Our observations of slow Vs (<3 km/s) at shallow depths beneath Afar, MER, and the plateau margin, which are consistent with previous research (Benoit et al., 006b), suggest that the crust in these areas is primarily composed of sedimentary and volcanic layers. We have also found support for this conclusion through gravity analysis, which has identified low-density lacustrine and clastic volcanic systems (Cornwell et al., 2006; Wolfenden et al., 2004).

Furthermore, the presence of low Vs (<3.5 km/s) in the lower crust above the Moho interface (<45 km) indicates the existence of less modified mafic crustal material with felsic intrusion or partial melt ($Vp/Vs > 1.9$), which is commonly found in regions where partial melting occurs (Chambers et al., 2019). This provides valuable insights into the geodynamic processes of the rift systems and the role played by magmatism.

At depths of $20-25$ km below the magmatic segment, we have observed slow Vs and high Vp/Vs, indicating the presence of partial melt, which serves as a major and long-term magma storage zone. Recent studies have confirmed that these regions are indicative of partial melting and have an influence on fault activity and thermal effects in the lower crust (Annen et al., 2006; Chambers et al., 2019). The presence of partial melt carries significant implications for the evolution of the rift system, necessitating further research.

In addition, the widespread distribution of melt-rich lower crust, as evidenced by slow Vs (< 3.5 km/s) in Afar, MER, and the NW plateau (Bastow et al., 2005; Ebinger, 2005; Wright et al., 2006), allows for significant transport of melt along the rift. The coexistence of slow Vp/Vs regions alongside fast Vs areas suggests the presence of subvolcanic melt reservoirs that episodically deliver melt through mafic intrusion along the rift axis (Albino and Biggs, 2021; Biggs et al., 2011).

Regarding the regions of slow Vs (< 3.2 km/s) beneath the NW plateau, we hypothesize that they can be explained by the presence of a fluid phase or warmer temperatures (Kibret et al., 2023). Computed Vp/Vs values provide further support for the existence of partial melt in specific localized areas beneath the NW plateau. This finding is additionally confirmed by seismic imaging, deep crustal earthquakes, electrical conductivities, and bulk crustal Vp/Vs observations (Bastow et al., 2005; Chambers et al., 2019; Dugda and Nyblade, 2006; Dugda et al., 2005; Keir et al., 2006b; Keranen et al., 2009; Samrock et al., 2018, 2015).

6.5 Crustal High Vs: A Causal Connection

Our 1D Vs modelling discovered seismic Vs variations at depths of 6-25 km in the Afar and MER rift systems (Kibret et al., 2022, 2023). High Vs values (up to ~4.5 km/s) in the upper to mid-crust of the Wonji fault belt and Afar rift axis indicate active magmatic intrusions (Cornwell et al., 2006; Mahatsente et al., 1999; Rooney et al., 2014, 2011; Tiberi et al., 2005). This suggests a significant role of magmatism in deformation and evolution (Cornwell et al., 2006, 2010; Keranen et al., 2004; Mackenzie et al., 2005; Mahatsente et al., 1999).

Notably, high Vs values exceeding 4.5 km/s beneath the NMER establish a connection between elevated Vs and magmatic intrusion, providing insights into continental rifting processes compared to adjacent plateaus (Birhanu et al., 2016; Stamps et al., 2015).

In the CMER crust, high Vs materials (>4.5 km/s) indicate an upper crustal magmatic plumbing system within the MER, similar to the Main Ethiopian Rift, and the presence of magma reservoirs near volcanic centers (Cornwell et al., 2006; Gleeson et al., 2017; Maguire et al., 2006; Mahatsente et al., 1999).

The interplay between magma-induced pressure and partially molten materials plays a crucial role in rifting initiation and the transition to seafloor spreading (Bastow et al., 2011; Ebinger and Casey, 2001; Makris and Ginzburg, 1987; Rooney et al., 2007; Stuart et al., 2006).

High Vs materials (>4.5 km/s) in the mid-to-lower crust beneath the NMER and CMER provide insights into rifting mechanisms (Chambers et al., 2019; Lavayssiere et al., 2018). The EAGLE experiment observed a fast Vp layer in the lower crust and a dense lower crust beneath the northwestern plateau, while receiver function analysis revealed reverberations from the underplate boundaries (Cornwell et al., 2006; Lavayssiere et al., 2018; Mackenzie et al., 2005; Maguire et al., 2006; Stuart et al., 2006). Extensive magmatic intrusion enables magma transport along the rift, influencing fault activity and thermal effects (Chambers et al., 2019).

6.6 The NW and SE Plateau crustal structure

The southeastern plateau of Ethiopia exhibits a uniform crustal structure with higher Vs values and minimal slow Vs observations, indicating stable continental crust (Thompson et al., 2010; Youssof et al., 2013, 2015). In contrast, the northwestern plateau shows a sharp contrast between the plateau and rift, with significant magmatic modification (Chambers et al., 2019; Mackenzie et al., 2005).

The presence of melt beneath the northwestern plateau can be attributed to decompression melting of the asthenosphere or lateral migration of magma from the rift. Slow Vs and high Vp/Vs regions are explained by the presence of a fluid phase, such as partial melt, sourced from the asthenosphere or rift migration.

The findings of slow Vs and high Vp/Vs beneath the northwestern plateau and partial melt in Afar shed light on rift-related magmatic processes, highlighting the role of pre-existing weaknesses and partial melt in accommodating extension. This supports the distinct crustal

structure of the northwestern plateau compared to Afar and contributes to our understanding of rift system evolution and geodynamic processes.

In Afar, the uppermost crust exhibits variability, with slow Vs and high Vp/Vs observed in regions containing sedimentary and volcanic materials, consistent with previous studies (Chambers et al., 2021; Hammond et al., 2011; Kibret et al., 2019). The lower crust is generally uniform, except in magmatic segments where strain is concentrated. East of the magmatic segments, high Vs and Vp/Vs consistent with intruded mafic rock are observed, while slower Vs and high Vp/Vs suggest mafic crust with limited partial melt to the west. This asymmetry in magmatic modification suggests ongoing processes between the magmatic segment and the western Afar margin.

In the upper crust beneath the magmatic segment, high Vs and anomalously low Vp/Vs indicate the presence of a gas phase and vigorous magmatic degassing from solidifying intrusions and a hydrothermal system (Ebinger et al., 2017; Lee et al., 2016; Roecker et al., 2017; Whittington et al., 2009).

6.7 Moho Depth

We constructed a continuous Moho map by interpolating RF constraints, capturing the variability of Vs and Moho in the NW plateau and Afar. Our interpretation assumes Moho depth at the large velocity gradient, consistent with previous studies (Ahmed et al., 2022; Bello et al., 2021; Clitheroe et al., 2000; Collins, 1999; Collins et al., 2003; Fontaine and Kennett, 2013; Hammond et al., 2011). Results revealed a well-defined velocity discontinuity at the Moho, but with smaller Vs values compared to the upper-to-mid crust at certain stations like KOBE and SRDE. This suggests intrusion and solidification of high-velocity materials or properties of the Moho altered by partial melting.

The NW plateau stations exhibit a sharp velocity contrast at the Moho, while the Afar region shows a more gradational Moho. We observed a gradational velocity gradient across the Afar Moho, possibly due to increasing mafic intrusion in the lower crust, reducing the contrast with the mantle. This is consistent with previous studies indicating mafic intrusions can alter the Moho to be more gradational (Hodgson et al., 2017; Thybo and Artemieva, 2019). We also found scattered Vs distribution beneath the rift axis, indicating potential crustal heterogeneity from repeated magmatic intrusion and solidification. Further investigation of local geological features and their impact on seismic wave velocities is warranted.

CHAPTER 7

CONCLUSIONS AND RECOMMENDATIONS

7.1 Conclusions

In this study, we analyzed teleseismic data from 44 broadband stations in Ethiopia and Eritrea ($2000 - 2017$) to investigate the region's crustal structure. Receiver function (RF) analysis was used to determine the Vs structure beneath profiles in NMER, CMER, Afar, NW plateau, and SW plateau. Our goal was to identify crustal structure, Moho depth, and the presence of lithospheric materials like magmatic intrusions and partial melting.

The uppermost crust exhibits low Vs ($\sim 2-3$ km/s), indicating sedimentary and/or volcanic layers. In the rift valley, Vs varies laterally and with depth. Slow Vs and high Vp/Vs ratios are observed beneath volcanic centers in the upper-mid crust, while the lower crust generally displays slow Vs. These observations align with previous studies that suggest the presence of a small fraction ($< 5\%$) of partial melt in the lower crust.

The NW plateau region's crustal structure and composition provide intriguing insights into its geodynamic evolution. Most of the NW plateau has faster Vs ($4 - 4.7$ km/s) compared to the rest of the region. However, in the mid-crust ($10 - 25$ km depth), Vs is slower (3.2 km/s), and the Vp/Vs ratio is high ($1.85 - 2.0$). This suggests the presence of partial melt covering over 1% of the crust, indicating mafic crust with fluid phases beneath the NW plateau. These findings have significant implications for understanding tectonic processes and the region's geodynamic evolution, potentially contributing to magmatic activity and extension.

In contrast, the SE Plateau exhibits a more homogeneous and faster Vs, with a distinct and sharp velocity contrast at the Moho interface, indicating minimal crustal modification from magmatism. The Afar region also shows homogeneous crust, except for faster material (4.5 km/s) in the upper-mid crust beneath the magmatic segment, where current extension is occurring. These findings shed light on the crustal structure and composition of these

regions and pave the way for further research on their geodynamic evolution.

The study reveals significant differences in seismic properties between the Eastern and NW plateaus. The SE Plateau displays homogeneous and faster Vs, with a distinct and sharp velocity contrast at the Moho, indicating minimal crustal modification from magmatism. In contrast, the NW plateau exhibits a more heterogeneous structure, with most of the crust showing faster Vs but also regionally slower Vs and higher Vp/Vs ratios in the mid-crust ($10 - 25$ km depth).

7.2 Future Work

The author's thesis convincingly demonstrates how the Receiver Functions technique is effective in studying what lies beneath the Earth's surface and its importance in understanding ongoing rifting. This method helps us accurately measure the thickness of the crust and composition of the lithosphere, giving us valuable insights that support findings from other geophysical methods like gravity modelling, magnetotelluric techniques, and ambient seismic noise tomography.

One significant discovery from the thesis is the presence of partial melting in specific locations deep within the crust, which may extend further up. This finding helps us understand the causes and effects of this phenomenon in unusual areas. To make our models of Vs and Vp/Vs more accurate, future research should focus on refining the Receiver Functions technique and exploring other complementary geophysical methods.

Looking ahead, ongoing research is crucial for us to gain a deeper understanding of the crust's structure, the distribution of partial melt, and how they influence seismic activity in the broader East African rift region. While our study provides valuable insights, there is still much to learn about the complex geological processes at work in this area. Future investigations should aim to develop detailed models of the underground magmatic plumbing system in volcanic regions like the MER, NW plateau, and Afar. Additionally, studying the relationship between partial melt and seismic activity can provide crucial insights into how rifting occurs. It's important that these efforts prioritize international collaboration and empower local scientists, as their expertise and knowledge will contribute to comprehensive research outcomes.

7.3 Recommendations

As we delve deeper into understanding the captivating geological processes of the East African rift, it becomes evident that collaboration on a global scale is vital. To unravel the

intricate crustal structure and distribution of partial melt, we need to join forces and tap into our collective expertise. While our study has uncovered valuable insights, there is still so much more to explore.

For a sustainable and enduring research effort, it is paramount that local scientists take the lead and guide us forward. By incorporating their knowledge and expertise, we can gain a richer understanding of the region's geology and appreciate the cultural and environmental factors that make it truly unique. Through collaborative and inclusive teamwork, we can unlock the full potential of this remarkable area and continue making groundbreaking discoveries that benefit the scientific community and society as a whole. Together, we can pave the way for an exciting future of exploration and innovation.

Annex 1: Performance report for PhD Degree

ADDIS ABABA UNIVERSITY

COLLEGE OF NATURAL AND
COMPUTATIONAL SCIENCE

PhD Degree Performance Certificate Form

Full Name **Birhanu Abera Kibret** ID NO:**GSR/1976/11**
Program Title **Doctor of Philosophy in Applied Geophysics**
I. Course Work

Course Code	Course Title	ECTS	Grade	Grade Point
ERSC 881	Geophysical Data Analysis	7.00	A+	12
ERSC 887	Earthquake Seismology	7.00	B+	10.5
ERSC 902	Seminar II	7.00	A+	4
ERSC 903	Seminar III	7.00	A	4
ERSC 920	Geodynamics	7.00	A	12
ERSC 981	Seminar I	7.00	A	4
ERSC 984	Dissertation	60.00		0
	Cumulative Average			46.5

II. Thesis Rating:_____

_____

III. Thesis Title: Crustal Structure of the Northeast African Rift System from Receiver Function Analysis
IV. Remarks by Examining Board: _____

_____

_____

V. **Publications:**

1. Kibret, B. A., Ayele, A. and Keir, D. (2019). Crustal thickness estimates beneath four seismic stations in Ethiopia inferred from p-wave receiver function studies. *J. African Earth Sciences*: **150**, 1–8, doi:10.1016/j.jafrearsci.2018.11.005

2. Kibret, B. A., Ayele, A. and Keir, D. (2022). Modelling S-Wave Velocity Structure Beneath the Central Main Ethiopian Rift Using Receiver Functions. *Front. Earth Sci.*: **10**, 773–783. doi:10.3389/feart.2022.773783

3. Kibret, B. A., Ayele, A. and Keir, D. (2023). Crustal Structure of the Ethiopian Northwestern Plateau and Central Afar from Receiver Function Analysis. *Front. Earth Sci.*: **11**, 1–13 doi:org/10.3389/feart.2023.1170907

4. Ogden, C. S., Keir, D., Bastow, I. D., Ayele, A., Marcou, S., Ugo, F., Woodward, A., Kibret, B. A. and Gudbrandsson, S. (2021). Seismicity and crustal structure of the southern Main Ethiopian Rift: New evidence from Lake Abaya. *Geochemistry, Geophysics, Geosystems*, **22**, 1–17. doi:org/10.1029/2021GC009831

5. Kounoudis, R., Bastow, I. D., Ebinger, C. J., Ogden, C. S., Ayele, A., Bendick, R., Mariita, N., Kianji, G., Wigham, G., Musila, M. and Kibret, B. A. (2021). Body-wave tomographic imaging of the Turkana Depression: Implications for rift development and plume-lithosphere interactions. *Geochemistry, Geophysics, Geosystems*, **22**, 1–27. doi:org/10.1029/2021GC009782

6. Ahmed, A., Doubre, C., Leroy, S., Keir, D., Pagli, C., Hammond, J. O. S., Ayele, A., Berc, M. B., Grunberg, M., Vergne, J., Pestourie, R., Mamo, D., Kibret, B. A., Cubas, N., Lavayssière, A., Janowski, M., Lengliné, O., La Rosa, A., Chambers, E. L., and Illsley-Kemp, F. (2022). Across and along-strike crustal structure variations of the western Afar margin and adjacent plateau: Insights from receiver functions analysis. *J. African Earth Sciences*, **192**, 1–17. doi: 10.1016/j.jafrearsci.2022.104570.

7. Ogden, C.S., Bastow, I.D., Ebinger, C., Ayele, A., Kounoudis, R., Musila, M., Bendick, R., Mariita, N., Kianji, G., Rooney, T.O., Sullivan, G., Kibret, B. (2023). The development of multiple phases of superposed rifting in the Turkana Depression, East Africa: Evidence from receiver functions. *Earth and Planetary Science Letters*, **609**, 1–13. doi:10.1016/j.epsl.2023.118088

VI. Approved By: Name and signature of the examining board members testifying that all program and legislation requirements are fulfilled.

Name	**Signature**	**Date**
1. Prof. Atalay Ayele (Advisor)	_____	_____
2. Prof. Tilahun Mammo (Internal Examiner)	_____	_____
3. ********** (External Examiner)	_____	_____
4. Prof. Worash Getaneh (Chairperson)	_____	_____

Dean of the College	**Signature**	**Date**
1. Prof. Tileye Feyissa	_____	_____

Bibliography

Abdulla, F., Hossain, M., and Rahman, M. (2014). On the Selection of Samples in Probability Proportional to Size Sampling: Cumulative Relative Frequency Method. *Mathematical Theory and Modeling*, 4:102–107.

Agostini, A., Bonini, M., Corti, G., Sani, F., and Mazzarini, F. (2011). Fault architecture in the Main Ethiopian Rift and comparison with experimental models: Implications for rift evolution and Nubia–Somalia kinematics. *Earth and Planetary Science Letters*, 301:479–492.

Ahmed, A., Doubre, C., Leroy, S., Keir, D., Pagli, C., Hammond, J. O. S., Ayele, A., Berc, M. B., Grunberg, M., Vergne, J., Pestourie, R., Mamo, D., Kibret, B. A., Cubas, N., Lavayssière, A., Janowski, M., Lengliné, O., La Rosa, A., Chambers, E. L., and Illsley-Kemp, F. (2022). Across and along-strike crustal structure variations of the western Afar margin and adjacent plateau: Insights from receiver functions analysis. *Journal of African Earth Sciences*, 192.

Aki, K. and Richards, P. (2002). *Quantitative Seismology*. G - Reference,Information and Interdisciplinary Subjects Series. University Science Books.

Albino, F. and Biggs, J. (2021). Magmatic Processes in the East African Rift System: Insights From a 2015–2020 Sentinel-1 InSAR Survey. *Geochem. Geophys. Geosyst.*, 22:1–24.

Ammon, C. (1991). The isolation of receiver effects from teleseismic P waveforms. *Bull. Seismol. Soc. Am.*, 81(6):2504–2510.

Ammon, C., Randall, G., and Zandt, G. (1990). On the nonuniqueness of receiver function inversions. *J. Geophys. Res.: Solid Earth*, 95(B10):15303–15318.

Annen, C., Blundy, J. D., and Sparks, R. S. J. (2006). The Genesis of Intermediate and Silicic Magmas in Deep Crustal Hot Zones. *Journal of Petrology*, 47:505–539.

Artemieva, I. M., Billien, M., Leveque, J. J., and Mooney, W. D. (2004). Shear wave velocity, seismic attenuation, and thermal structure of the continental upper mantle. *Geophysical Journal International*, 157(2):607–628.

Ayele, A., Stuart, G., and Kendall, J. (2004). Insights into rifting from shear wave splitting and receiver functions: An example from Ethiopia. *Geophys. J. Int.*, 157:354–362.

Barnie, T. D., Oppenheimer, C., and Pagli, C. (2016). Does the lava lake of Erta 'Ale volcano respond to regional magmatic and tectonic events? An investigation using Earth Observation data, in Wright, T. J., Ayele, A., Ferguson, D. J., Kidane,T. and Vye-Brown, C., eds,. *Geological Society, London, Special Publications*.

Bastow, I. D., Keir, D., and Daly, E. (2011). The Ethiopia Afar Geoscientific Lithospheric Experiment (EAGLE): Probing the transition from continental rifting to incipient seafloor spreading. *Geological Society of America Bulletin*, 478:51–76.

Bastow, I. D., Nyblade, A. A., Stuart, G. W., Rooney, T. O., and Benoit, M. H. (2008). Upper mantle seismic structure beneath the Ethiopian hot spot: Rifting at the edge of the African low-velocity anomaly. *Geochemistry, Geophysics, Geosystems*, 9(12).

Bastow, I. D., Pilidou, S., Kendall, J. M., and Stuart, G. W. (2010). Melt-induced seismic anisotropy and magma assisted rifting in Ethiopia: Evidence from surface waves. *Geochemistry, Geophysics, Geosystems*, 11.

Bastow, I. D., Stuart, G. W., Kendall, J. M., and Ebinger, C. J. (2005). Upper-mantle seismic structure in a region of incipient continental breakup: Northern Ethiopian rift. *Geophysical Journal International*, 162(2):479–493.

Beccaluva, L., Bianchini, G., Natali, C., and Siena, F. (2009). Continental Flood Basalts and Mantle Plumes: A Case Study of the Northern Ethiopian Plateau. *Journal of Petrology*, 50(7):1377–1403.

Bello, M., ell, D. G., Rawlinson, N., Reading, A. M., and Likkason, O. K. (2021). Crustal structure of southeast Australia from teleseismic receiver functionsv. *Solid Earth*, 12:463–481.

Benoit, M. H., Nyblade, A. A., and VanDecar, J. C. (2006b). Upper mantle P-wave speed variations beneath Ethiopia and the origin of the Afar hotspot. *Geology*, 34:329–332.

Berhe, S. M., Desta, B., Nicoletti, M., and Teferra, M. (1987). Geology, geochronology and geodynamic implications of the Cenozoic magmatic province in Wand SE Ethiopia. *Journal of the Geological Society of London*, 144:213–226.

Bialas, R. W., Buck, W. R., and Qin, R. (2010). How much magma is required to rift a continent? *Earth and Planetary Science Letters*, 292(1-2):68–78.

Biggs, J., Bastow, I. D., Keir, D., and Lewi, E. (2011). Pulses of deformation reveal frequently recurring shallow magmatic activity beneath the Main Ethiopian Rift. *Geochem. Geophys. Geosyst.*, 12:1–11.

Bilham, R., Bendick, R., Larson, K., Mohr, P., Braun, J., Tesfaye, S., and Asfaw, L. (1999). Secular and tidal strain across the Main Ethiopian Rift. *Geophysical Research Letters*, 26(18):2789–2792.

Birch, F. (1960). The velocity of compressional waves in rocks to 10 kilobars, part 1. *J. Geophys. Res.*, 65:1083–1102.

Birhanu, Y., Bendick, R., Fisseha, S., Lewi, E., Floyd, M., King, R., and Reilinger, R. (2016). GPS constraints on broad scale extension in the Ethiopian Highlands and Main Ethiopian Rift. *Geophys. Res. Lett.*, 43:6844–6851.

Boccaletti, M., Bonini, M., Mazzuoli, R., Abebe, B., Piccardi, L., and Tortorici, L. (1998). Quaternary oblique extensional tectonics in the Ethiopian Rift (Horn of Africa). *Tectonophysics*, 287(1):97–116.

Bonini, M., Corti, G., Innocenti, F., Manetti, P., Mazzarini, F., Abebe, T., and Pecskay, Z. (2005). Evolution of the Main Ethiopian Rift in the frame of Afar and Kenya rifts propagation. *Tectonics*, 24(1).

Buck, W. R. (1991). Modes of continental lithospheric extension. *J. Geophys. Res.*, 96(B12):20161–20178.

Buck, W. R. (2004). *Consequences of Asthenospheric Variability on Continental Rifting*, pages 1–30. Columbia University Press, New York Chichester, West Sussex.

Buck, W. R., Einarsson, P., and Brandsdóttir, B. (2006). Tectonic stress and magma chamber size as controls on dike propagation: Constraints from the 1975–1984 Krafla rifting episode. *J. Geophys. Res.: Solid Earth*, 111(B12).

Campione, M., Malaspina, N., and Frezzotti, M. L. (2015). Threshold size for fluid inclusion decrepitation. *J. Geophys. Res. Solid Earth*, 120:1–8.

Cassidy, J. F. (1992). Numerical experiments in broadband receiver function analysis. *Bulletin of the Seismological Society of America*, 82(3):1453–1474.

Chambers, E. L., Harmon, N., Keir, D., and Rychert, C. A. (2019). Using ambient noise to image the northern East African Rift. *Geochem. Geophys. Geosyst.*, 20:2091–2109.

Chambers, E. L., Harmon, N., Rychert, C., and Keir, D. (2021). Variations in melt emplacement beneath the northern East African Rift from radial anisotropy. *Earth and Planetary Science Letters*, 573:1–13.

Chiasera, B., Rooney, T. O., Girard, G., Yirgu, G., Grosfils, E., Ayalew, D., Mohr, P., Zimbelman, J., and Ramsey, M. S. (2018). Magmatically assisted off-rift extension-The case for broadly distributed strain accommodation. *Geosphere*, 14:1544–1563.

Christensen, N. I. (1996). Poisson's ratio and crustal seismology. *J. Geophys. Res.*, 101(B2):3139–3156.

Christensen, N. I. and Mooney, W. D. (1995). Seismic velocity structure and composition of the continental crust: A global view. *J. Geophys. Res.*, 100:9761–9788.

Clayton, R. W. and Wiggins, R. A. (1976). Source shape estimation and deconvolution of teleseismic bodywaves. *Geophys. J. Int.*, 47(1):151–177.

Clitheroe, G., Gudmundsson, O., and Kennett, B. (2000). The crustal thickness of australia. *J. Geophys. Res.*, 105(1):13697–13713.

Collins, C. D. N. (1999). The nature of crust-mantle boundary under australia from seismic evidence in the australian lithosphere, edited by: Drummond, b. j. *Geol. Soc. Aust. Spec. Pub.*, 17:67–80.

Collins, C. D. N., Drummond, B. J., and Nicoll, M. G. (2003). Crustal thickness patterns in the australian continent. *Geol. Soc. Ame. Spec. Papers*, 372:121–128.

Cornwell, D. G., Mackenzie, G. D., England, R. W., Maguire, P. K. H., Asfaw, L. M., and Oluma, B. (2006). Northern Main Ethiopian Rift crustal structure from new high-precision gravity data. In: Yirgu, G., Ebinger, C., Maguire, P. (Eds.), The Afar Volcanic Province within the East African Rift System. *Special Publication of the Geological Society London*, 259:307–322.

Cornwell, D. G., Maguire, P. K. H., England, R. W., and Stuart, G. W. (2010). Imaging detailed crustal structure and magmatic intrusion across the Ethiopian Rift using a dense linear broadband array. *Geochemistry, Geophysics, Geosystems*, 11.

Corti, G. (2008). Control of rift obliquity on the evolution and segmentation of the main Ethiopian rift. *Nature Geoscience*, 1:258–262.

Corti, G. (2009). Continental rift evolution: From rift initiation to incipient break-up in the Main Ethiopian Rift, East Africa. *Earth-Science Reviews*, 96:1–53.

Corti, G. (2012). Evolution and characteristics of continental rifting: Analog modeling-inspired view and comparison with examples from the East African Rift System. *Tectonophysics*, 522–523:1–33.

Corti, G., Bonini, M., Conticelli, S., Innocenti, F., Manetti, P., and Sokoutis, D. (2003). Analogue modelling of continental extension: A review focused on the relations between the patterns of deformation and the presence of magma. *Earth-Science Reviews*, 63:169–247.

Corti, G., Sani, F., Agostini, S., Philippon, M., Sokoutis, D., and Willingshofer, E. (2018). Off-axis volcano-tectonic activity during continental rifting: Insights from the transversal Goba-Bonga lineament, Main Ethiopian Rift (East Africa). *Tectonophysics*, 728–729:75–91.

Corti, G., Sani, F., Florio, A. A., Greenfield, T., Keir, D., Erbello, A., Muluneh, A. A., and Ayele, A. (2020). Tectonics of the Asela-Langano margin, Main Ethiopian Rift (East Africa). *America Geophysical Union, in press.*, pages 1–43.

Corti, G., Sani, F., Philippon, M., Sokoutis, D., Willingshofer, E., and Molin, P. (2013). Quaternary volcano-tectonic activity in the Soddo region, western margin of the Southern Main Ethiopian Rift. *Tectonics*.

Daly, E., Keir, D., Ebinger, C., Stuart, G. W., Bastow, I. D., and Ayele, A. (2008). Crustal tomographic imaging of a transitional continental rift: The Ethiopian rift. *Geophysical Journal International*, 172(3):1033–1048.

Daniels, K. A., Bastow, I. D., Keir, D., Sparksa, R. S. J., and T, M. (2014). Thermal models of dyke intrusion during development of continent–ocean transition. *Earth and Planetary Science Letters*, 385:145–153.

Desissa, M., Johnson, N. E., Whaler, K. A., Hautot, S., Fisseha, S., and Dawes, G. J. K. (2013). A mantle magma reservoir beneath an incipient mid-ocean ridge in Afar, Ethiopia. *Nature Geoscience*, 6(10):861–865.

Diaferia, G. and Cammarano, F. (2017). Seismic signature of the continental crust: What thermodynamics says. An example from the Italian peninsula. *Tectonics*, 36:3192–3208.

Didana, Y. L., Thiel, S., and Heinson, G. (2014). Magnetotelluric imaging of upper crustal partial melt at Tendaho graben in Afar, Ethiopia. *Geophysics Research Letter*, 41:3089–3095.

Doubre, C., Deprez, A., Masson, F., Socquet, A., Lewi, E., Grandin, R., and al., e. (2017). Current deformation in central afar and triple junction kinematics deduced from gps and insar measurements. *Geophys. J. Int.*, 208 (2):936–953.

Dugda, M. T. and Nyblade, A. A. (2006). New constraints on crustal structure in eastern Afar from the analysis of receiver functions and surface wave dispersion in Djibouti. *Geological Society London Special Publications*, 259(1):239–251.

Dugda, M. T., Nyblade, A. A., and Julia, J. (2007). Thin Lithosphere Beneath the Ethiopian Plateau Revealed by a Joint Inversion of Rayleigh Wave Group Velocities and Receiver Functions. *J. Geophys. Res.: Solid Earth*, 112(B8).

Dugda, M. T., Nyblade, A. A., Julia, J., Langston, C. A., Ammon, C. J., and Simiyu, S. (2005). Crustal structure in Ethiopia and Kenya from receiver function analysis: Implications for rift development in eastern Africa. *J. Geophys. Res.*, 110.

Dvorkin, J. (2021). Rock Physics: Recent History and Advances. In: Khalid S. Essa, Marcello Di Risio, Daniele Celli, Davide Pasquali (Eds.). *Geophysics and Ocean Waves Studies*, pages 1–24.

Ebinger, C. (2007). Afar07. Data set.

Ebinger, C. J. (2005). Continental break-up: The East African perspective. *The Bullerwell Lecture*, 64:16–20.

Ebinger, C. J. and Casey, M. (2001). Continental breakup in magmatic provinces: An Ethiopian example. *Geology*, 29.

Ebinger, C. J., Keir, D., Bastow, I., Whaler, K., Hammond, J. O. S., Ayele, A., Miller, M., Tiberi, C., and Hautot, S. (2017). Crustal structure of active deformation zones in Africa: Implications for global crustal processes: Africa crust. *Tectonics*, 36.

Ebinger, C. J. and Sleep, N. H. (1998). Cenozoic magmatism throughout east Africa resulting from impact of a single plume. *Nature*, 395(6704):788–791.

Ebinger, C. J. and Wijk, J. V. (2014). Roadmap to continental rupture: Is obliquity the route to success? *Geology*, 42:271–272.

Eckhardt, C. and Rabbel, W. (2011). P-receiver functions of anisotropic continental crust: A hierarchic catalogue of crustal models and azimuthal waveform patterns. *Geophys. J. Int.*, 187(1):439–479.

Emishaw, L., Laó-Dávila, D. A., Abdelsalam, M. G., Atekwana, E. A., and Gao, S. S. (2017). Evolution of the broadly rifted zone in southern Ethiopia through gravitational collapse and extension of dynamic topography. *Tectonophysics*, 699:213–226.

Eshetu, A., Mammo, T., and Tilmann, F. (2021). Imaging the Ethiopian Rift Region Using Transdimensional Hierarchical Seismic Noise Tomography. *Pure Appl. Geophys.*, 178:4367–4388.

Ferguson, D. J., Keir, D., and et al (2013). Melting during late-stage rifting in Afar is hot and deep. *Nature*, 499:70–73.

Fontaine, F. R. Tkalcic, H. and Kennett, B. L. N. (2013). Crustal complexity in the lachlan orogen revealed from teleseismic receiver functions. *Aust. J. Earth Sci.*, 60:413–430.

Gani, N. D. S. and Gani, N. R. (2007). Blue Nile incision on the Ethiopian Plateau: Pulsed plateau growth, Pliocene uplift, and hominin evolution. *Geological Society of America*.

George, R., Rogers, N., and Kelley, S. (1998). Earliest magmatism in Ethiopia: Evidence for two mantle plumes in one flood basalt province. *Geology*, 26(10):923–926.

Gleeson, M. L. M., Michael, J. S., David, M. P., Tamsin, A. M., William, H., Gezahegn, Y., and Jon, W. (2017). Constraining magma storage conditions at a restless volcano in the Main Ethiopian Rift using phase equilibria models. *Journal of Volcanology and Geothermal Research*, 337:44–61.

Greenfield, T., Keir, D., Kendall, J., and Ayele, A. (2019a). Low-frequency earthquakes beneath Tullu Moye volcano, Ethiopia, reveal fluid pulses from shallow magma chamber. *Earth and Planetary Science Letters*, 526:1–11.

Greenfield, T., Keir, D., Kendall, J.-M., and Ayele, A. (2019b). Seismicity of the Bora-Tullu Moye volcanicfield, 2016-2017. *Geochem. Geophys. Geosyst.*, 20:548–570.

Guerri, M., Cammarano, F., and Connolly, J. A. D. (2015). Effects of chemical composition, water and temperature on the physical properties of the continental crust. *Geochem. Geophys. Geosyst.*, 16:2431–2449.

Guidarelli, M., Stuart, G., Hammond, J. O. S., Kendall, J. M., Ayele, A., and Belachew, M. (2011). Surface wave tomography across Afar, Ethiopia: Crustal structure at a rift triple-junction zone. 38(24).

Gurrola, H., Baker, G. E., and Minster, J. B. (1995). Simultaneous time-domain deconvolution with application to the computation of receiver functions. *Geophysical Journal International*, 120(3):537–543.

Hacker, B. R. and Abers, G. A. (2004). Subduction Factory 3: An Excel worksheet and macro for calculating the densities, seismic wave speeds, and H2O contents of minerals and rocks at pressure and temperature. *Geochemistry Geophysics Geosystems*, 5(1–7).

Hamling, I. J., Ayele, A., Bennati, L., Calais, E., Ebinger, C. J., Keir, D., Lewi, E., Wright, T. J., and Yirgu, G. (2009). Geodetic observations of the ongoing Dabbahu rifting episode: New dyke intrusions in 2006 and 2007. *Geophys. J. Int.*, 178(2):989–1003.

Hammond, J. O. S. (2011). Eritrea seismic project. international federation of digital seismograph networks.

Hammond, J. O. S. (2014). Constraining melt geometries beneath the Afar Depression, Ethiopia from teleseismic receiver functions: The anisotropic H-k stacking technique. *Geochem. Geophys. Geosyst.*, 15:1316–1332.

Hammond, J. O. S., Kendall, J. M., Stuart, G., Ebinger, C., Bastow, I., Keir, D., Ayele, A., Belachew, M., Goitom, B., Ogubazghi, G., and Wright, T. J. (2013). Mantle upwelling and initiation of rift segmentation beneath the Afar Depression. *Geology*, 41:635–638.

Hammond, J. O. S., Kendall, J. M., Stuart, G., Keir, D., Ebinger, C., Ayele, A., and Belachew, M. (2011). The nature of the crust beneath the Afar triple junction: Evidence from receiver functions. *Geochem. Geophys. Geosyst.*, 12:1–24.

Hayward, N. and Ebinger, C. J. (1996). Variations in the along-axis segmentation of the Afar rift system. *Tectonics*, 15:244–257.

Herrmann, R. B. (2013). Computer programs in seismology: An evolving tool for instruction and research. *Seism.Res.Lettr*, 84:1081–1088.

Herrmann, R. B. and Ammon, C. J. (2002). Surface waves, receiver functions and crustal structure, computer programs in seismology version 3.30. saint louis, mo: Saint louis university.

Hodgson, I., Illsley-Kemp, F., Gallacher, R. J., Keir, D., Ebinger, C. J., and Mtelela, K. (2017). Crustal structure at a young continental rift: A receiver function study from the tanganyika rift. *Tectonics*, 36.

Hofmann, C., Courtillot, V., Féraud, G., Rochette, P., Yirgu, G., Ketefo, E., and Pik, R. (1997). Timing of the Ethiopian flood basalt event and implications for plume birth and global change. *Nature*, 389(6653):838–841.

Hübert, J., Whaler, K., and Fisseha, S. (2018). The electrical structure of the Central Main Ethiopian Rift as imaged by magnetotellurics: Implications for magma storage and pathways. *J. Geophys. Res.*, 123:6019–6032.

Hutchison, W., Mather, T. A., Pyle, D. M., Boyce, A. J., Gleeson, M. L. M., Yirgu, G., Blundy, J. D., Ferguson, D. J., Vye-Brown, C., Millar, I. L., Sims, K. W. W., and Finch, A. A. (2018/05/01/). The evolution of magma during continental rifting: New constraints from the isotopic and trace element signatures of silicic magmas from Ethiopian volcanoes. *Earth and Planetary Science Letters*, 489:203–218.

Ismail, E. H. and Abdelsalam, M. G. (2012). Morpho-tectonic analysis of the Tekeze River and the Blue Nile drainage systems on the Northwestern Plateau, Ethiopia. *Journal of African Earth Sciences*, 69:34–47.

Jentzsch, G., Mahatsente, R., and Jahr, T. (2000). Three Dimensional Inversion of Gravity Data from the Main Ethiopian Rift. *Phys. Chem. Earth*, 25:365–373.

Johnson, N. (2012). Magnetotelluric Studies of the Crust and Upper Mantle in a Zone of Active Continental Breakup, Afar, Ethiopia, PhD thesis. *University of Edinburgh*.

Julia, J., Ammon, C., Herrmann, R. B., and Correig, A. M. (2000). Joint inversion of receiver function and surface wave dispersion observation. *Geophys. J. Int.*, 143:99–112.

Keir, D., Bastow, I. D., Whaler, K. A., Daly, E., Cornwell, D. G., and Hautot, S. (2009). Lower crustal earthquakes near the Ethiopian rift induced by magmatic processes. *Geochemistry, Geophysics, Geosystems*, 10(6).

Keir, D., Belachew, M., Ebinger, C., Kendall, J., Hammond, J. O. S., Stuart, G., Ayele, A., and Rowland, J. (2011). Mapping the evolving strain field during continental breakup from crustal anisotropy in the Afar Depression. *Nature communications*, 2:285.

Keir, D., Ebinger, C. J., Stuart, G. W., Daly, E., and Ayele, A. (2006a). Strain accommodation by magmatism and faulting as rifting proceeds to breakup: Seismicity of the northern ethiopian rift. *Journal of Geophysical Research: Solid Earth*, 111(B5).

Keir, D., Ebinger, C. J., Stuart, G. W., Daly, E., and Ayele, A. (2006b). Strain accommodation by magmatism and faulting as rifting proceeds to breakup: Seismicity of the northern Ethiopian rift. *J. Geophys. Res.: Solid Earth*, 111(B5).

Keir, D., Hamling, I. J., Ayele, A., Calais, E., Ebinger, C., Wright, T., Jacques, E., Mohamed, K., Hammond, J. O. S., Belachew, M., Baker, E., Rowland, J., Lewi, E., and Bennati, L. (2009b). Evidence for focused magmatic accretion at segment centers from lateral dike injections captured beneath the Red Sea rift in Afar. *The Geological Society of America*, 37:59–62.

Keir, D., Stuart, G. W., Jackson, A., and Ayele, A. (2006b). Local Earthquake Magnitude Scale and Seismicity Rate forthe Ethiopian Rift. *Bull. Seismol. Soc. Am.*, 96:2221–2230.

Kendall, J. M., Pilidou, S., Keir, D., Bastow, I. D., Stuart, G. W., and Ayele, A. (2006). Mantle upwellings, melt migration and the rifting of Africa: Insights from seismic anisotropy, in Fitton, J.G., and Upton, B.G.J., eds., Alkaline Igneous Rocks. *Geological Society of London, Special Publications*, 259.

Kendall, J. M., Stuart, G., Ebinger, C., Bastow, I., and Keir, D. (2005). Magma-assisted rifting in Ethiopia. *Nature*, 433:146–8.

Kennett, B. L. N. (1983). Seismic Wave Propagation in Stratified Media. *Cambridge University Press, New York*, page 342.

Kennett, B. L. N., Engdah, E. R., and Buland, R. (1995). Constraints on seismic velocities in the Earth from traveltimes. *Geophys. J. Int.*, 122:108–124.

Keranen, K. M. and Klemperer, S. L. (2008). Discontinuous and diachronous evolution of the Main Ethiopian Rift: Implications for development of continental rifts. *Earth and Planetary Science Letters*, 265:96–111.

Keranen, K. M., Klemperer, S. L., and Gloaguen, R. (2004). Three-dimensional seismic imaging of a proto-ridge axis in the Main Ethiopian Rift. *Geology*, 32:949–952.

Keranen, K. M., Klemperer, S. L., Julia, J., Lawrence, J. F., and Nyblade, A. A. (2009). Low lower crustal velocity across Ethiopia: Is the Main Ethiopian Rift a narrow rift in a hot craton? *Geochemistry, Geophysics, Geosystems*, 10(5).

Kibret, B. A., Ayele, A., and Keir, D. (2019). Crustal thickness estimates beneath four seismic stations in Ethiopia inferred from p-wave receiver function studies. *Journal of African Earth Sciences*, 150:264–271.

Kibret, B. A., Ayele, A., and Keir, D. (2022). Modelling S-Wave Velocity Structure Beneath the Central Main Ethiopian Rift Using Receiver Functions. *Front. Earth Sci.*, 10:1–13.

Kibret, B. A., Ayele, A., and Keir, D. (2023). Crustal structure of the ethiopian northwestern plateau and central afar from receiver function analysis. *Front. Earth Sci.*, 11:1–13.

Kieffer, B., Arndt, N., Lapierre, H., Bastien, F., Bosch, D., Pecher, A., Yirgu, G., Ayalew, D., Weis, D., Jerram, D. A., Keller, F., and Meugniot, C. (2004). Flood and Shield Basalts from Ethiopia: Magmas from the African Superswell. *J. Petrology*, 45.

Kikuchi, M. and Kanamori, H. (1982). Inversion of complex body waves. *Bulletin of the Seismological Society of America*, 72(2):491–506.

Kim, S., Nyblade, A. A., Rhie, J., Baag, C. E., and Kang, T. S. (2012). Crustal S-wave velocity structure of the Main Ethiopian Rift from ambient noise tomography. *Geophysical Journal International*, 191(2):865–878.

Kind, R., Yuan, X., and Kumar, P. (2012). Seismic receiver functions and the lithosphere-asthenosphere boundary. *Tectonophysics*, 536-537:25–43.

Koptev, A., Calais, E., Burov, E., Leroy, S., and Gerya, T. (2015). Dual continental rift systems generated by plume–lithosphere interaction. *Nature Geoscience*, 8(5):388–392.

Korostelev, F., Weemstra, C., Leroy, S., Boschi, L., Keir, D., Ren, Y., Molinari, I., Ahmed, A., Stuart, G. W., Rolandone, F., Khanbari, K., Hammond, J. O. S., Kendall, J. M., Doubre, C., Ganad, I. A., Goitom, B., and Ayele, A. (2015). Magmatism on rift flanks: Insights from ambient noise phase velocity in Afar region. *Geophys. Res. Lett.*, 42:2179–2188.

La Rosa, A., Pagli, C., Wang, H., Doubre, C., Leroy, S., Sani, F., and al., e. (2021). Plateboundary kinematics of the afrera linkage zone (afar) from insar and seismicity. *J. Geophys. Res. Solid Earth*, 126.

Langston, C. A. (1979). Structure under Mount Rainier, Washington, inferred from teleseismic body waves. *J. Geophys. Res.*, 84(B9):4749.

Last, R. J., Nyblade, A. A., and Langston, C. A. (1997). Crustal structure of the East African Plateau from receiver functions and Rayleigh wave phase velocities. *J. Geophys. Res.*, 102:24,469–24,483.

Lavayssiere, A., et al Rychert, C., Hammond, J. O. S., Harmon, N., Kendall, J. M., Doubre, C., Keir, D., and Leroy, S. (2018). Imaging lithospheric discontinuities beneath the northern East African Rift usingS-to-Preceiverfunctions. *Geochem. Geophys. Geosyst.*, 19:4048–4062.

Lavayssiere, A., Greenfield, T., Keir, D., Ayele, A., and Kendall, J. (2019). Local seismicity near the actively deforming Corbetti volcano in the Main Ethiopian Rift. *Journal of Volcanology and Geothermal Research*, 381:227–237.

Lee, H., Muirhead, J. D., Fischer, T. P., Ebinger, C. J., Kattenhorn, S. A., Sharp, Z. D., and Kianji, G. (2016). Massive and prolonged deep carbon emissions associated with continental riftingv. *Nature Geoscience*, 9:145–149.

Lewi, E., Keir, D., Birhanu, Y., Blundy, J., Stuart, G., Wright, T., and Calais, E. (2016). Use of a High-precision Gravity Survey to Understand the Formation of Oceanic Crust and the Role of Melt at the Southern Red Sea Rift in Afar, Ethiopia. *Geological Society of London, Special Publications*, 420:165–180.

Ligorria, J. P. and Ammon, C. (1999). Iterative deconvolution and receiver function estimation,. *Bull. Seismol. Soc. Am.*, 89:1395–1400.

Liu, H. and Niu, F. (2012). Estimating crustal seismic anisotropy with a joint analysis of radial and transverse receiver function data. *Geophys. J. Int.*, 188:144–164.

Maccaferri, F., Rivalta, E., Keir, D., and Acocella, V. (2014). Off-rift volcanism in rift zones determined by crustal unloading. *Nature Geoscience*, 7(4):297–300.

Mackenzie, G. D., Thybo, H., and Maguire, P. K. H. (2005). Crustal velocity structure across the Main Ethiopian Rift: Results from two-dimensional wide-angle seismic modelling. *Geophys. J. Int.*, 162:994–1006.

Maguire, P., Keller, R., Klemperer, S., Mackenzie, G. D., Keranen, K., Harder, S., O'Reilly, B., Thybo, H., Asfaw, L., Khan, M., and Amha, M. (2006). Crustal structure of the Northern Main Ethiopian Rift from the EAGLE controlled source survey; a snapshot of incipient lithospheric break-up. *Geological Society Special Publication*, 259:269–292.

Mahatsente, R., Jentzsch, G., and Jahr, T. (1999). Crustal structure of the Main Ethiopian Rift from gravity data: 3-dimensional modeling. *Tectonophysics*, 313:363–382.

Makris, J. and Ginzburg, A. (1987). The Afar Depression: Transition between continental rifting and sea-floor spreading. *Tectonophysics*, 141:199–214.

Mammo, T. (2013). Crustal Structure of the Flood Basalt Province of Ethiopia from Constrained 3-D Gravity Inversion. *Pure Appl. Geophys.*, pages 1–22.

Mickus, K., Tadesse, K., Keller, G. R., and Oluma, B. (2007). Gravity analysis of the main Ethiopian rift. *Journal of African Earth Sciences*, 48:59–69.

Niu, F. and James, D. E. (2002). Fine structure of the lowermost crust beneath the Kaapvaal craton and its implications for crustal formation and evolution. *Earth and Planetary Science Letters*, 200.

Nyblade, A. A. (2002). Crust and upper mantle structure in East Africa: Implications for the origin of Cenozoic rifting and volcanism and the formation of magmatic rifted margins, inMenzies, M.A., Klemperer, S.L., Ebinger, C.J., and Baker, J., eds. Volcanic Rifted Margins: Boulder, Colorado. *Geol. Soc. Am., Spec. Pap.*, 362:15–26.

Nyblade, A. A., Owens, T. J., Gurrola, H., Ritsema, J., and Langston, C. A. (2000). Seismic evidence for a deep upper mantle thermal anomaly beneath East Africa. *Geology*, 28(7):599–602.

Ogden, C. S., Bastow, I. D., Gilligan, A., and Rondenay, S. (2019). A reappraisal of the H–κ stacking technique: Implications for global crustal structure. *Geophys. J. Int.*, 219:1491–1513.

Ogden, C. S., Keir, D., Bastow, I., Ayele, A., Marcou, S., Ugo, F., Woodward, A., Kibret, B. A., and Gudbrandsson, S. (2021). Seismicity and Crustal Structure of the Southern Main Ethiopian Rift: New Evidence From Lake Abaya. *Geochem. Geophys. Geosyst.*, 22:1–17.

Ott, R. L. and Longneckerv, M. T. (2001). *An Introduction to Statistical Methods and Data Analysis*. Thomson Brooks.

Owens, T. J. and Zandt, G. (1985). The response of the continental crust-mantle boundary observed on broadband teleseismic receiver functions. *Geophysical Research Letters*, 12:705–708.

Owens, T. J., Zandt, G., and Taylor, S. R. (1984). Seismic evidence for an Ancient Rift beneath the Cumberland Plateau, Tennessee: A detailed analysis of broadband teleseismic P waveforms. *J. Geophys. Res.*, 89:7783–7795.

Pagli, C., Mazzarini, F., Keir, D., Rivalta, E., Rooney, T. O., Pisa, U., al., e., of rifting: Tectonics, I. A., magmatism in continental rifts, o. s. c., and transforms (2015). *Geosphere*, 11(5):1256–1261.

Pagli, C., Yun, S.-H., Ebinger, C., Keir, D., and Wang, H. (2019). Strike-slip tectonics during rift linkage. *Geology*, 47(1):31–34.

Paulatto, M., Annen, C., Henstock, T. J., Kiddle, E., Minshull, T. A., Sparks, R. S. J., and Voight, B. (2012). Magma chamber properties fromintegrated seismic tomography and thermal modeling at Montserrat. *Geochem. Geophys. Geosyst.*, 13:1–18.

Paulatto, M., Minshull, T. A., Baptie, B., Dean, S., Hammond, J. O. S., Henstock, T., Kenedi, C. L., Kiddle, E. J., Malin, P., Peirce, C., Ryan, G., Shalev, E., Sparks, R. S. J., and Voight, B. (2010). Upper crustal structure of an active volcano from refraction/reflection tomography, Montserrat, Lesser Antilles. *Geophys. J. Int.*, 180(2):685–696.

Paulatto, M., Moorkamp, M., Hautmann, S., Hooft, E., Morgan, J. V., and Sparks, R. S. J. (2019). Vertically extensive magma reservoir revealed from joint inversion and quantitative interpretation of seismic and gravity data. *J. Geophys. Res.*, 124:11,170–11,191.

Peck, R., Olsen, C., and Devore, J. (2008). *Introduction to Statistics and Data Analysis*. Thomson Brooks/Cole.

Pik, R., Deniel, C., Coulon, C., Yirgu, G., Hofmann, C., and Ayalew, D. (1998). The northwestern Ethiopian Plateau flood basalts: Classification and spatial distribution of magma types. *J. Volcanol. Geotherm. Res.*, 81:91–111.

Pik, R., Deniel, C., Coulon, C., Yirgu, G., and Marty, B. (1999). Isotopic and trace element signatures of Ethiopian flood basalts: Evidence for plume–lithosphere interactions. *Geochimica et Cosmochimica Acta*, pages 2263–2279.

Pik, R., Marty, B., Carignan, J., and Lave, J. (2003). Stability of the Upper Nile drainage network (Ethiopia) deduced from (U-Th)/He thermochronometry: Implications for uplift and erosion of the Afar plume dome. *Earth and Planetary Science Letters*, 215:73–88.

Pik, R., Marty, B., Carignan, J., Yirgu, G., and Ayalew, T. (2008). Timing of East African Rift development in southern Ethiopia: Implication for mantle plume activity and evolution of topography. *Geology*, 36(2):167–170.

Ping, D., Jiatian, L., Xiaoqing, Z., and Jia, L. (2009). A new Interpolation Model of Convex Hull in Delaunay Triangulation. *International Symposium on Spatial Analysis, Spatial-Temporal Data Modeling, and Data Mining, edited by Yaolin Liu, Xinming Tang, Proc. of SPIE*, 7492:1–9.

Randall, G. E. (1989). Efficient calculation of differential seismograms for lithospheric receiver functions. *Geophys. J. Int.*, 99:469–481.

Reed, C. A., Almadani, S., Gao, S. S., Elsheikh, A. A., Cherie, S., Abdelsalam, M. G., Thurmond, A. K., and Liu, K. H. (2014). Receiver function constraints on crustal seismic velocities and partial melting beneath the Red Sea rift and adjacent regions, Afar Depression. *J. Geophys. Res. Solid Earth*, 119 (3):2,138–2,152.

Robinson, E. A. (1982). A historical perspective of spectrum estimation. *in Proceedings of the IEEE*, 70:885–907.

Roecker, S., Ebinger, C., Tiberi, C., Mulibo, G., Ferdinand-Wambura, R., Mtelela, K., Kianji, G., Muzuka, A., Gautier, S., Albaric, J., and Peyrat, S. (2017). Subsurface images of the Eastern Rift, Africa, from the joint inversion of body waves, surface waves and gravity: Investigating the role of fluids in early-stage continental rifting. *Geophys. J. Int.*, 210:931–950.

Rogers, N. W. (2006). Basaltic magmatism and the geodynamics of the East African Rift System. *Geological Society, London, Special Publications*, 259:77–93.

Rogers, N. W., Macdonald, R., Fitton, J., George, R., Smith, M., and Barreiro, B. (2000). Two mantle plumes beneath the East African rift system: Sr, Nd and Pb isotope evidence from Kenya Rift basalts. *Earth and Planetary Science Letters*, 176:387–400.

Rooney, T., Furman, T., Yirgu, G., and Ayalew, D. (2005). Structure of the Ethiopian lithosphere: Evidence from mantle xenoliths. *Geochim. Cosmochim. Acta*, 69(15):3889–3910.

Rooney, T. O. (2010). Geochemical evidence of lithospheric thinning in the southern Main Ethiopian Rift. *Lithos*, 117:33–48.

Rooney, T. O. (2017). The Cenozoic magmatism of East-Africa: Part I — Flood basalts and pulsed magmatism. *Lithos*, 286–287:264–301.

Rooney, T. O., Bastow, I. D., Keir, D., Mazzarini, F., Movsesian, E., Grosfils, E., Zimbelman, J., Ramsey, M., Ayalew, D., and Yirgu, G. (2014). The protracted development of focused magmatic intrusion during continental rifting. *Tectonics*, 33:875–897.

Rooney, T. O., Furman, T., Bastow, I., Ayalew, D., and Yirgu, G. (2007). Lithospheric modification during crustal extension in the Main Ethiopian Rift. *J. Geophys. Res.*, 112.

Rooney, T. O., Herzberg, C., and Bastow, I. D. (2011). Elevated mantle temperature beneath East Africa. *Geology*, 40:27–30.

Rooney, T. O., Krans, S. R., Mège, D., Arnaud, N., Korme, T., Kappelman, J., and Yirgu, G. (2018). Constraining the magmatic plumbing system in a zoned continental flood basalt province. *Geochem. Geophys. Geosyst.*, 19:3917–3944.

Rowland, J. V., Baker, E., Ebinger, C. J., Keir, D., Kidane, T., Biggs, J., Hayward, N., and Wright, T. J. (2007). Fault growth at a nascent slow-spreading ridge: 2005 Dabbahu rifting episode, Afar. *Geophysical Journal International*, 171:1226–1246.

Rychert, C., Hammond, J. O. S., Harmon, N., Kendall, J., Keir, D., Ebinger, C., Bastow, I., Ayele, A., Belachew, M., and Stuart, G. (2012). Volcanism in the Afar Rift sustained by decompression melting with minimal plume influence. *Nature Geoscience*, 5:406–409.

Samrock, F., Grayver, A. V., Eysteinsson, H., and Saar, M. (2018). Magnetotelluric image of transcrustal magmatic system beneath the Tulu Moye geothermal prospect in the Ethiopian Rift. *Geophys. Res. Lett.*, 45:12,847–12,855.

Samrock, F., Kuvshinov, A., Bakker, J., Jackson, A., and Fisseha, S. (2015). 3-D analysis and interpretation of magnetotelluric data from the Aluto-Langano geothermal field, Ethiopia. *Geophysical Journal International*, 202(3):1923–1948.

Sembroni, A., Faccenna, C., Becker, T., Molin, P., and Bekele, A. (2016). Long-term, deep-mantle support of the Ethiopia-Yemen Plateau. *Tectonics*, 35:469–488.

Sengor, A. M. C. (2001). Elevation as indicator of mantle-plume activity. *Geol. Soc. Am., Spec. Pap.*, 352:183–225.

Simmons, G. (1964). The velocity of shear waves in rocks to 10 kilobars. *J. Geophys. Res.*, 69(6):1123–1130.

Stamps, D. S., Iaffaldano, G., and Calais, E. (2015). Role of mantle flow in Nubia-Somalia plate divergence. *Geophys. Res. Lett.*, 42:290–296.

Steiner, R. A., Rooney, T. O., Girard, G., Rogers, N., Ebinger, C. J., Peterson, L., and Phillips, R. K. (2021). Initial Cenozoic magmatic activity in East Africa: New geochemical constraints on magma distribution within the Eocene continental flood basalt province. *Geological Society, London, Special Publications*, 518(1):435–465.

Stuart, G., Bastow, I. D., and Ebinger, C. J. (2006). Crustal structure of the northern Main Ethiopian Rift from receiver function studies, in The Afar Volcanic Province Within the East African Rift System, edited by G. Yirgu, C. J. Ebinger, and P. K. H. Maguire. *Geological Society London Special Publications*, 259:253–267.

Tessema, A. and Antoine, L. A. G. (2004). Processing and interpretation of the gravity field of the East African Rift: Implication for crustal extension. *Tectonophysics*, 394:87–110.

Thompson, D. A., Bastow, I. D., Helffrich, G., Kendall, J. M., Wookey, J., Snyder, D. B., Thompson, D. A., and Eaton, D. W. (2010). Precambrian crustal evolution: Seismic constraints from the Canadian Shield. *Earth and Planetary Science Letters*, 297(3-4):655–666.

Thybo, H. and Artemieva, I. M. (2019). Moho and magmatic underplating in continental lithosphere. *Tectonophysics*, 609:605–619.

Thybo, H., Youssof, M., and Artemieva, I. M. (2019). Southern Africa crustal anisotropy reveals coupled crust-mantle evolution for over 2 billion years. *Nature communications*, 10:1–10.

Tiberi, C., Ebinger, C., Ballu, V., Stuart, G., and Oluma, B. (2005). Inverse models of gravity data from the Red Sea–Aden–East African rifts triple junction zone. *Geophysical Journal International*, 163(2):775–787.

Viltres, R., Jonsson, S., Ruch, J., Doubre, C., Reilinger, R., Floyd, M., and Ogubazghi, G. (2020). Kinematics and deformation of the southern red sea region from gps observations. *Geophys. J. Int.*, 221(3):2143–2154.

Wang, T., Gao, S. S., Yang, Q., and Liu, K. H. (2021). Crustal structure beneath the Ethiopian Plateau and adjacent areas from receiver functions: Implications for partial melting and magmatic underplating. *Tectonophysics*, 889:1–12.

Weissel, J. K. and Karner, G. D. (1989). Flexural uplift of riftflanks due to mechanical unloading of the lithosphere during extension. *J. Geophys. Res.*, 94:13,919–13,950.

Wessel, P., Luis, J. F., Uieda, L., Scharroo, R., Wobbe, F., Smith, W. H. F., and Tian, D. (2019). The Generic Mapping Tools Version 6. *Geochemistry, Geophysics, Geosystems*, 20:1–9.

Whaler, K. A. and Hautot, S. (2006). The electrical resistivity structure of the crust beneath the northern Main Ethiopian Rift. *Geological Society, London, Special Publications*, 259(1):293–305.

Whittington, A. G., Hofmeister, A. M., and Nabelek, P. I. (2009). Temperature-dependent thermal diffusivity of the Earth's crust and implications for magmatism. *Nature*, 458(7236):319–321.

Woldegabriel, G., Aronson, J., and Walter, R. (1990). Geology, geochronology, and rift basin development in the central sector of the Main Ethiopia Rift. *Geological Society of America Bulletin*, 102:439–458.

Woldetinsae, G. and Gotze, H. J. (2005). Gravity field and isostatic state of Ethiopia and adjacent areas. *Journal of African Earth Sciences*, 41:103–117.

Wolfenden, E., Ebinger, C., Yirgu, G., Deino, A., and Ayalew, D. (2004). Evolution of the northern Main Ethiopian Rift: Birth of a triple junction. *Earth and Planetary Science Letters*, 224:213–228.

Wolfenden, E., Ebinger, C. J., Yirgu, G., Renne, P. R., and Kelley, S. P. (2005). Evolution of a volcanic rifted margin: Southern Red Sea, Ethiopia. *J Geological Society of America Bulletin*, 117:846–864.

Wright, T., Ebinger, C., Biggs, J., Ayele, A., Yirgu, G., Keir, D., and Stork, A. (2006). Magma-maintained rift segmentation at continental rupture in the 2005 Afar dyking episode. *Nature*, 442:291–294.

Wright, T., Sigmundsson, F., Pagli, C., Belachew, M., Hamling, I., Brandsdóttir, B., Keir, D., Pedersen, R., Ayele, A., Ebinger, C., Einarsson, P., Lewi, E., and Calais, E. (2012). Geophysical constraints on the dynamics of spreading centres from rifting episodes on land. *Nature Geoscience*, 5:242–250.

Yang, H., Chemia, Z., Artemieva, I. M., and Thybo, H. (2018). Control on off-rift magmatism: A case study of the Baikal Rift Zone. *Earth and Planetary Science Letters*, 482:501–509.

Yilmaz, Ö. and Doherty, S. M. (1987). *Seismic Data Processing*. Society of Exploration Geophysicists.

Youssof, M., Thybo, H., Artemieva, I. M., and Levander, A. (2013). Moho depth and crustal composition in the Southern Africa. *Tectonophysics*.

Youssof, M., Thybo, H., Artemieva, I. M., and Levander, A. (2015). Upper mantle structure beneath southern African cratons from seismic finite-frequency P- and S-body wave tomography. *Earth and Planetary Science Letters*, 420:174–186.

Zandt, G. and Ammon, C. J. (1995). Continental Crustal composition constrained by measurements of crustal Poisson's ratio. *Nature*, 374:152–154.

Zhu, L. and Kanamori, H. (2000). Moho depth variation in southern California from teleseismic receiver functions. *J. Geophys. Res.: Solid Earth*, 105(B2):2969–2980.